Con Edison

Indian Point Unit 2
1991 Steam Generator Inspection, Evaluation and Repair Activities

December, 1991

Consolidated Edison Company of New York, Inc.
4 Irving Place
New York, NY 10003

Indian Point Unit 2
1991 Steam Generator Inspection, Evaluation and Repair Activities

December, 1991

Consolidated Edison Company of New York, Inc.
4 Irving Place
New York, NY 10003

Table of Contents

This page intentionally left blank.

1.0 INTRODUCTION

1.1 Overview

Indian Point Unit 2 is a Pressurized Water Reactor with four Westinghouse designed Model 44 steam generators. During the scheduled refueling outage in 1987, cracks were discovered on the inside surface of each of the four steam generators at the girth weld connecting the upper cylinder to the transition cone [1]*. These cracks were repaired by grinding and the unit was returned to service. During the next refueling outage in 1989, additional cracks were identified in the girth weld region and also in the area of the feedwater ring tee support bracket [2]. The feedwater ring tee support brackets were repaired by grinding and shielded metal arc welding using the half bead technique. The girth weld cracks were repaired by grinding and by localized weld buildup by gas tungsten arc welding and full circumferential stress relief in one steam generator (Steam Generator 22). During November, 1989, while the unit was in operation, a leak was detected in an inspection port. The leak was caused by a crack close to the outside of the vessel shell and it was repaired by grinding, rewelding, and installation of a bolted cover plate. During a midcycle inspection in 1990, additional cracks were discovered in the girth weld, the feedwater nozzle bores, and the feedwater tee and ring support brackets [3]. These cracks were repaired by grinding and localized temper bead and half bead welding. The tee support brackets were moved to minimize the bracket stresses caused by the nozzle thermal sleeve bypass flow.

As a result of this crack recurrence, Consolidated Edison, in May of 1990, initiated a program of investigation to reassess the cause of the cracking and to recommend steps that could be taken to prevent further cracking.

*Numbers in Brackets Refer to References in Section 10.0.

Several activities were initiated as a part of a multi-faceted program. One activity of this program was the monitoring of temperature data from thermocouples that were mounted at strategic locations on the outside surface of the feedwater pipe, feedwater nozzle, and girth weld of Steam Generator 21. A second activity was the selection of a group of independent industry consultants to work with the Consolidated Edison Engineering Department to investigate the cause of steam generator cracking. This team, called the Steam Generator Review Team (SGRT), included Dr. Thomas Esselman of Altran Corporation as lead investigator, Professor Ronald Ballinger of MIT, Professor Robert Wei of Lehigh University, and Dr. Robert Vecchio of Lucius Pitkin Inc. The SGRT initiated a coordinated program to investigate:

- the pitting that occurred at the inside surface of the steam generators,

- the data from the thermocouple monitoring program measuring the shell temperatures near the feedwater nozzle, and

- the fracture mechanics aspects of the cracking at the girth weld location.

The results from this program provided an understanding of the failure mechanism and root cause. The causes of the surface pitting were identified. A quantitative assessment of the operational thermal transients occurring at the region of cracking was made. Additional information on the fracture mechanics implications of the nature of the crack growth in the girth weld of the steam generator shell was obtained. The SGRT concluded that the primary cause of the cracking was stress corrosion.

As a result of work performed by Consolidated Edison and the SGRT, extensive repairs were made to the steam generators

during the Spring 1991 Refueling Outage. The girth weld repair consisted of removal of a section of the girth weld to a nominal depth of 3/4 inch. A band of approximately six inches of the weld was removed in the axial direction around the entire circumference of the shell. The band was centered about the existing weld. The area was rewelded with a carefully selected weld material and weld contour with smooth finish. Weld repairs were also made at locations of cracks in regions above and below the girth weld. A feedwater nozzle sealing sleeve was installed to eliminate the leakage of cold water into the region beneath the thermal sleeve.

The repair addressed all interacting contributors to stress corrosion cracking (SCC). This resulted in the reduction of high stresses, the mitigation of the aggressive environment, and the use of more corrosion resistant materials. The improvements in each of these areas are as follows:

- High Stresses - A specifically selected contour in the replacement weld reduced the stress concentration previously caused by the "knee" at the girth weld region. An effective post weld heat treatment reduced the residual stresses in the girth weld. Modifications made earlier to the feedwater system reduced the severity of the transient at the girth weld following a reactor trip.

- Environment - Oxygen control measures during auxiliary feedwater injection have been added to reduce the likelihood of pitting and cracking.

- Material - Low sulphur material was utilized in the replacement weld. This material will have a higher resistance to pit formation.

1.2 Conclusions

The objectives of the steam generator activities reported herein were to develop a thorough understanding of the mechanism and root cause of girth weld crack initiation and propagation, and to develop and implement a high quality repair that would effectively retard further cracking. This has been accomplished through a thorough analytical and experimental investigation of the cracking phenomena, analysis of boat samples removed from the steam generator, and development and implementation of a girth weld repair.

The primary conclusions regarding the root cause of the cracking in the steam generator are the following:

- The girth weld cracking was preceded by pitting.
- The cracks are propagated primarily by stress corrosion cracking.
- The field and analytical data have shown that the cracks have a tendency to grow partially through-wall and then decelerate. This is due to the interaction of operating stresses and residual stresses.

A repair and plant modification which effectively addressed the root cause contributors has been implemented. The repair and modification included selection of a replacement weld material which minimizes pit formation locations, selection of a weld contour which reduces and controls the operating stress at the girth weld, implementation of an effective and well controlled post weld heat treatment, and reduction of oxygen in the auxiliary feedwater. The replacement weld repair and improved auxiliary feedwater oxygen control have been implemented to eliminate further cracking in the girth weld region of the steam generators.

Cracking had been noted in the bore and knuckle of the feedwater nozzles. This cracking was caused by the leakage of cold auxiliary feedwater under the existing thermal sleeve during low flow cold water injection. A sealing sleeve was installed in the feedwater nozzle which will mitigate the mechanism responsible for cracks in the nozzle region.

This page intentionally left blank.

2.0 **1991 INSPECTIONS**

2.1 Girth Weld

The internal surface of the girth welds of all four steam generators was inspected. A horizontal reference line was established and the girth weld region was divided into 12 circumferential zones to assist in record keeping. The inspection area included a band nominally 7 inches above and below the centerline of the girth weld. Figure 2.1 shows the girth weld region of the steam generators.

The magnetic particle examination (MT) of the girth welds in Steam Generators 21 and 24 showed them to be crack free. The initial MT examinations of the girth weld showed a total of 9 cracks in Steam Generator 22 and 1 crack in Steam Generator 23. All the girth weld cracks were localized within two zones in Steam Generators 22 and 23.

Table 2.1 lists the cracks found during the initial inspection in the girth weld (noted by "GW" in the position column). The horizontal location is determined from the start of the zone and is measured clockwise when viewing the feedring from above. The vertical locations are measured relative to the milling machine trackline. The location of these Steam Generator 22 and 23 cracks is presented graphically in Figure 2.2. None of the cracks found in 1991 were located in the weld repair areas of 1989 or 1990.

2.2 Near Girth Weld Region

In addition to inspection band described above which included areas above and below the girth weld, the internal surface of the steam generators was also MT examined in a band 7 to 14 inches below the girth weld

centerline. Cracks were found above and below the girth weld. These cracks were found at temporary attachment fit-up welds installed during fabrication or field assembly of the vessel. There were four cracks found above the girth weld area in Steam Generator 21. Below the girth weld, twenty three cracks were found in Steam Generator 22 and five cracks were found in Steam Generator 23. No cracks were found in Steam Generator 24.

A band of 7 to 14 inches below the girth weld of Steam Generator 22 was examined from the external surface of the vessel by ultrasonics (UT). All UT surface indications were investigated by MT examination and grinding.

Table 2.1 lists the cracks found during the initial inspection in the near girth weld area (noted by "A" or "B" in the position column for above or below the girth weld). The locations of these Steam Generator 21, 22, and 23 cracks are presented graphically in Figure 2.3. No cracks were detected in Steam Generator 24.

2.3 Feedwater Nozzle

A UT examination was conducted on the feedwater nozzle of Steam Generator 24. Portions of the bore and part of the knuckle area were inspected by UT from the external surface. Figure 2.4 shows the feedwater nozzle. In this UT inspection on the knuckle in Steam Generator 24, no cracking was detected.

The UT examination of the bore region of the Steam Generator 24 nozzle, using a high sensitivity technique, showed reflectors in the area of a cross section change. In order to determine the nature of the reflectors, a fiberscope was used to view the area. Results of the fiberscope examination were inconclusive and the thermal

sleeve was removed. Examination of the bore by MT after removal of the sleeve indicated no cracking.

On all four steam generators, the knuckle of the feedwater nozzle forging was also inspected by liquid penetrant (PT). One crack was found on the face near the knuckle in Steam Generator 22. The crack was located near the 7 o'clock position and measured 1/2 inch long. The crack was removed by grinding to a depth of 0.050 inch. The location of this crack was dimensionally consistent with the location of one of the original welded feedwater tee support brackets.

2.4 Feedwater Pipe Inspection

A one foot square area on the internal surface of the feedwater pipe leading to Steam Generator 22 was examined by UT from the external surface. No cracks were found. Visual examination of the interior surface during installation of the thermal sleeve also confirmed the absence of cracks.

A nozzle to pipe weld on Steam Generator 24 was examined by radiography. Comparison of the current with the previous as-left radiographs from the 1990 Midcycle Outage revealed no differences.

2.5 Feedring Bracket Inspection

The bracket welds supporting the feedwater ring and the feedwater tee were examined by MT or PT, depending upon physical accessibility. No cracks were found. The examinations revealed two indications in the base material that were unrelated to previous repairs. The indications were surface imperfections in the original material and were removed. A feedring support bracket is shown in Figure 2.5.

2.6 Inspection Ports

Shortly before the beginning of the 1991 Refueling Outage, Inspection Port 2 on Steam Generator 24 developed a leak. The Steam Generator 24 Inspection Ports 1, 2, 3 and 4 and Steam Generator 22 hillside port had been enlarged from 1 inch to 2 inch diameters during the November 1989 outage.

After cooling down and draining, the cover of Inspection Port 2 of Steam Generator 24 was removed and the area of the leak was examined. The leak was at the gasket. PT examination of the bore of the port revealed a crack. The crack was etched and shown to be at the edge of the original repair, coincident with a previous crack that was repaired when the port was enlarged. The crack is believed to have been missed by the original repair inspection because of very limited visibility and physical access for the PT examination.

The bore of the other three ports was examined by PT. No cracks were found. Figure 2.6 shows a typical 2 inch diameter inspection port.

The other inspection ports examined were the 1 inch diameter hillside port on Steam Generator 23 and the 2 inch diameter hillside port on Steam Generator 22. The 1 inch diameter hillside port on Steam Generator 23 was examined by a fiberscope. No cracks were found by this examination. The 2 inch diameter hillside inspection port on Steam Generator 22 was examined by PT. No cracks were found. Figures 2.7 and 2.8 show the 1 inch diameter and 2 inch diameter hillside ports, respectively.

An upper and a lower level (3/4 inch diameter) instrument tap port in Steam Generator 21 were examined by PT. No cracks were found.

One of the 6 inch diameter handholes located above the tubesheet on Steam Generator 22 and the upper 8 inch diameter handhole on Steam Generator 23 were examined by PT. No cracks were found.

The bore of the 16 inch diameter manway of Steam Generator 21 was examined by MT. No cracks were found.

2.7 Comparison To Previous Inspections

The number of girth weld cracks, as well as their maximum and average depths, were compiled from inspections performed during 1987 to 1991. The trends for the number of cracks, maximum depth and average depth were decreasing. Table 2.2 summarizes the current and previous examinations. It should be noted that the depth of cracks in 1991 are not available in all cases because the robotic milling machine depth of cut is approximately 1/8 inch. Since the lengths of the current cracks are short, 1/4 inch maximum, the depth would be correspondingly shallow and they were readily removed by initial passes of the milling machine.

SG	Zone	Crack	Length in.	Depth in.	Pos.	Loc.	Horiz in.	Vert. in.	Remarks crack orient.;
21	7	1	0.25	<0.16	A	O	21.13	7.82	-; Below tap
		2	0.25	<0.16	A	O	20.38	7.82	-; Below tap
		3	0.75	0.16	A	O	21.25	8.19	-; Below tap
		4	1.50	0.11	A	O	15.75	7.93	-; Below tap
22	1	1	1.50	0.06	B	S	8.50	21.50	-; } Boat
		2	0.50	0.03	B	S	10.00	21.75	-;
		3	0.25	-	GW	O	0.50	15.70	-;
		4	0.25	-	GW	O	20.50	16.70	-;
		5	0.25	0.10	GW	O	24.00	17.20	-; } Boat; HAZ
		6	0.25	0.13	GW	O	25.25	17.20	-;
		7	0.25	-	GW	O	29.00	17.20	-;
		8	0.25	-	GW	O	31.00	17.40	-;
		9	0.75	0.20	GW	O	35.75	17.00	-; Boat; HAZ
		10	0.25	-	GW	O	33.00	17.20	-;
		11	0.25	-	GW	O	34.00	17.40	-;
	3	1	1.00	0.31	B	O	2.50	22.69	I; Boat; HAZ
	4	1	1.13	0.35	B	O	30.25	21.20	\; Boat; HAZ
		3	1.19	0.21	B	O	30.81	22.25	-; HAZ
	5	1	0.25	<0.20	B	O	2.62	22.31	-; HAZ
		2	0.25	0.20	B	O	3.62	22.31	/; HAZ
	7	1	2.00	0.43	B	O	4.00	22.69	-; HAZ
		2	1.38	0.15	B	S	36.62	22.31	-;
	8	1	0.88	0.19	B	S	0.88	19.00	I; Boat
		2	0.88	0.04	B	S	38.50	22.19	-;

KEY
A Above Girth Weld
B Below Girth Weld
GW Girth Weld
O Original Surface
S Slope of 1990 Repair
H HAZ Observed

TABLE 2-1

Steam Generator Girth Weld Cracks - 1991

SG	Zone	Crack	Length in.	Depth in.	Pos.	Loc.	Horiz in.	Vert. in.	Remarks crack orient.;
22	10	1	0.50	0.22	B	O	31.37	20.00	-; HAZ
		2	0.25	<0.22	B	O	32.75	20.19	-; HAZ
		3	0.38	0.22	B	O	36.00	20.19	-; HAZ
	11	1	0.13	<0.48	B	O	1.25	21.31	-; HAZ
		2	0.50	<0.48	B	O	3.25	21.06	I; HAZ
		3	0.50	<0.48	B	O	3.88	20.94	I; HAZ
		4	1.31	0.48	B	O	5.63	21.63	-; HAZ
		5	1.00	0.41	B	O	35.87	22.06	-; HAZ
	12	1	0.25	<0.15	B	O	5.00	21.44	-; HAZ
		2	0.25	0.15	B	O	5.50	22.00	-; HAZ
		3	0.38	0.15	B	O	5.63	21.69	I; HAZ
		4	0.31	0.15	B	O	31.50	22.19	-; HAZ
23	3	1	2.13	0.25	B	O	25.63	23.13	-; BOAT; HAZ
	5	1	0.63	0.22	B	O	22.00	21.69	/; } Joined HAZ
		2	0.50	0.13	B	O	24.00	27.69	/; subsurface
	6	1	2.50	0.06	B	O	26.50	23.07	-; BOAT; HAZ
	8	1	1.63	0.35	B	O	25.00	23.34	I; BOAT; HAZ
	12	1	0.25	-	GW	O	7.25	16.25	I;
24	NONE								

NOTES:

- Vertical measurements were made from the horizontal track line
- Horizontal measurements were taken from the start of the zone and were measured clockwise when viewed from above the feedring
- All girth weld cracks (10) were on original surfaces

  Largest - 0.75" long x 0.20" deep (22-1-9 Boat)
- Below girth weld - 25 cracks were on original surfaces

  All 5 slope cracks were in 1990 grindouts (3 areas)
  Longest in grindout - 1.5" long x 0.06" deep (22-1-1 Boat)
  Deepest in grindout - 0.88" long x 0.19 deep (22-8-1 Boat)

  Longest on original surface - 2.50" long x 0.06" deep (23-6-1 Boat)
  Deepest on original surface - 1.31" long x 0.48" deep (22-11-4)

TABLE 2-1 (Cont.)

Steam Generator Girth Weld Cracks - 1991

OUTAGE PERIOD	SG 21	SG 22	SG 23	SG 24	OPERATING PERIOD
1987 Refueling					
Number of Cracks	38	101	102	50	UP TO
Maximum Depth	0.56	1.07	1.01	0.57	1987
Average Depth	0.29	0.49	0.31	0.29	
1989 Refueling					
Number of Cracks	5	49	15	7	BETWEEN 1987
Maximum Depth	0.3	0.95	0.33	0.34	AND
Average Depth	0.21	0.26	0.16	0.14	1989
1990 Mid-Cycle					
Number of Cracks	42	23	14	10	BETWEEN 1989
Maximum depth	0.48	0.51	0.27	0.33	AND
Average Depth	0.11	0.09	0.08	0.17	1990
1991 Refueling					
Number of Cracks	0	9	1	0	BETWEEN 1990
Maximum Depth	-	0.20*	*	-	AND
Average Depth	-	0.14*	*	-	1991

* - Measurements were based on boat samples removed. The deepest crack was 3/4" long, all others were 1/4" long.

TABLE 2.2

Girth Weld Crack Summary

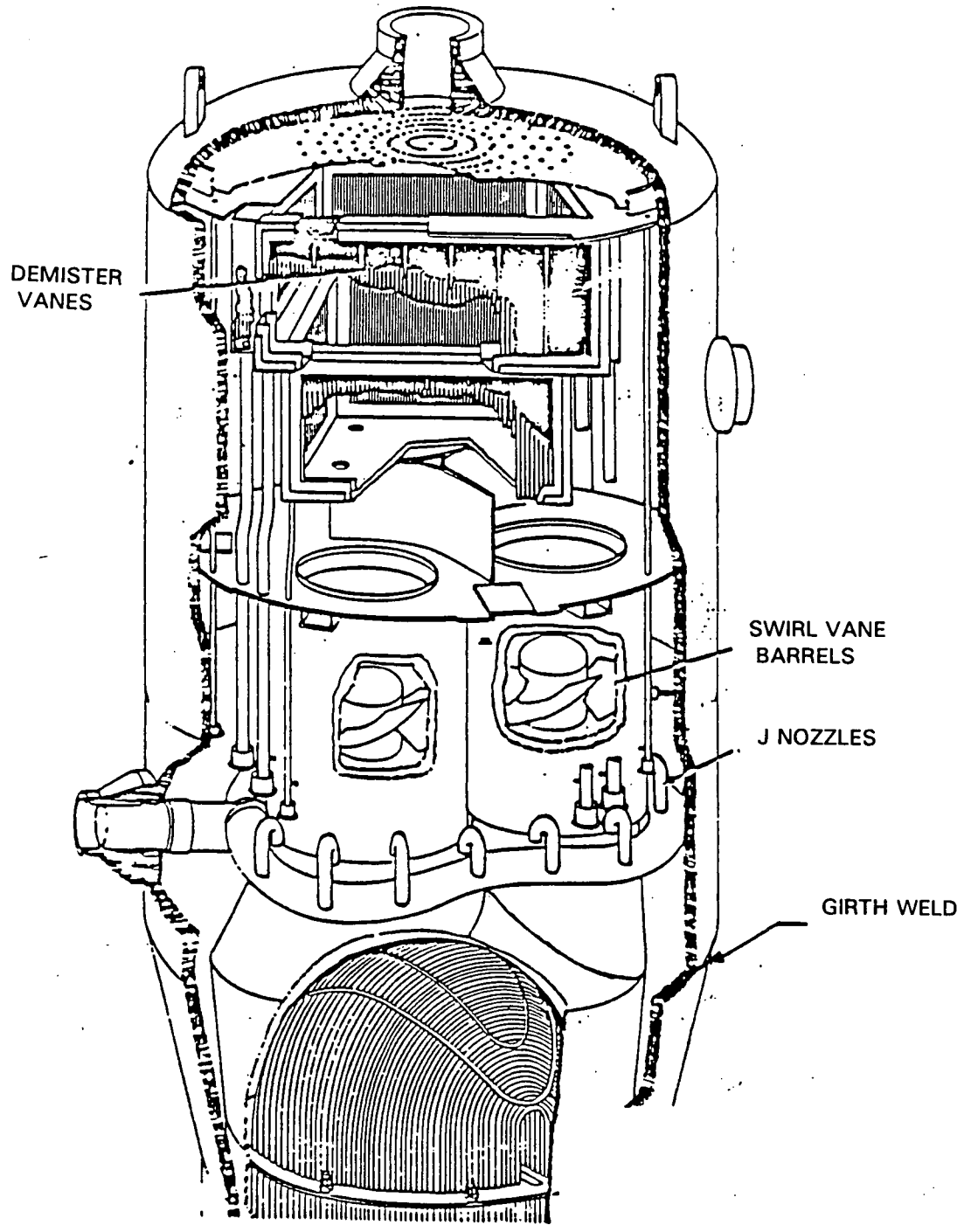

FIGURE 2.1

General Outline of Westinghouse Model 44
Steam Generator Showing Girth Weld Region

This page intentionally left blank.

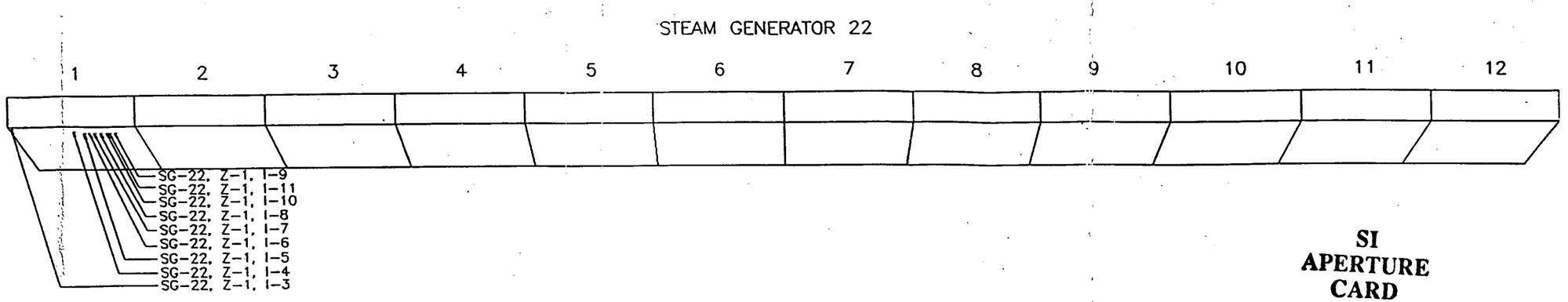

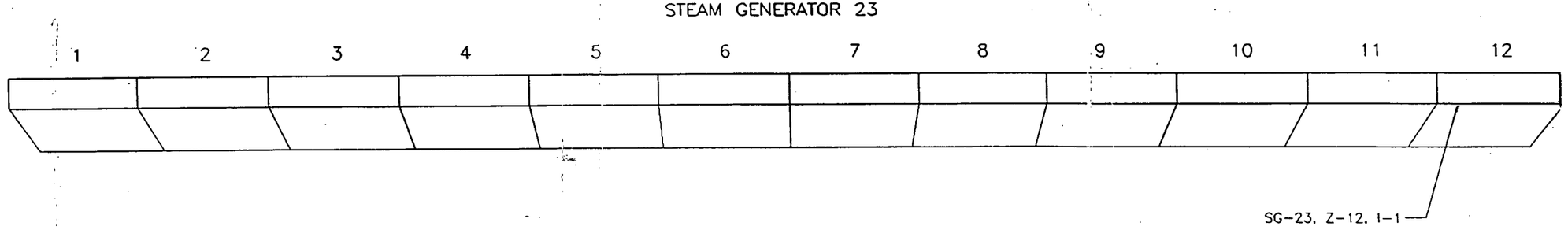

FIGURE 2.2

1991 Girth Weld Cracks
Steam Generator 22 and 23

Locations of Cracks

SI APERTURE CARD

Also Available On Aperture Card

STEAM GENERATOR 21

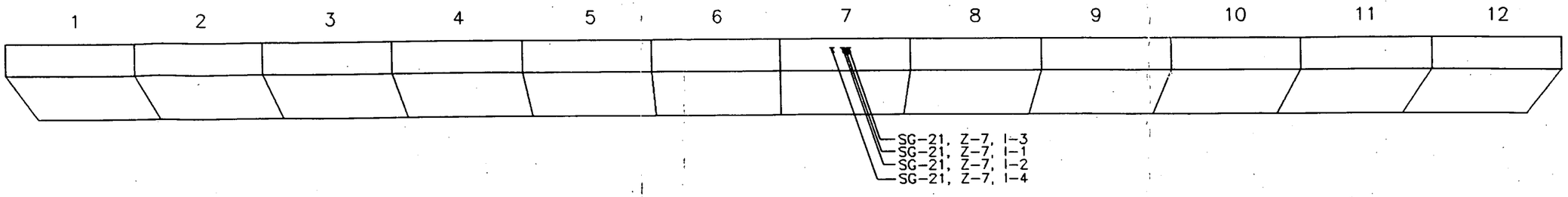

STEAM GENERATOR 22

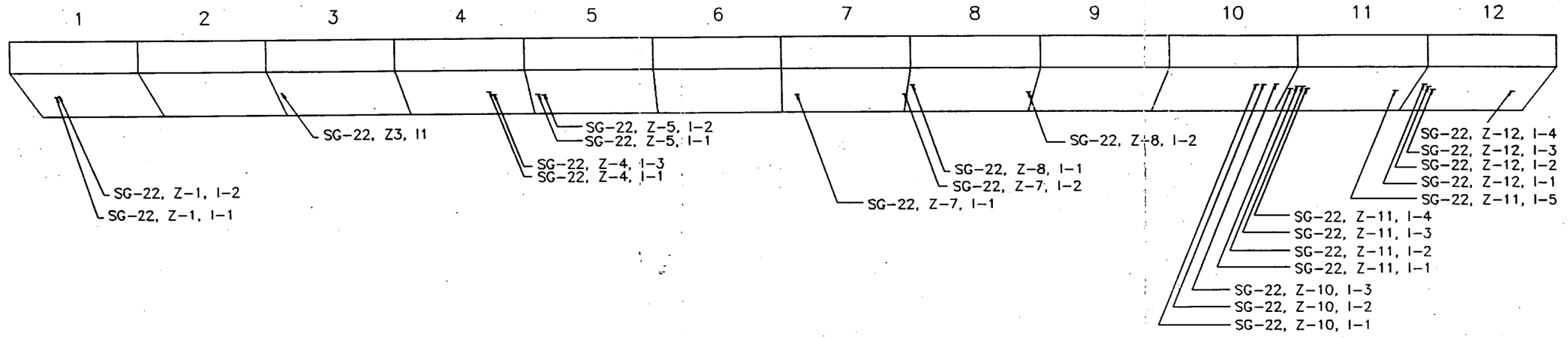

STEAM GENERATOR 23

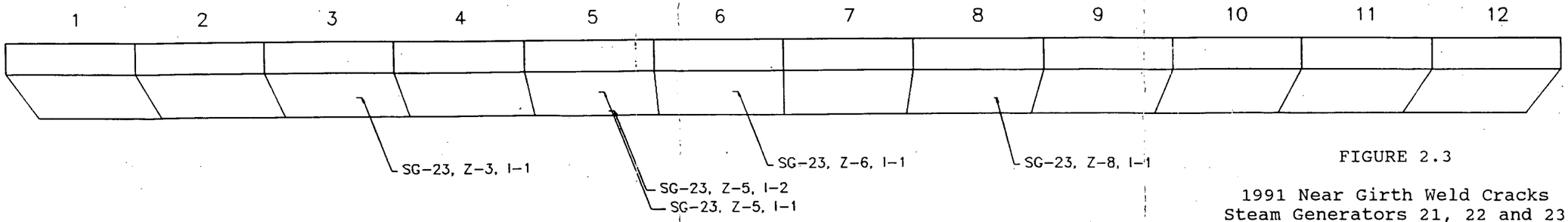

FIGURE 2.3

1991 Near Girth Weld Cracks
Steam Generators 21, 22 and 23

Locations of Cracks

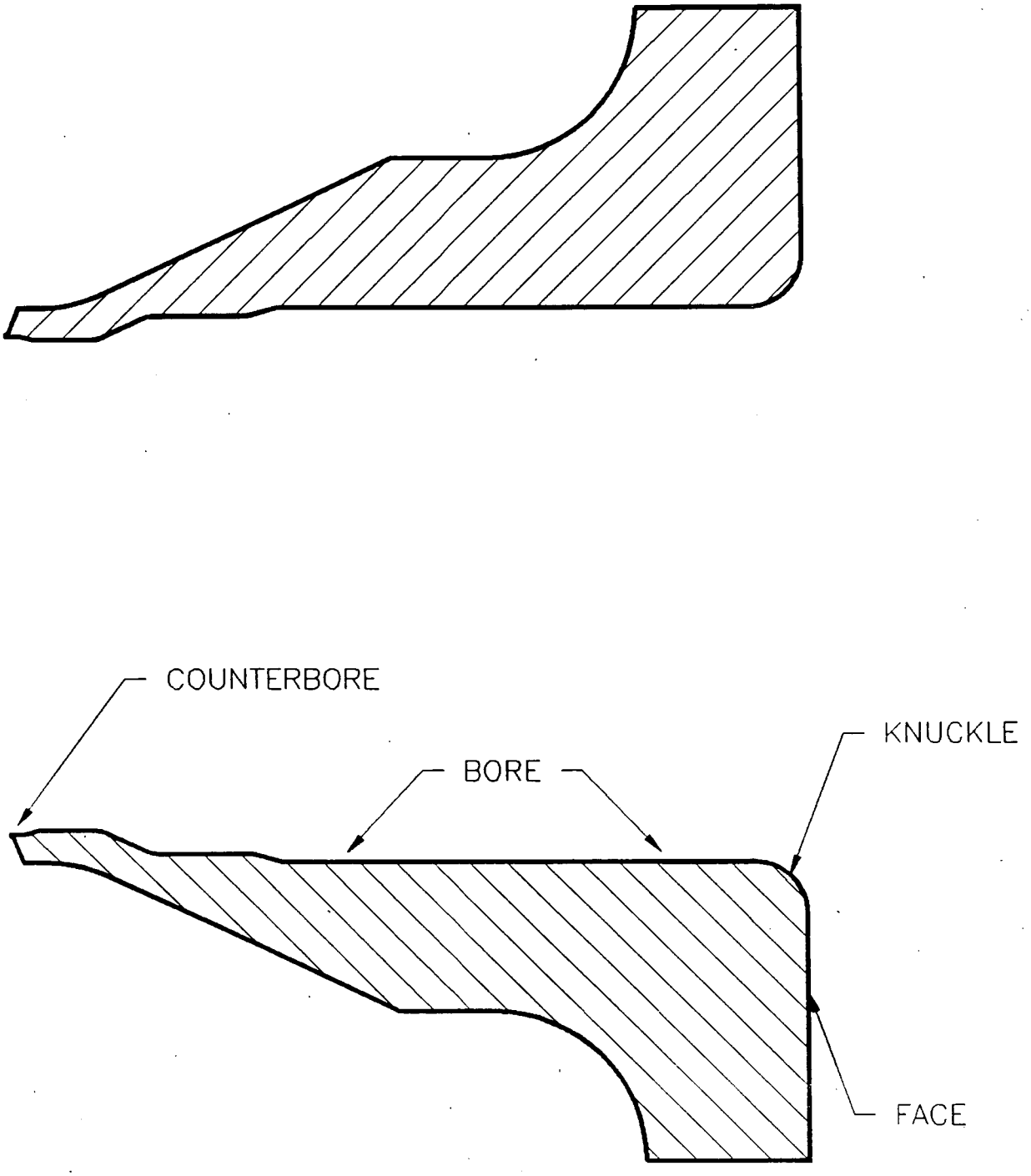

FIGURE 2.4

Feedwater Nozzle

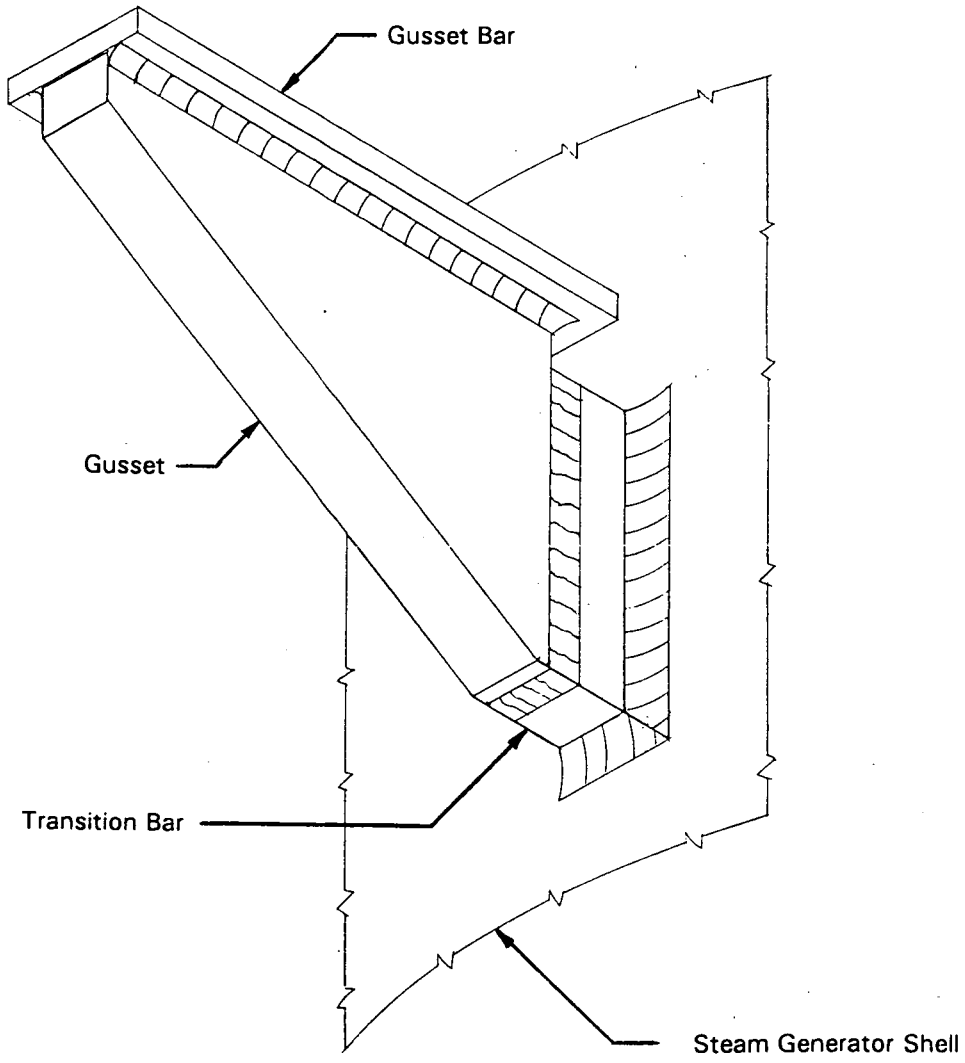

FIGURE 2.5

Feedring Support Bracket

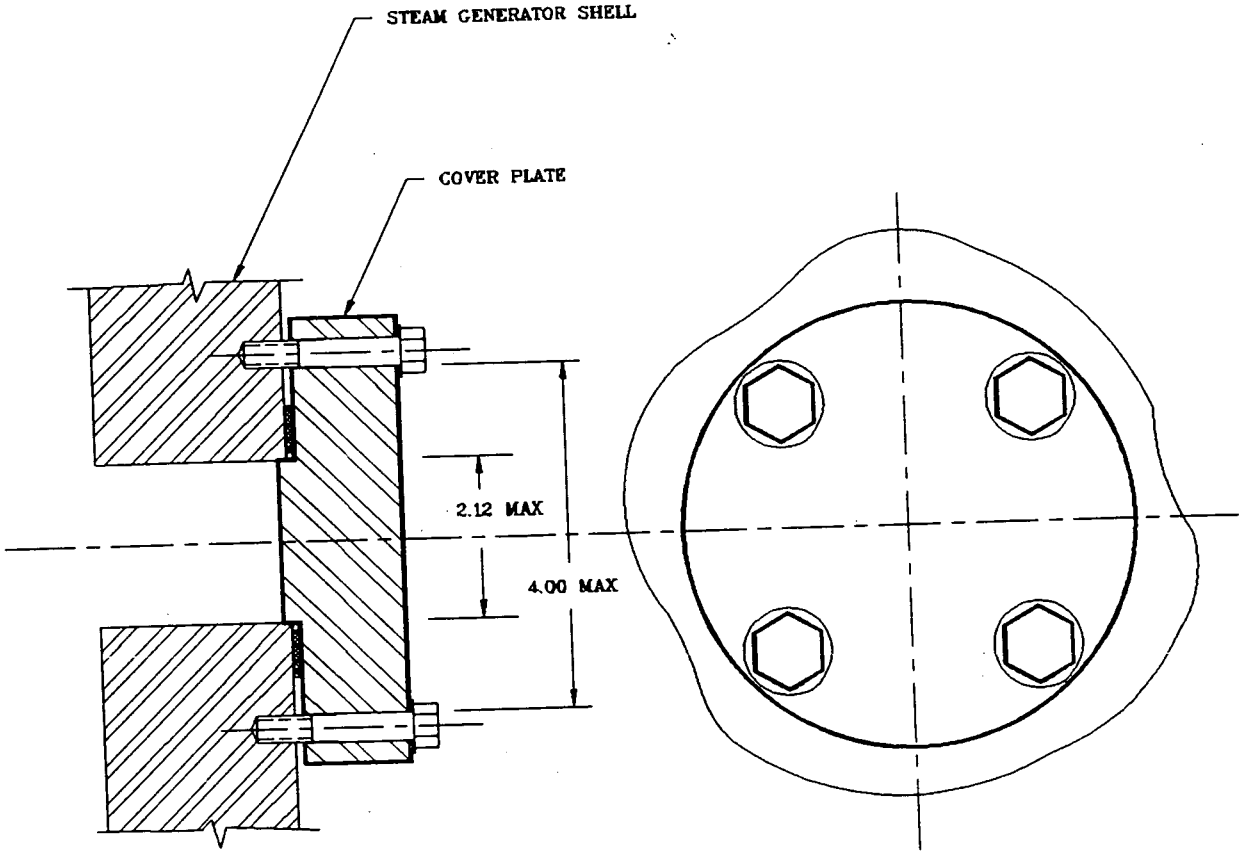

FIGURE 2.6

2 Inch Diameter Inspection Port Cover Plate Detail

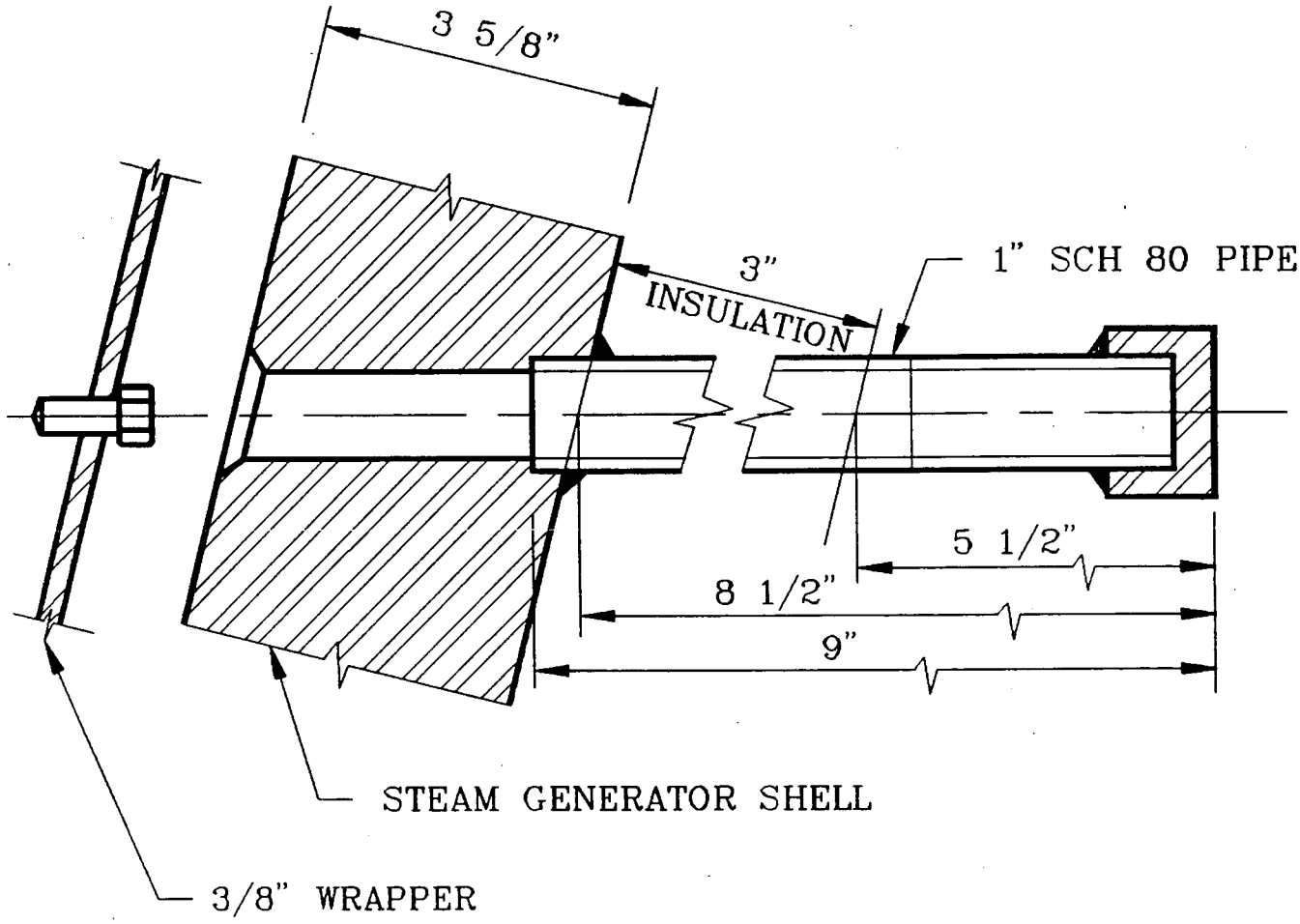

FIGURE 2.7

1 Inch Diameter Hillside Port

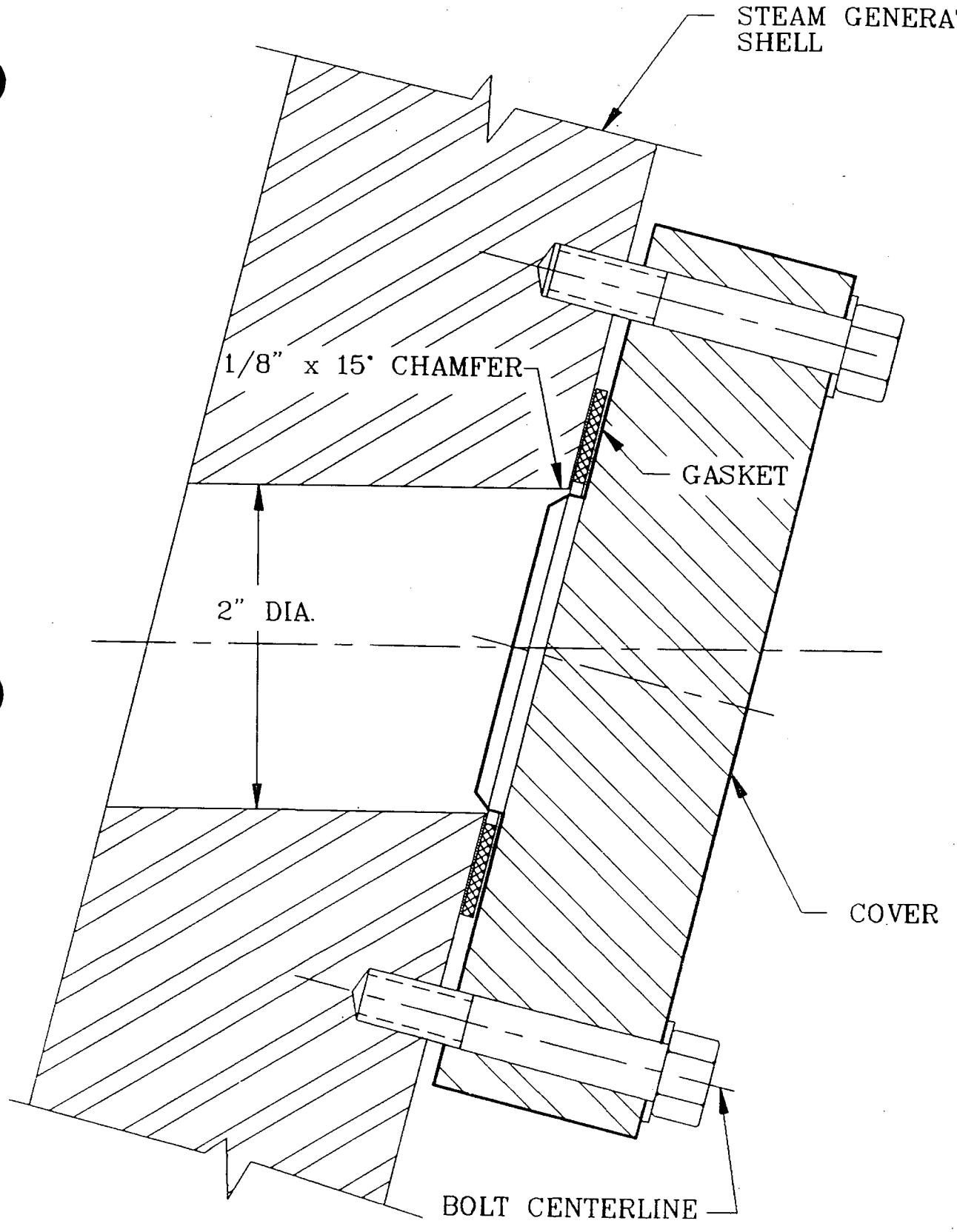

FIGURE 2.8

2 Inch Diameter Hillside Port Cover Detail

This page intentionally left blank.

3.0 METALLURGICAL EVALUATION

As part of the development of the root cause of the cracking phenomena, a number of cracks were removed as boat samples and analyzed. This section provides a description of the analyses performed on the boats and the results.

The objective of the analysis of the boat samples was to investigate the mechanisms of crack initiation and crack propagation in the girth weld and the nearby regions, and to provide insight into the root cause. The areas investigated include:

1) the crack initiation site and the extent of pitting present on the surface,

2) the presence of welds at the location of the cracks,

3) the path of the crack propagation and the degree to which the crack has the appearance of being active or inactive,

4) the characteristics of the fracture surface, and

5) the chemistry of the oxide on the fracture surface.

Nine boat samples containing eleven cracks were removed and analyzed. The boats were from Steam Generators 22 and 23. Two of the boat samples were from the girth weld and seven were from the region approximately 5 inches to 8 inches below the centerline of the girth weld. The location of the boat samples relative to the center line of the girth weld in Steam Generators 22 and 23 are shown in Figure 3.1. The cracks are identified by reference to the steam generator number, the zone number, and the crack number.

The following specific evaluations were performed on these boat samples:

1) Fractographic examination of the samples including optical and scanning electron microscopy to characterize the surface of the boat samples and the fracture surface.

2) Metallographic examinations of sections to observe and characterize crack growth details, microstructural details (weld, heat affected zone, etc.), and other aspects of each crack.

3) X-Ray Dispersion analysis for chemistry of fracture surface.

3.1 Analysis Procedures

The general procedure for analysis of each boat was similar. The following is a description of this procedure.

3.1.1 Macro-Analysis

Upon receipt of a boat sample, the boat surface was visually examined and then photographed using macro and/or stereo techniques. Special care was taken to determine the extent of surface pitting and the relation of the pits to the crack. The sides of the boat were then polished and etched to show microstructural detail. In some cases, the surface of the boat was ground to allow clearer definition of the crack geometry.

Based on the results of the preliminary analysis, a detailed cutting map was prepared to guide the more detailed analysis. The boats were then sectioned at

selected locations. From these sections, samples for metallography, fractography, hardness testing, and chemical analysis were prepared. Detailed maps of each cut surface were prepared.

3.1.2 Micro-Analysis

Boat samples were analyzed using optical and scanning electron microscopy. In addition, hardness measurements were made to identify heat affected zones. Chemical analyses using X-ray techniques were made at locations of hardness measurements.

3.1.3 Fractographic Analysis

Selected samples were sectioned to expose crack surfaces for analysis of fracture features. These samples were gold coated and analyzed using the Scanning Electron Microscope (SEM). Chemical analyses of the fracture surfaces using X-Ray dispersion were also performed. The corrosion product on the surface of the fracture surfaces was evaluated to determine if copper was present.

3.2 Summary of Boat Analysis

The key observations and similarities between the boats are as follows:

1) All the boats removed were found to be at locations of welds. These welds were either at the girth weld or at temporary fabrication or repair weld remnants below the girth weld. Some of the boats were removed because it could not be specifically verified by an in-plant etch that a weld was present - all other cracks were verified to be at locations of welds. In one boat sample, it could not be specifically verified that a weld

was present since the sample had been heavily ground prior to removal. The probable weld and heat affected zone had been removed by grinding.

Photographs from boat samples showing the proximity of welds and cracks are shown in Figures 3.2 and 3.3. No cracks in or near the girth weld have been found to have initiated in base material.

2) All cracks initiated at pits. A clear example of this is in the boat shown in Figure 3.4. The surface of this boat was progressively ground to allow the observation of cracks in the initiation phase which were not evident during in-plant inspection nor identified by surface examination in the laboratory. Microcracks forming at the boundaries of the pits were detected as seen in Figure 3.4. Figure 3.5 and 3.6 also show clear evidence of surface pitting and crack initiation at the pits.

3) There was evidence in several boat samples of crack tip blunting. This was most evident in Figure 3.7, in which the crack tip was wide and blunt. Other cracks showed evidence of crack deceleration - see Figure 3.8. Some of the cracks had very tight crack tips suggesting continuing crack growth.

4) Two different crack growth characteristics were seen. In one case, the crack grew straight down into the boat and in the other the crack turned to follow the heat affected zone of the weld. These two conditions are shown in Figure 3.9 and Figure 3.10 respectively.

Each of these cracks began growing in a direction perpendicular to the maximum stress direction, but the difference in crack behavior was a result of different stress states. The residual tensile stress between the boundary of the weld and the heat affected zone was so great in the first case, Figure 3.9, that the crack followed this maximum tensile stress region and did not leave the heat affected zone. In the second case, Figure 3.10, with the crack growing straight into the shell, the stresses were more balanced and the resultant stress direction was parallel to the surface of the boat. In several boats, the crack growth behavior was as shown in Figure 3.11; cracks grew straight into the boat, but lateral cracks started to form at the boundary between the weld and the heat affected zone, indicating the presence of a "secondary" residual stress field. This stress was not large enough to overcome the balanced stress driving the crack into the boat.

5) Copper was found on the fracture surfaces of several of the boat samples. Copper appeared as elemental copper and as copper sulfide. The copper was detected in globules and discrete particles. Figures 3.12 and 3.13 show examples of elemental copper particles and copper sulfide particles.

6) The mechanism of cracking is predominantly stress corrosion. There are some signs of differing crack growth rates in several of the boats, as seen, for example, in Figure 3.14, but these do not appear to be due to mechanical fatigue loadings. The differing rates of crack growth

could be caused by chemistry or oxygen changes or plant operating mode changes.

3.3 Conclusions of Boat Analysis

The boat analysis provided important information about the mechanism of cracking. Two primary conclusions are drawn from the evaluation, one regarding residual stresses and the other regarding pitting. Both of these conclusions are utilized in the definition of the repair to prevent cracking.

1) Residual stresses from the welds contributed to the crack growth. The direction of crack growth was affected by the residual stress fields. Since the original girth weld post weld heat treatment was performed at lower temperatures than optimum, residual stresses from the welding process remain and contribute to the cracking. In regions away from the welds and the residual stress fields, cracks did not form.

   An effective heat treatment that significantly reduces residual stresses will reduce the initiation of cracks in the material, particularly at the location of pits.

2) Pits provided locations for crack initiation. These boat samples confirm that crack initiation was linked to pitting. The pits provided both amplified stresses and localized chemistry concentration. Reducing the formation of pits will assist in preventing the initiation of cracks.

STEAM GENERATOR 22

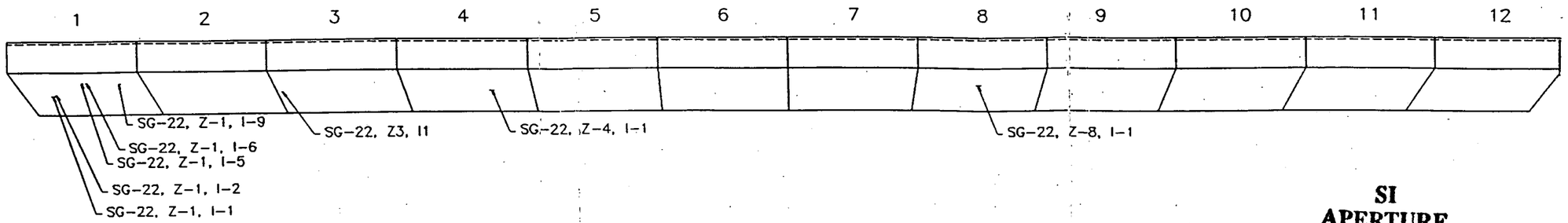

STEAM GENERATOR 23

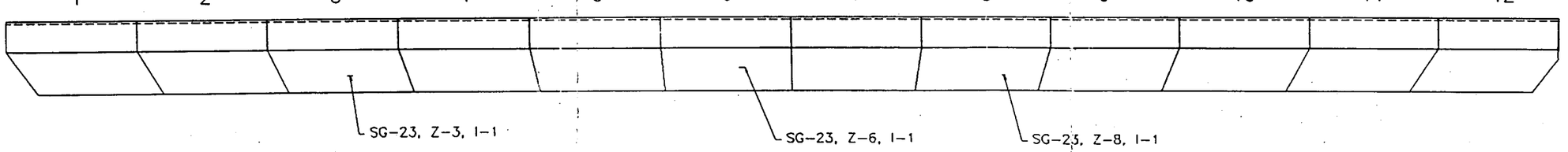

FIGURE 3.1

The Location of the Boat Samples
Relative to the Center Line of the Girth Weld
in Steam Generators 22 and 23

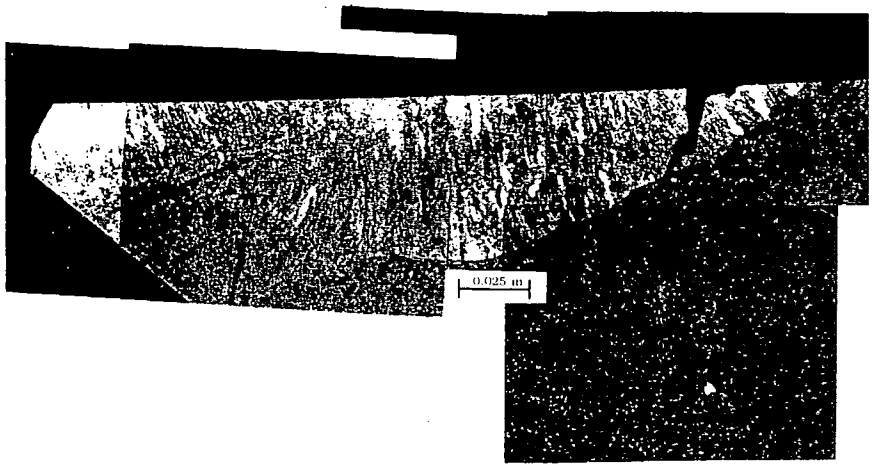

FIGURE 3.2

Section Through Crack Showing Weld and Heat Affected Zone
(Boat From Steam Generator 22, Zone 1, Indications 5 & 6)

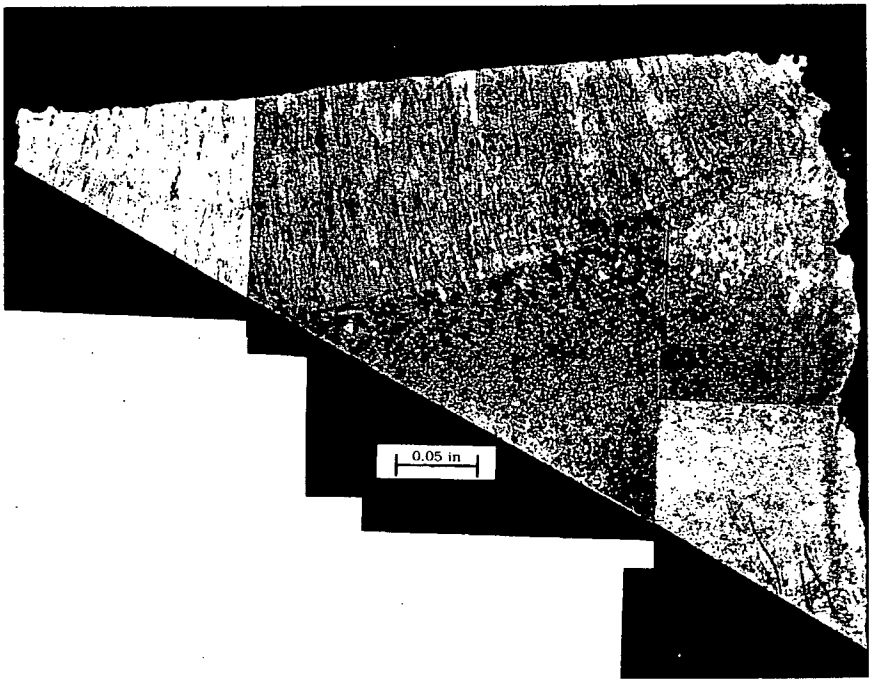

FIGURE 3.3

Section Through Crack Showing Proximity of Crack
to Two Weld Passes and Heat Affected Zones -
Crack is at the Right Hand Side of the Sample
(Boat From Steam Generator 22, Zone 1, Indication 9)

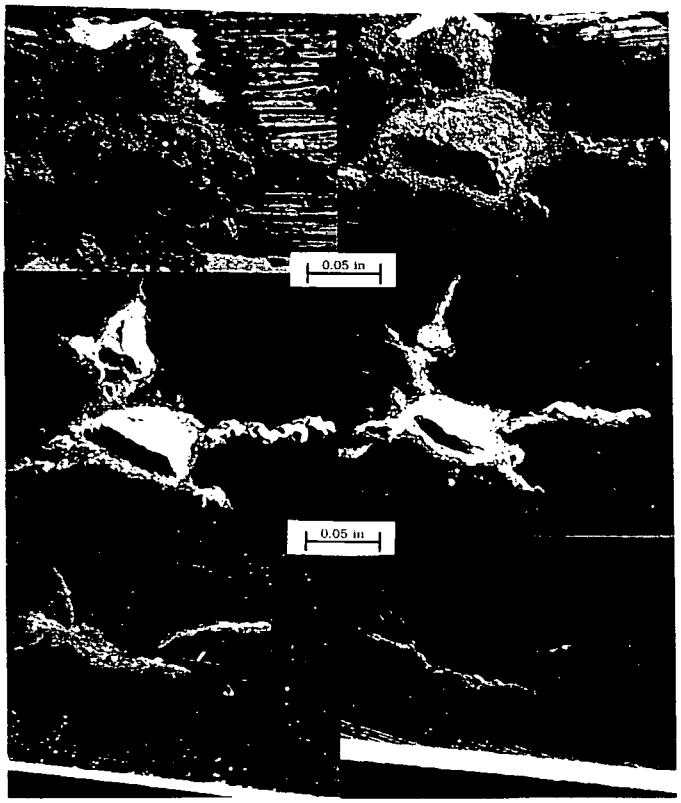

FIGURE 3.4

Photographs Showing Grinding Sequence for Pit and Crack Characterization. Grinding Sequence is Upper Left, Upper Right, Middle Left, Middle Right, Lower Left, Lower Right. Grind Increments are 0.012", 0.013", 0.005", 0.010", and 0.010" (Boat From Steam Generator 22, Zone 1, Indications 5 & 6)

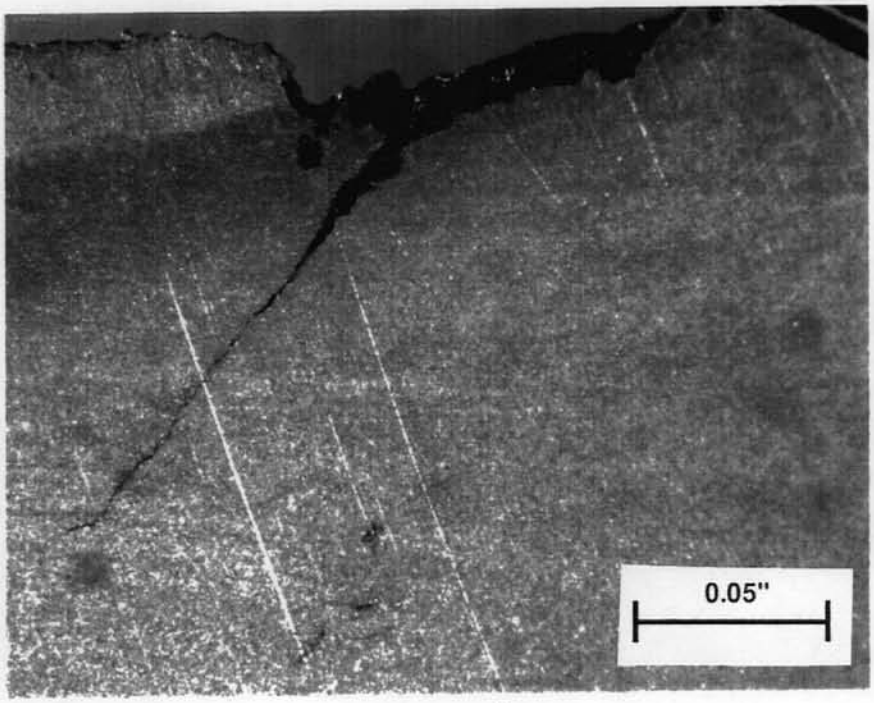

FIGURE 3.5

Section Through Crack Showing Pit Initiation Site
(Boat From Steam Generator 22, Zone 1, Indications 5 & 6)

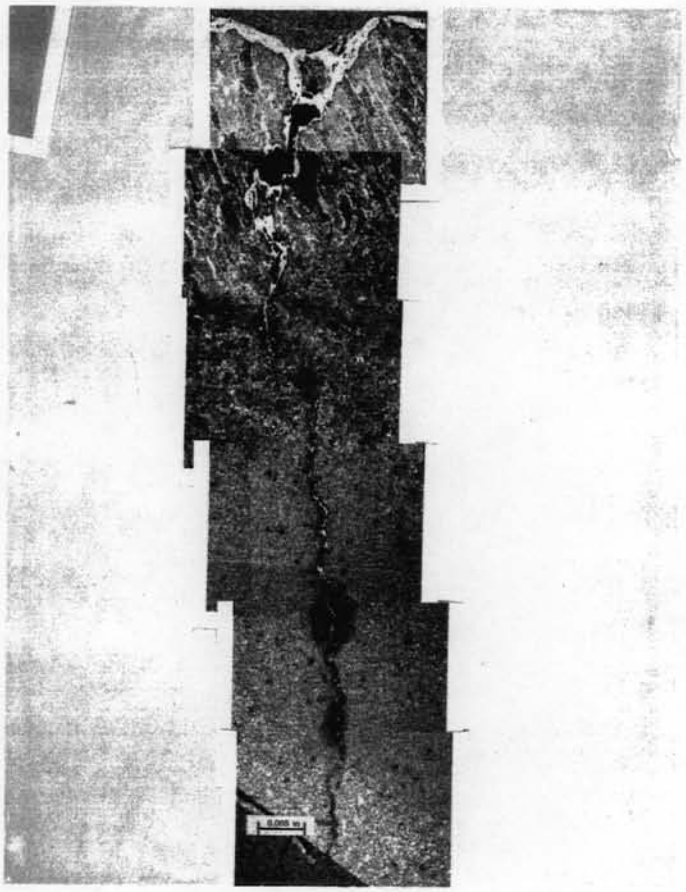

FIGURE 3.6

Section Through Crack Showing Pit Initiation Location
(Boat From Steam Generator 22, Zone 1, Indication 9)

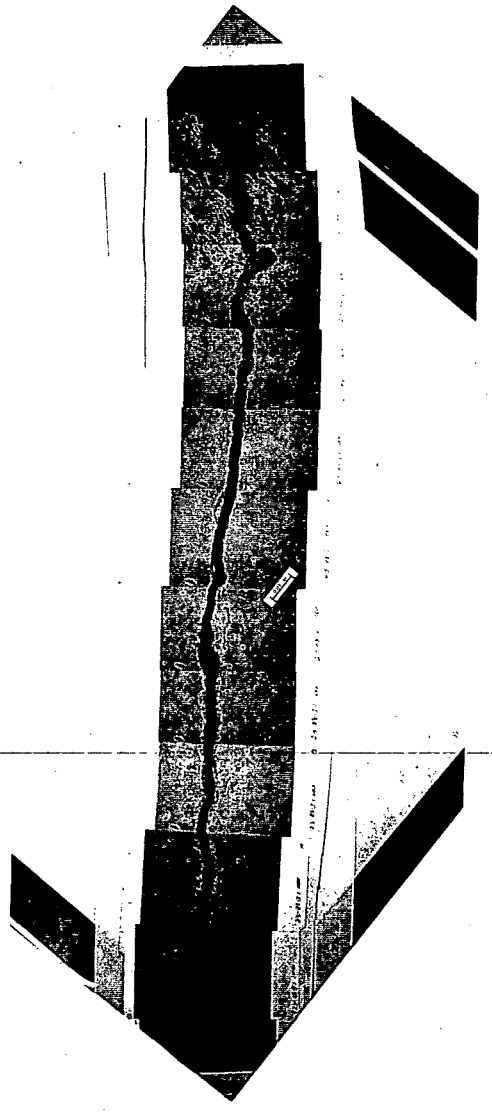

FIGURE 3.7

Section Through Crack. Note Weld at
Initiation Site and Crack Tip Blunting
(Boat From Steam Generator 23, Zone 8, Indication 1)

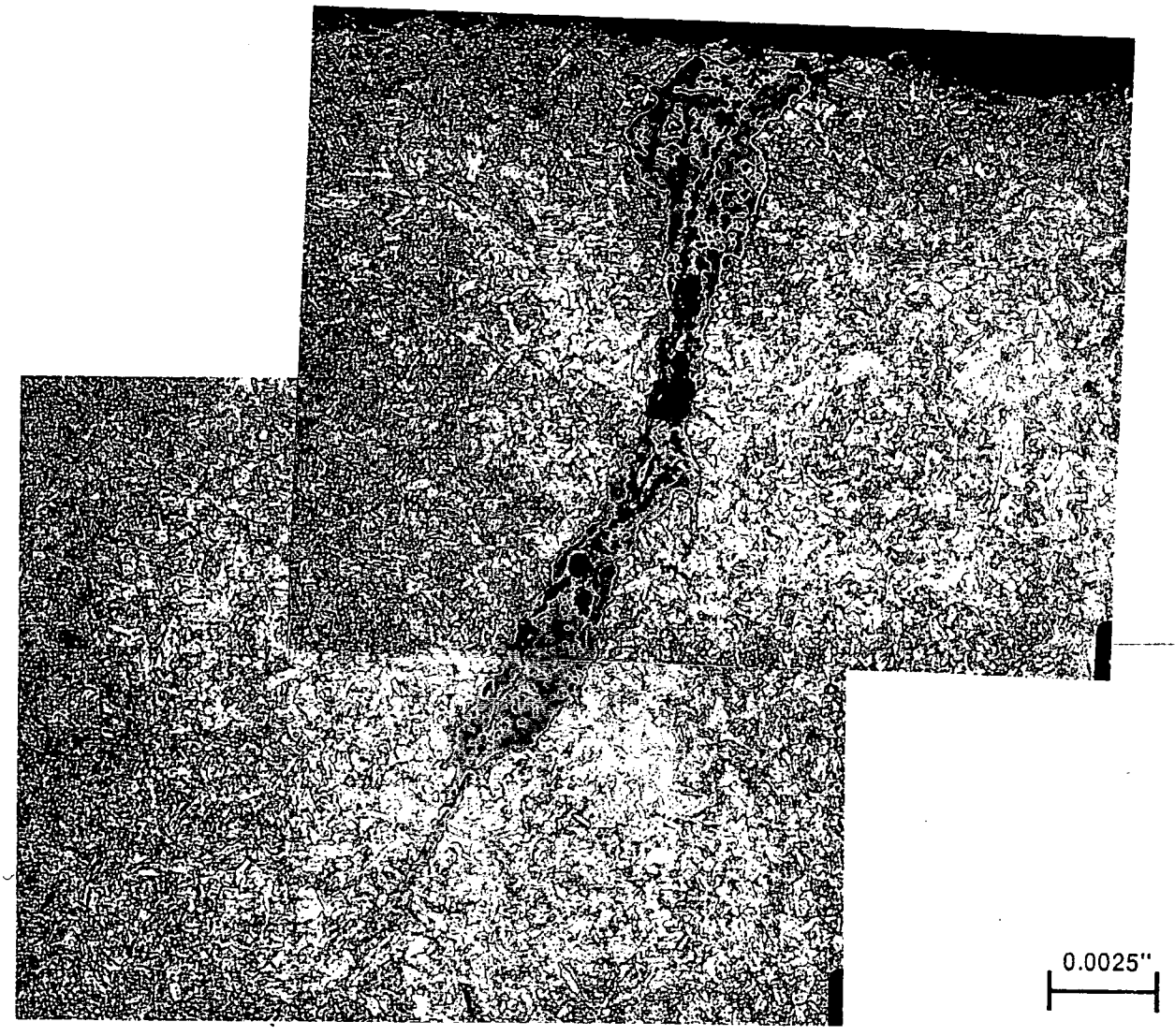

FIGURE 3.8

Section Through Crack
Showing Blunting at Crack Tip
(Boat From Steam Generator 22, Zone 1, Indication 2)

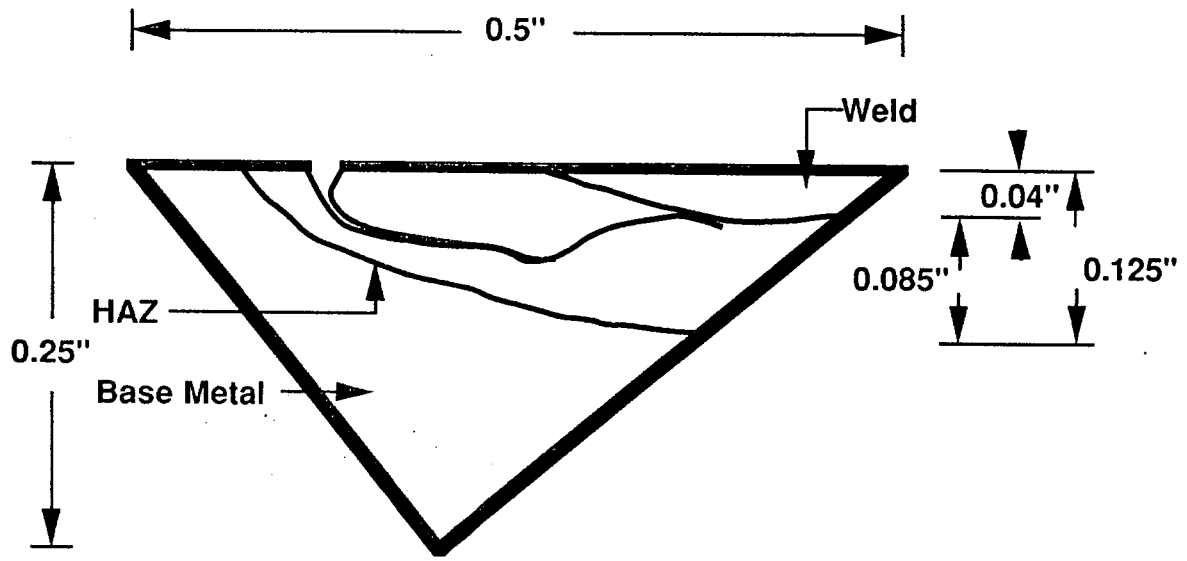

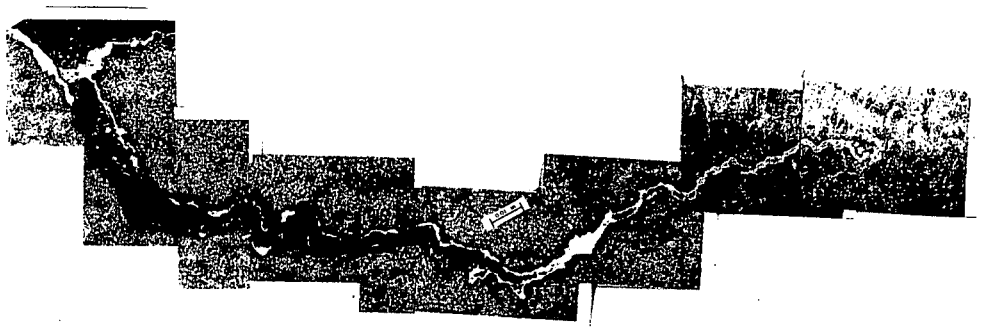

FIGURE 3.9

Section Perpendicular to Crack Plane
Showing Initiation, Turning of Crack to Follow HAZ,
and Intersection With Weld Region
(Boat From Steam Generator 23, Zone 6, Indication 1)

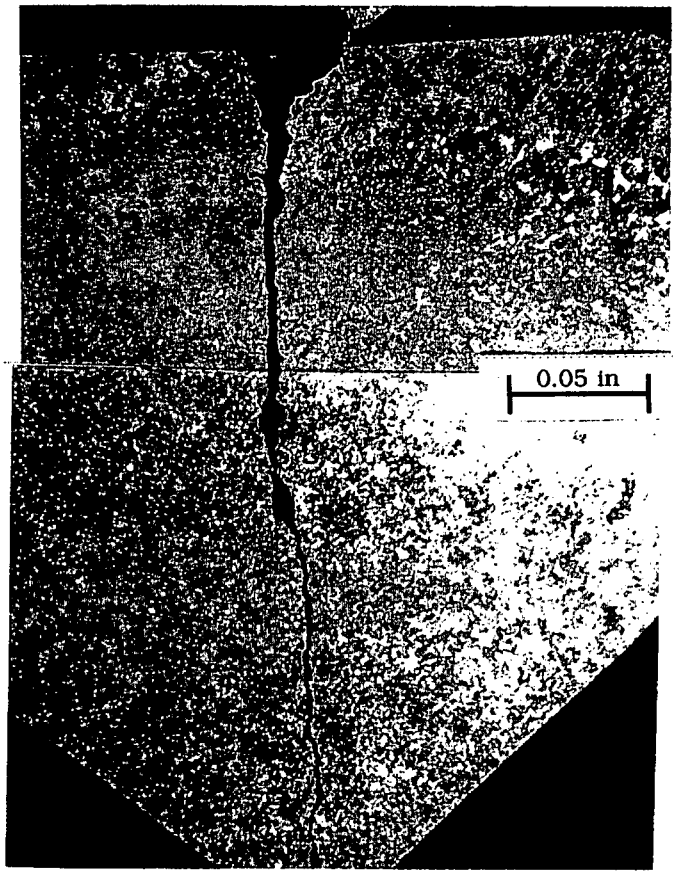

FIGURE 3.10

Etched Section Through Crack to Show Crack Morphology and Weld/Heat Affected Zone. This Crack Formed Near Two Weld Passes and Grew Straight Into the Shell (Boat From Steam Generator 22, Zone 4, Indication 1)

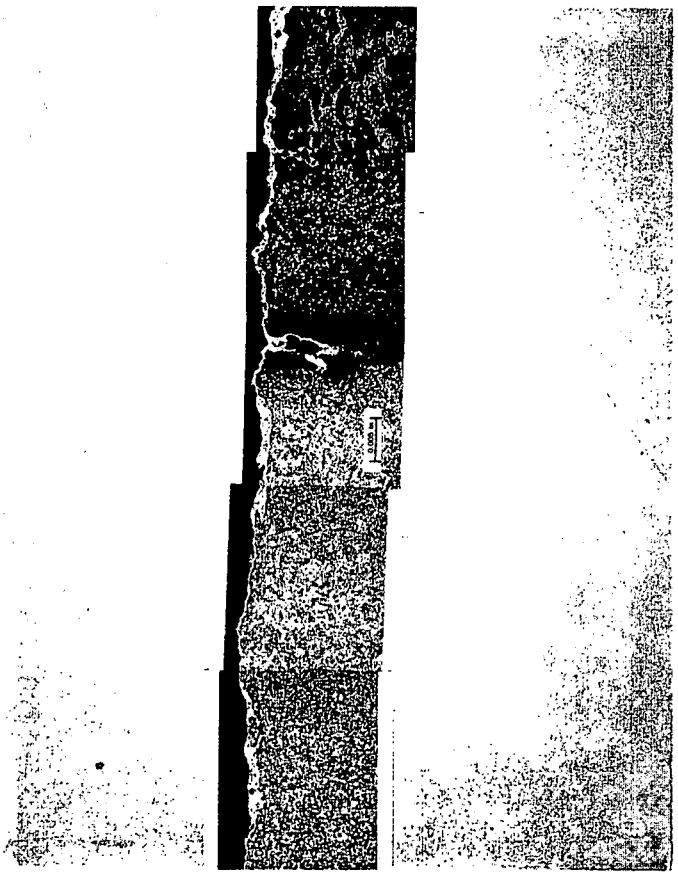

FIGURE 3.11

Section Through Crack Edge. Note Lateral Cracks at Boundary Between the Weld and Heat Affected Zone and Between Heat Affected Zone and Base Metal (Boat From Steam Generator 22, Zone 4, Indication 1)

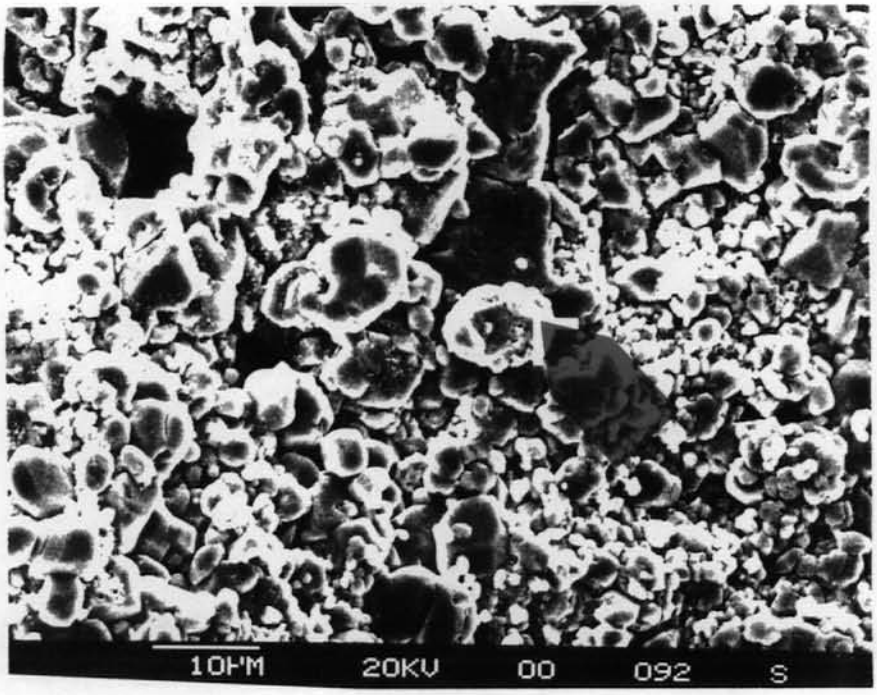

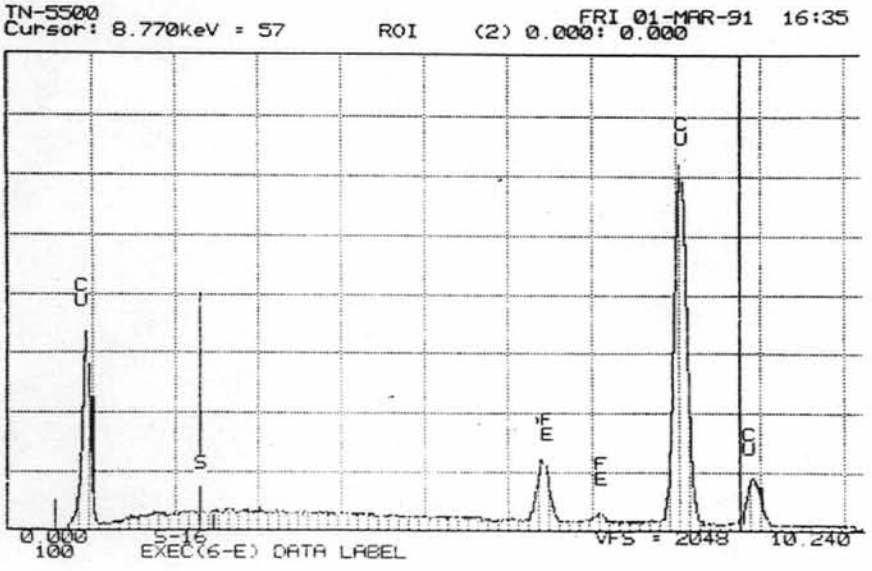

FIGURE 3.12

Fracture Surface Showing Morphology of Copper Particle, and X-Ray Spectra for the Copper Particle (Boat From Steam Generator 22, Zone 1, Indication 9)

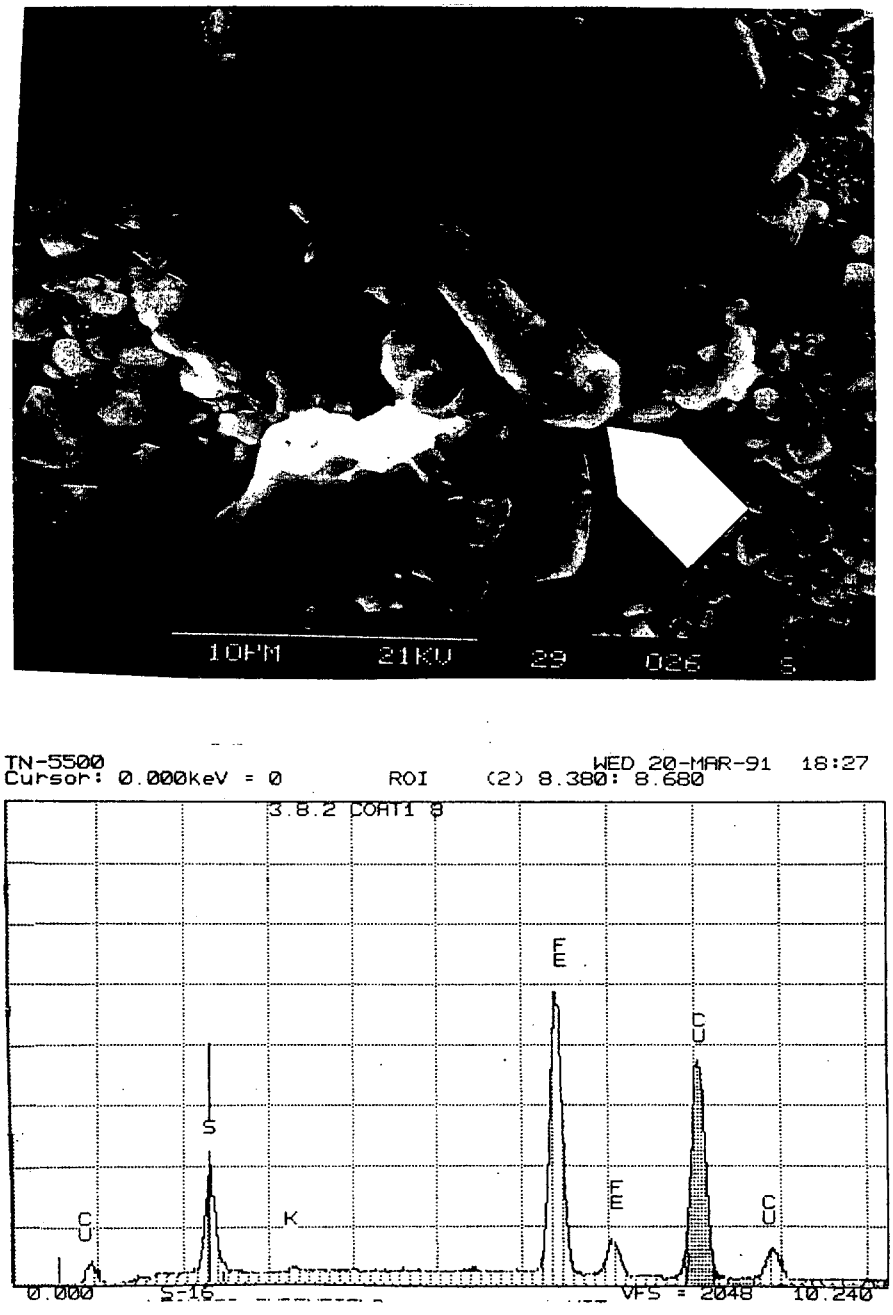

FIGURE 3.13

Fracture Showing Morphology of Copper Sulfide Particle, and X-Ray Spectra for the Copper Sulfide Particle (Boat From Steam Generator 22, Zone 1, Indications 5 & 6)

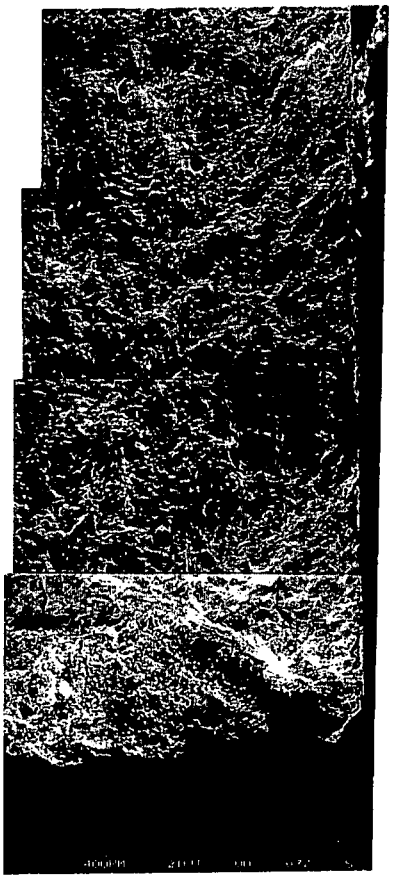

FIGURE 3.14

Fracture Surface Showing Initiation Site
at the Bottom of the Photo and a Location of
Crack Growth Rate Change Near the Top
(Boat From Steam Generator 22, Zone 1, Indication 9)

4.0 PITTING TESTS

4.1 Introduction and Objectives

As was discussed in Section 3.0, the girth weld cracking involved initiation and propagation of stress corrosion cracks. All of the observed cracks initiated from pits; consequently, it was essential that the pitting process be characterized as to (1) the source, (2) the key controlling variables, and (3) the appropriate mitigating actions. A pitting program was designed and implemented to address the issue of pitting in the Indian Point Unit 2 steam generators.

4.2 Background

The effect of environment on cracking is in some respects well characterized from efforts underway to characterize environmentally assisted cracking (EAC) in pressure vessel steels for PWR and BWR systems in high purity water. However, the situation is more complex on the secondary side of the steam generator due to a more undefined, varied and potentially more aggressive environment.

As with virtually all forms of EAC, the phenomena requires the simultaneous presence of (1) a tensile stress, (2) an aggressive environment, and (3) a susceptible material. Tensile stresses can be provided by the general operating stress, thermal transients, residual stresses from welds, or stress concentrations due to geometric discontinuities. The environment in the steam generator is one with variable oxygen (ppb - ppm range), temperature range of 25 - 290°C, and various levels of contaminants that include copper, chloride, sulphur, and other impurities. The material, low alloy steel, has been shown to be susceptible to EAC in these environments.

There is ample evidence that the electrochemical potential (ECP) is the unifying variable in the environment. Pitting occurs for potentials above a fairly well defined "pitting potential". In the steam generator environment the ECP is dominated by the oxygen concentration in a clean system but can be influenced by ionic impurities, especially copper, chloride and sulphur ions. Copper is often present as a result of corrosion of materials in the feed train. Chloride ions may result from condenser leaks. Sulphur is present because of in-leakage and dissolution of inclusions in the steel itself. Consideration of the levels of copper, chlorides, and sulphur in the secondary water environment has lead to the conclusion that oxygen is the primary variable which controls the ECP.

While the key variables appear to be identified, the details of the process and their combined role in initiation and propagation are much less clear. For example, it is likely that pitting initiated during hot standby or startup conditions where temperatures are lower and/or the oxygen concentration is higher and that crack propagation occurs at operating conditions. It has also been assumed that the temperature and oxygen concentration dependence of the pit initiation process is related to the nature of the surface oxide film.

Little is known about the details of the transition from pit to crack or the initiation of a crack from a pit. However, it has been shown that, in some cases, the pits blunt and cracks do not initiate. In other cases, pit blunting does not occur and cracks initiate. It is well known that the pit environment can be different, and more aggressive, than the bulk environment. Sulfide dissolution is thought to play a critical role in not only pit chemistry, but in crack propagation in pressure vessel steels. While it is fairly well established that pitting

can be suppressed if the ECP is maintained below the pitting potential, its exact value in the steam generator environment is unknown. The objective of the Pitting Test Program was to determine the appropriate means to reduce the ECP to a level that is below the pitting potential, knowing that the elimination of pitting should greatly reduce the incidence of cracking.

4.3 Test Program

As discussed above, the test program was designed to characterize the pitting behavior of the steam generator shell material and to make recommendations as to the appropriate course of action to minimize future pitting in the steam generators. To accomplish these goals the pitting program had the following major tasks:

1. To determine the electrochemical potential (ECP) as a function of temperature and oxygen concentration.

2. To determine the pitting susceptibility of the steam generator shell material as a function of temperature, pH, oxygen level, and surface condition.

4.3.1 Materials

The materials used in the test program were as follows:

1. A302 Grade B plate material fabricated by Lukens Steel at approximately the same time that the Indian Point Unit 2 plate was fabricated.

2. Peened samples with two degrees of peening.

3. Samples coated with several nickel based coating materials.

Samples were cut from these materials for testing.

4.3.2 Program Variables

The test program variables were as follows:

Temperatures:	25, 175, 250°C
pH:	7, 9
Oxygen Concentration:	50, 100, 150, 300, 7000 ppb
Surface Finish:	3μm, 60 grit SiC, Mild Peen, Severe Peen

4.3.3 Test Facilities and Procedures

4.3.3.1 Pitting Tests

Pitting tests were conducted in a glass cell for room temperature tests, and in a titanium autoclave system for elevated temperature tests. Electrochemical potential (ECP) was monitored using a saturated KCl reference electrode at room temperature and a Ag/AgCl reference electrode at elevated temperatures.

Samples for testing were prepared in accordance with the desired surface finish and then cleaned with acetone prior to insertion into the test facility. A minimum of three samples were run per condition. After insertion in the test chamber, the testing sequence was as illustrated in Figure 4.1 and described below.

The initial conditions were first established using a low oxygen environment (<5 ppb O_2) by purging with hydrogen gas. The ECP and temperature were continuously monitored during this period to verify the initial conditions. After the initial, low oxygen condition was established, the temperature was adjusted to the desired test temperature. After temperature adjustment, the test oxygen concentration was adjusted. The test was then run for the desired period (50 hours in all tests except one 1000 hour test). At the end of the test period, the oxygen concentration was reduced to less than 5 ppb prior to cool down.

This procedure provided assurance that the test startup and shutdown periods would not influence the pitting behavior of the material and complicate data interpretation. Temperature and ECP were monitored continuously during all tests. Figure 4.2 shows a typical ECP and Temperature versus Time record for a test.

After testing, samples were removed from the autoclave or cell and examined for pitting. Optical and/or scanning electron microscopy techniques were used. EDX analysis was conducted for identification of inclusion chemistry.

4.3.3.2 Chemistry Control and Monitoring

As discussed above, the primary chemistry/environmental variables for the program were temperature, oxygen concentration, and pH. These variables were monitored continuously during testing. In addition, the ECP was also monitored during each test.

The water chemistry was established by starting with distilled and demineralized water. Desired pH adjustments were made with ammonium hydroxide and the oxygen

concentration was established by bubbling the makeup tank with selected oxygen/argon gas mixtures.

Water purity was verified using ion chromatography. Ions analyzed for were Cl^-, SO_4^-, Na^+, and Cu^{2+}. The pH, conductivity and oxygen concentration were continuously monitored at the effluent of the autoclave using Beckman pH, conductivity, and oxygen monitors.

4.3.3.3 Potential versus Oxygen Measurements

The potential versus oxygen relationship for the shell material was evaluated over the oxygen range 1 to 800 ppb at a temperature of 175°C. Test conditions were established as discussed above after which the oxygen concentration was adjusted by changing the gas mixture used to bubble the makeup tank. The oxygen concentration in the tank was allowed to stabilize at the new equilibrium value and the ECP monitored. When the ECP and oxygen concentration were steady, the ECP was recorded.

4.3.3.4 Potential versus Temperature Measurements

The relationship between potential of the shell material and temperature was determined in 50 ppb oxygen water at pH 9.

4.4 Results

4.4.1 Potential versus Oxygen and Temperature

Figure 4.3 shows the relationship between ECP and oxygen concentration at 175°C. Figure 4.4 shows the ECP versus temperature relationship.

4.4.2 Pitting Tests

4.4.2.1 Microstructural Characterization

The A302 Grade B plate material was characterized using optical, SEM and EDX for inclusion chemistry. Figure 4.5 shows the as-polished, unetched surface that was typical of the material. The plate rolling direction is from left to right as the stringer elongation indicates. Figures 4.6 and 4.7 show the same orientation in the etched condition (2% nital) at two magnifications. The microstructure is typical of a quenched and tempered material.

Figures 4.8 to 4.12 show the results of the chemical characterization of the inclusions using the SEM and EDX. Figure 4.8 shows an SEM micrograph of an inclusion in the etched condition. Figures 4.9 and 4.10 show X-ray dot maps for aluminum and sulphur respectively. Figures 4.11 and 4.12 show X-ray spot analysis results for the aluminum and sulphur rich inclusions. It is clear from this analysis that the inclusions are a mixture of MnS and aluminum oxide.

4.4.2.2 Pre-Test Characterization

Figure 4.13 shows the surface of a typical 3μm ground specimen. The specimens were ground using a diamond compound in order to produce the required finish without contamination of the surface with grinding compound. The particles shown in Figure 4.13 were analyzed in the SEM and shown to be MnS inclusions.

4.4.2.3 Post-Test Characterization

Table 4.1 shows the results of the 50 hour tests in the pitting program. As the data shows, an oxygen

concentration of 100 ppb would appear to be the concentration above which pitting occurs. This threshold was verified by conducting a 1000 hour test at 175°C and 100 ppb O_2 concentration. This long duration test resulted in no pitting.

High Oxygen Results

Figures 4.14 to 4.21 show the results of Test #HT-1 (250°C, pH 9, 300 ppb O_2). This test was typical of all of the tests with oxygen concentrations of 150 ppb or higher. Figure 4.14 shows the samples after the 50 hour exposure. Samples were suspended in the autoclave using steel wire which was sheathed with teflon tubing and shrunk on to eliminate any galvanic effects due to the connection. The specimen at the upper right is a 3μm finish sample while the sample immediately below is a 60 grit finish sample. The surface was characterized by a soft oxide and pits. Figure 4.15 shows an SEM micrograph of the surface that was typical of the 3μm samples after exposure. In general, the finer finish samples showed a lower density of pits than the coarse finish samples. The pits are evident. Figures 4.16 and 4.17 show micrographs of a sample that was sectioned normal to the exposed surface. Figure 4.16, in the unetched condition, shows the nature of the pitting. Figure 4.17 shows the same region in the etched condition.

Figure 4.18 shows the severely peened sample, and Figure 4.19 shows the mildly peened sample. In general, the peened surfaces showed a higher density of pits than the un-peened surfaces.

Figures 4.20 and 4.21 show a "coated surface" sample. Figure 4.20 shows a macro-photo of the as-tested sample. The upper half of the sample had been plasma sprayed while the lower half had not. Figure 4.21 shows a higher

magnification photograph of the interface between the sprayed and un-sprayed regions. The interface region shows extensive local corrosion due to the galvanic couple between the more noble coating and the steel surface. The low conductivity of the environment acts to aggravate the localization of the corrosion.

Low Oxygen Results

Figures 4.22 to 4.27 show results of Test #HT-3 (175°C, pH 9, 50 ppb O_2). This test was typical of all of the tests with oxygen concentrations below 150 ppb. There was no noticeable difference between the 250°C and the 175°C test results. Figure 4.22 shows the samples after testing. The surface was characterized by a thin dark oxide as opposed to the lighter colored and thicker oxide on the high oxygen samples. Figure 4.23 shows an SEM micrograph of a typical surface. While it was possible to find regions where inclusions had fallen, or were dissolved out of position, the density of these regions was at least a factor of 100 lower that in the high oxygen environment. There was no corrosion noted.

Figures 4.24 and 4.25 show the surfaces of the peened samples. As the photographs show, when compared with the high oxygen environment, the surface oxide is thin and adherent with little evidence of localized corrosion.

Figures 4.26 and 4.27 show the coated sample. Due to the galvanic couple between the more noble coating and the steel surface and despite the lower oxygen level, the interface region shows similar localized corrosion to that present in the high oxygen environment.

4.5 Conclusions from Pitting Program

The pitting program provides the following conclusions:

1. Pitting can be minimized if the oxygen concentration is maintained at 100 ppb or less.

2. Peening of surfaces does not help and appears to increase the susceptibility to pitting.

3. Coating of the surface to eliminate pitting will result in localized corrosion at the coating/base metal interface that is potentially a more serious problem than the pitting.

4. A fine surface finish has fewer pits than a coarse surface finish.

Test ID#	Temp. (°C)	pH	O_2(ppb)	Pitting
HT-1	250	9	300	Y
HT-2	175	9	300	Y
HT-3	175	9	50	N
HT-4	175	7	50	N
HT-5	175	9	50	N
HT-6	175	9	150	Y
HT-7	175	9	100	N
RT-1	25	9	300	Y
RT-2	25	9	150	Y
RT-3	25	9	50	N
RT-4	25	7	300	Y
RT-5	25	7	150	Y
RT-6	25	7	50	N
RT-7	25	7	7000	Y

TABLE 4.1

Pitting Test Results
All Tests Performed for 50 Hours

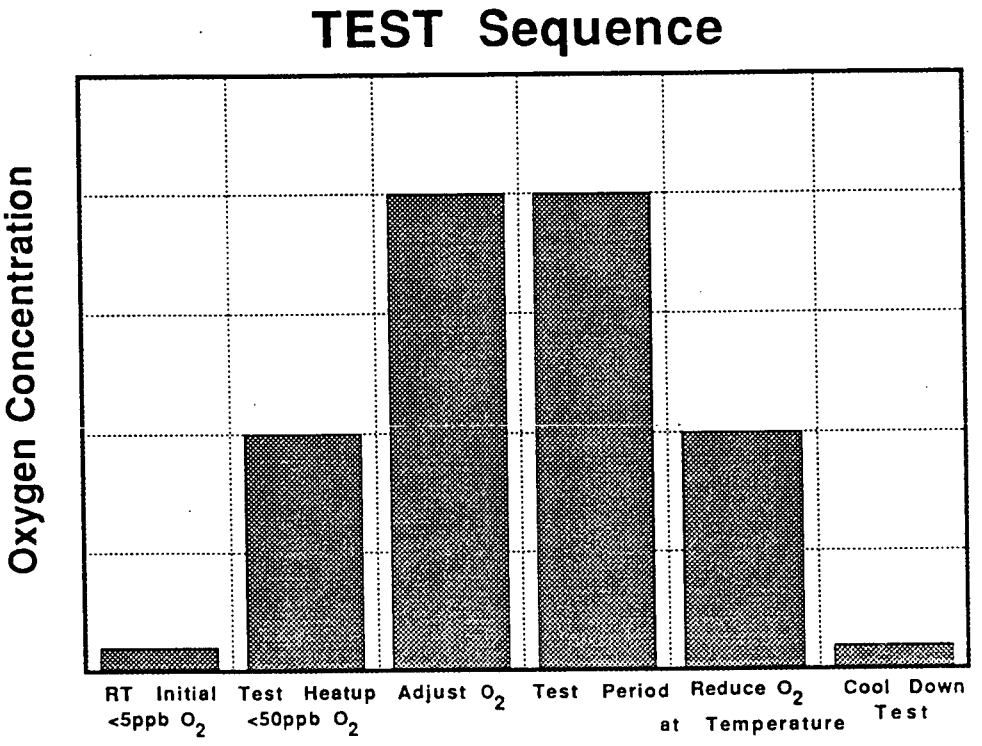

FIGURE 4.1

Pitting Test Experimental Sequence

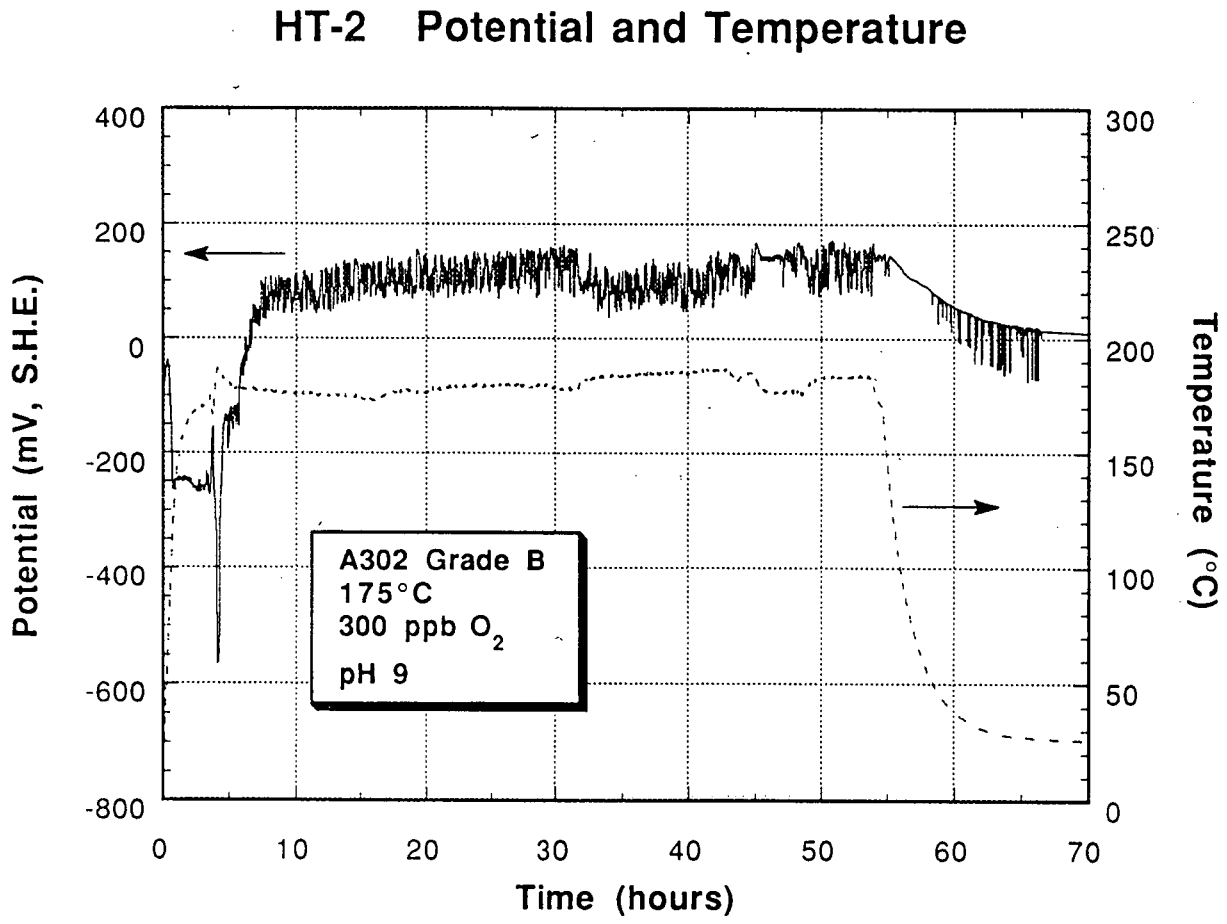

FIGURE 4.2

Potential and Temperature Variation with Time During Test HT-2

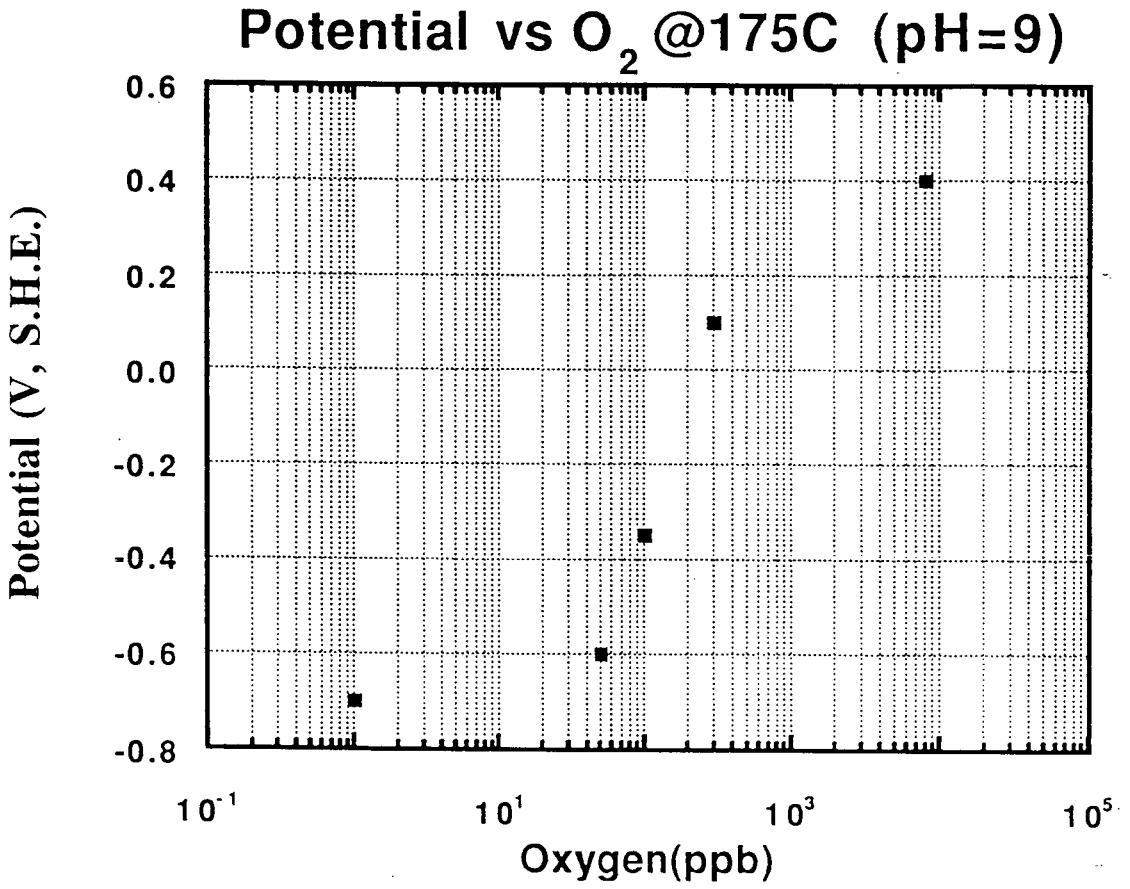

FIGURE 4.3

Electrochemical Potential vs. Oxygen Concentration of A302B Steam Generator Shell Material at 175°C, pH 9

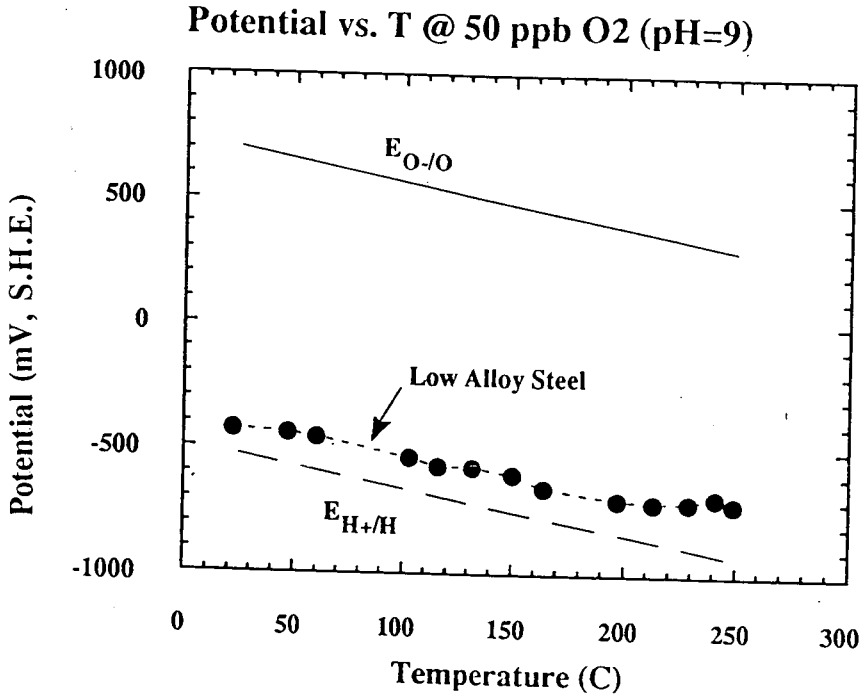

FIGURE 4.4

Electrochemical Potential vs. Temperature for A302B Steam Generator Shell Material at 50 ppb O_2 and pH 9

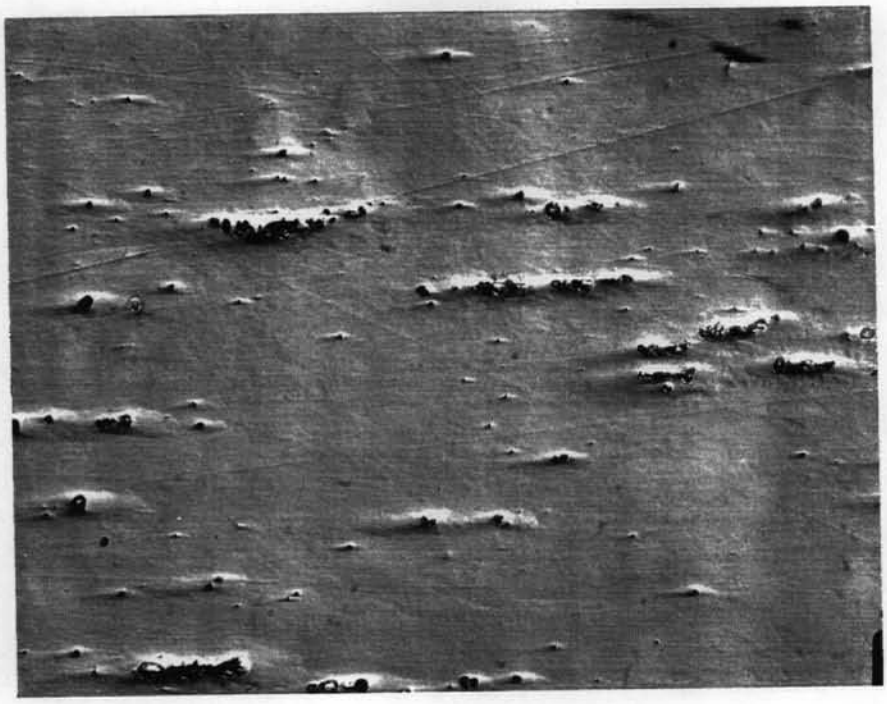

FIGURE 4.5

As-Polished Surface of A302B Steel Surface
Showing Orientation of Inclusions (200X)

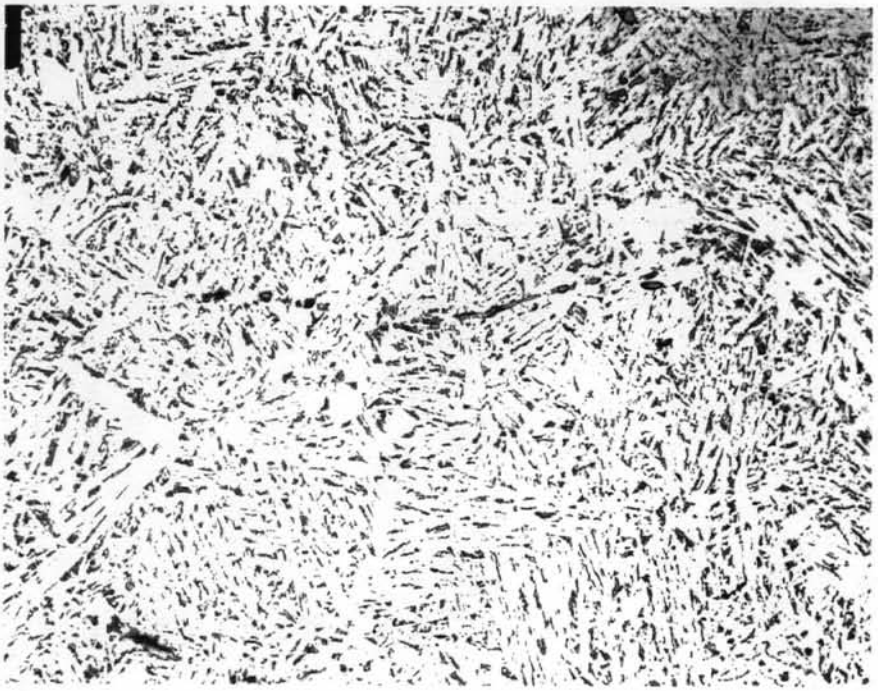

FIGURE 4.6

Optical Micrograph of the A302B Steel
used for the Pitting Tests, Nital Etch, 200X.
Inclusion Stringers are Shown in a Quenched and Tempered Matrix

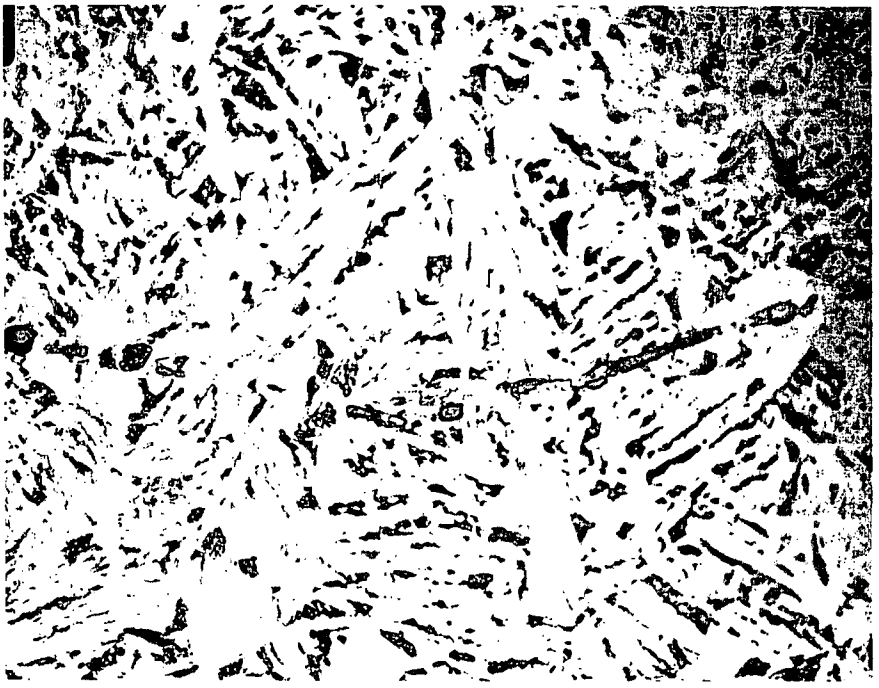

FIGURE 4.7

Higher Magnification Micrograph of
the A302B Steel, 500X

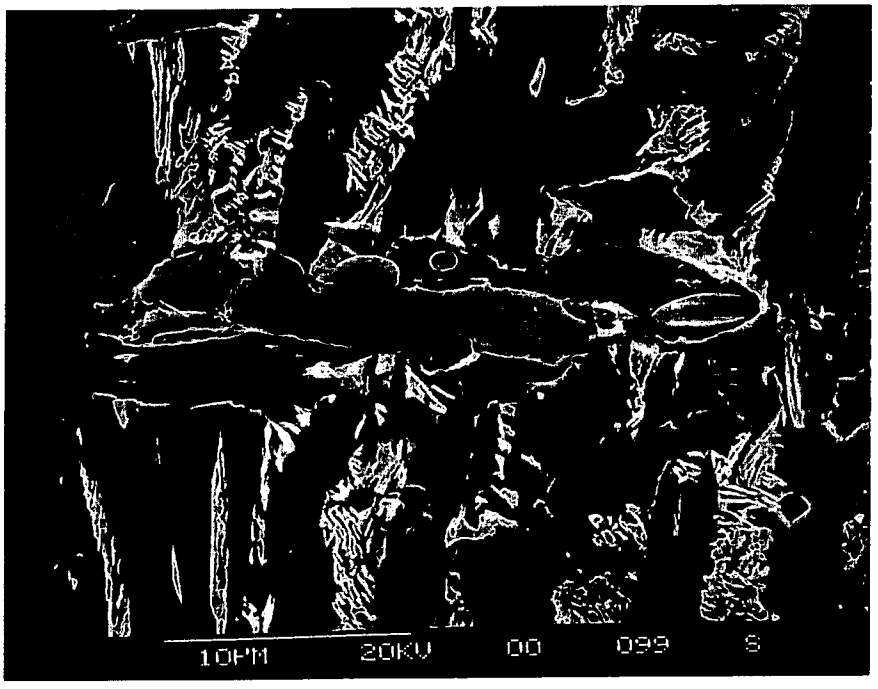

FIGURE 4.8

SEM Micrograph of the A302B Steel
Showing a Typical Inclusion

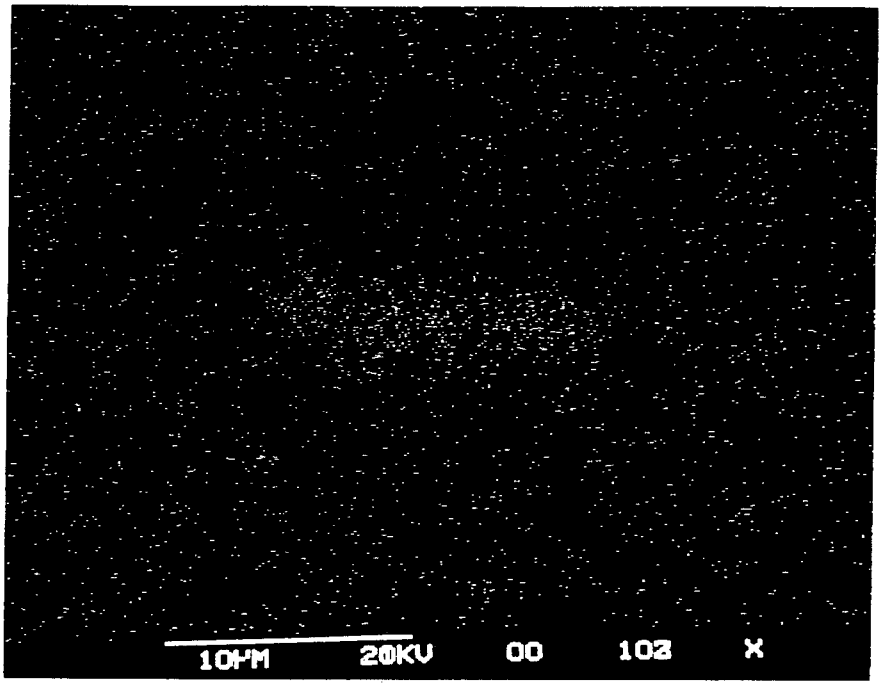

FIGURE 4.9

Aluminum X-Ray Dot Map of Inclusion Stringer in Figure 4.8. Note Increased Aluminum Concentration in Region of Large Particle.

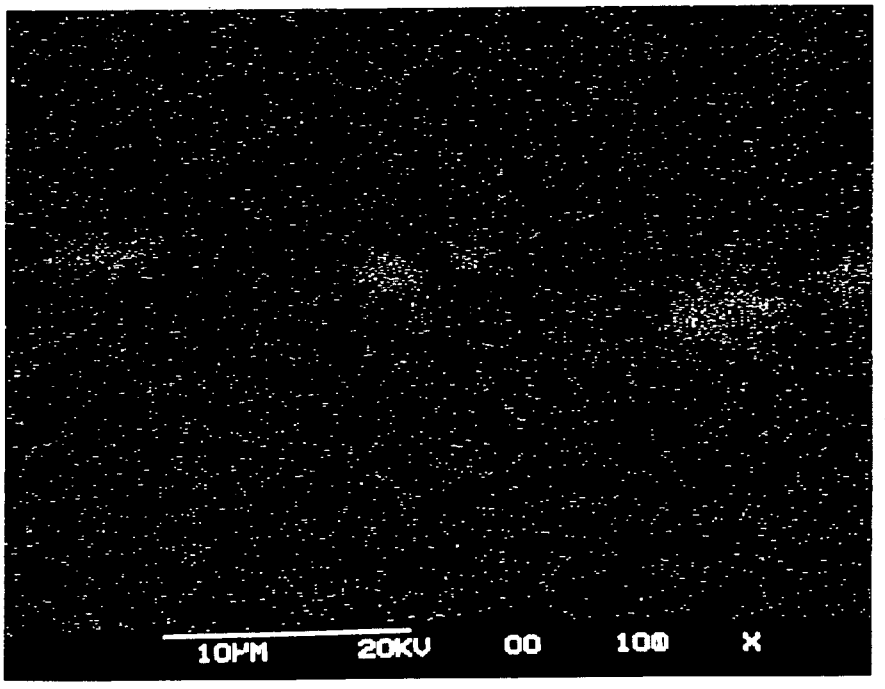

FIGURE 4.10

Sulphur X-Ray Dot Map of Figure 4.8 Showing Concentration of Sulphur in Regions of Small Particles

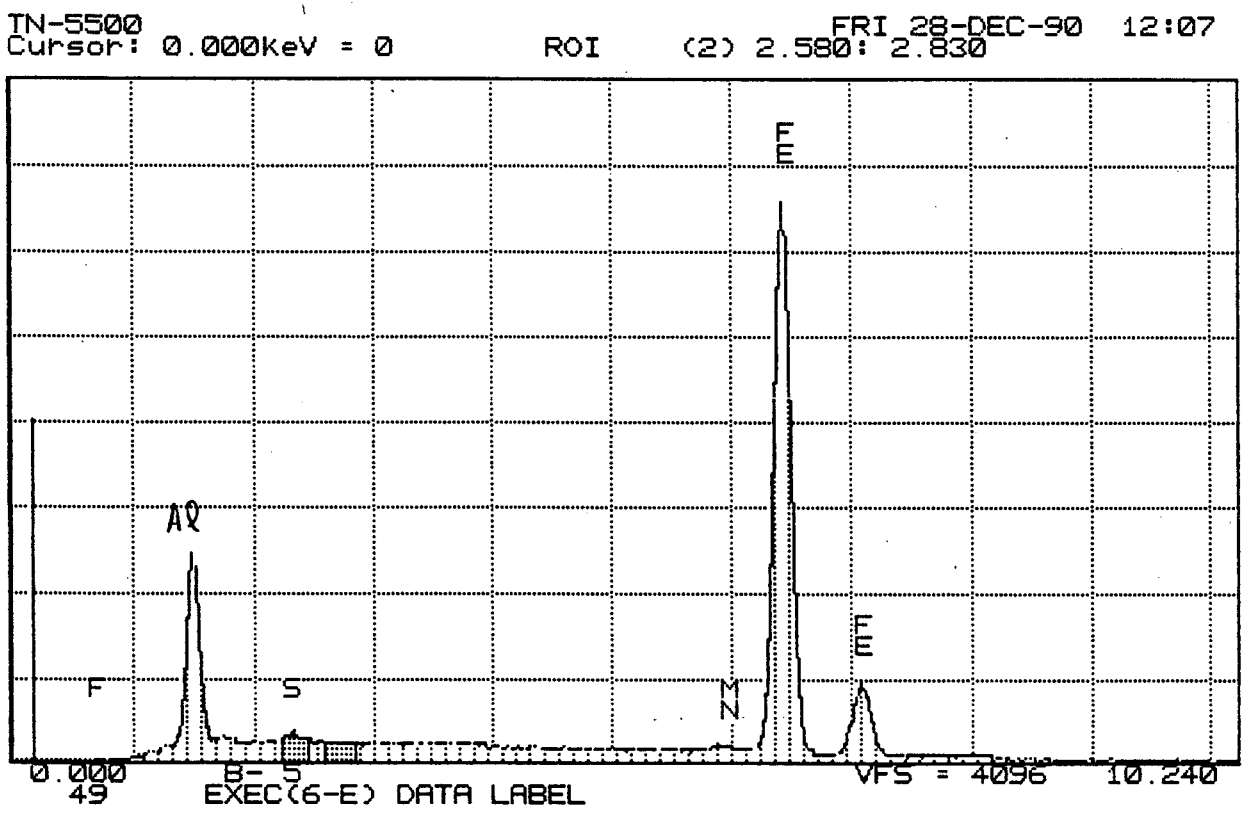

FIGURE 4.11

X-Ray Spectrum for High Aluminum Particle in Figure 4.8

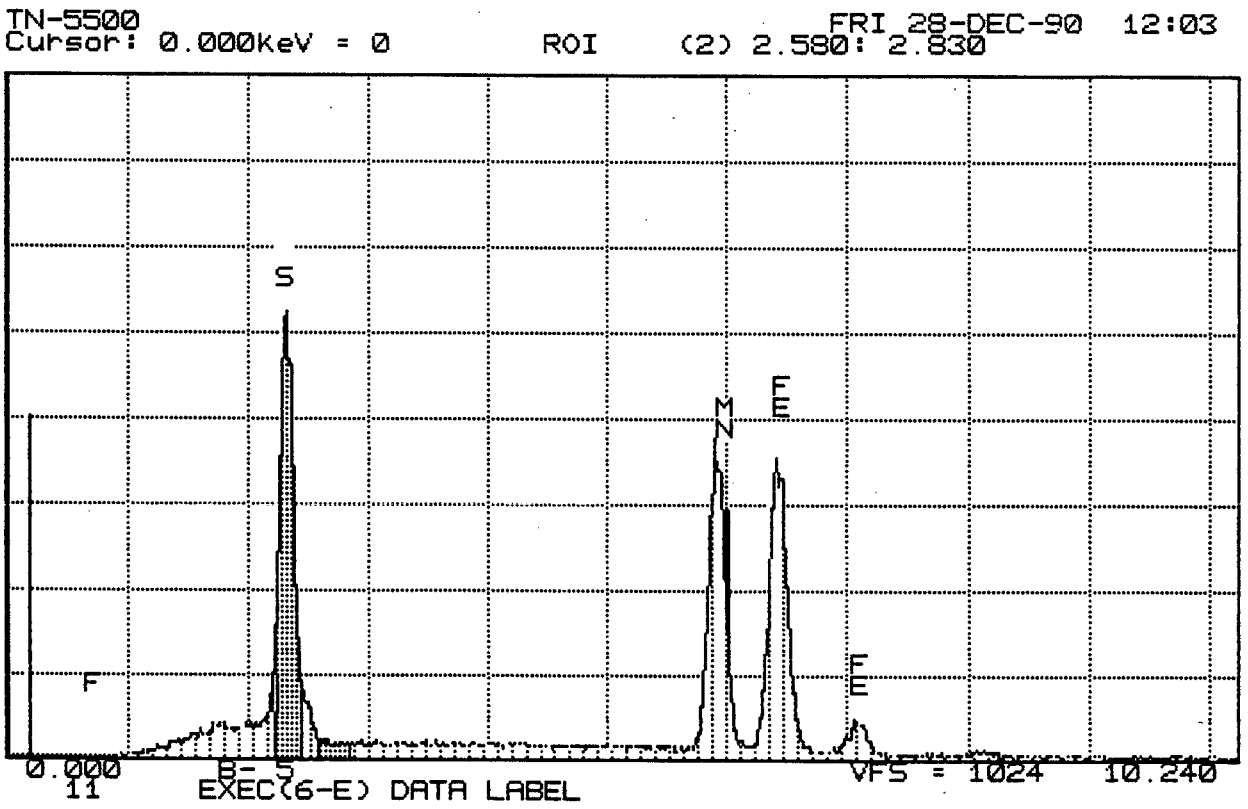

FIGURE 4.12

X-Ray Spectrum for High Sulphur Particle in Figure 4.8.

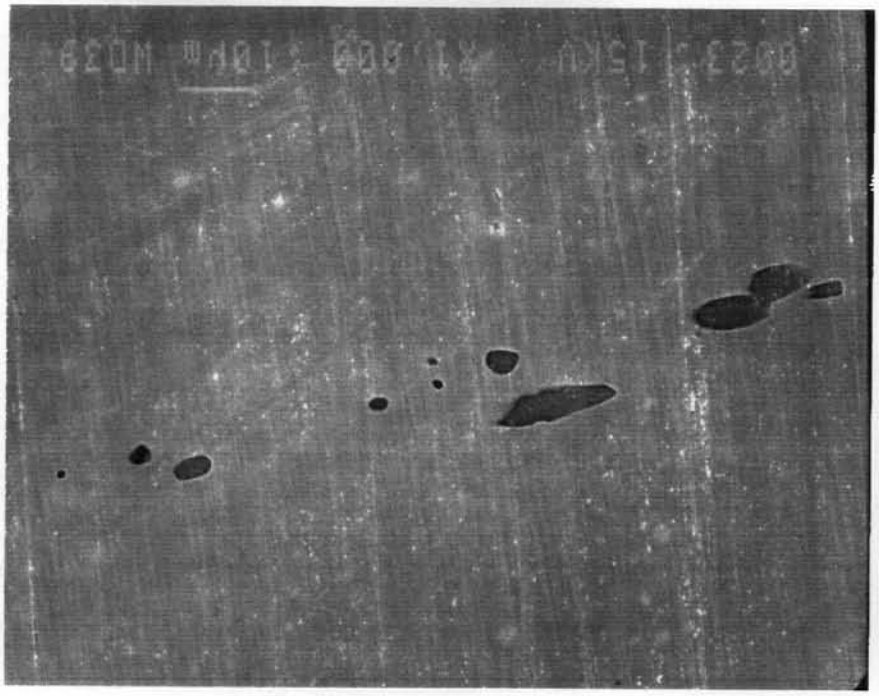

FIGURE 4.13

SEM Micrograph of 3μm Surface Finish Sample Prior to Testing. Inclusions are MnS.

FIGURE 4.14

Photograph of As-Tested Samples for Test HT-1.

FIGURE 4.15

SEM Micrograph of As-Tested HT-1 Sample Surface Showing Pits

FIGURE 4.16

Optical Micrograph of HT-1 Sample Sectioned Normal to the Exposed Surface Showing Pitted Region, 500X, Unetched.

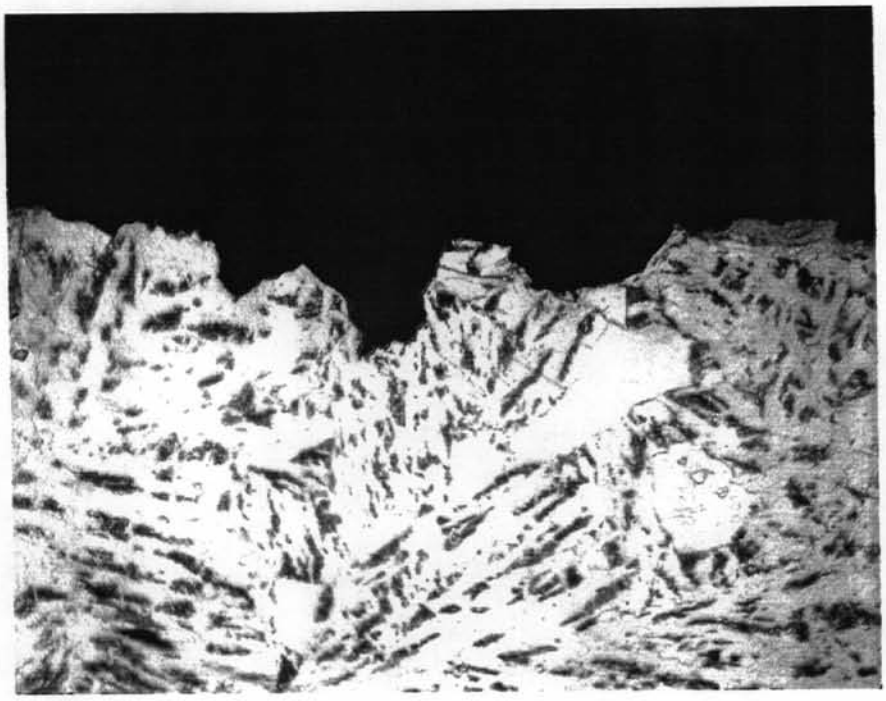

FIGURE 4.17

Optical Micrograph of HT-1 Sample Sectioned Normal to the Exposed Surface Showing Pitted Region of Figure 4.16, 500X, Etched.

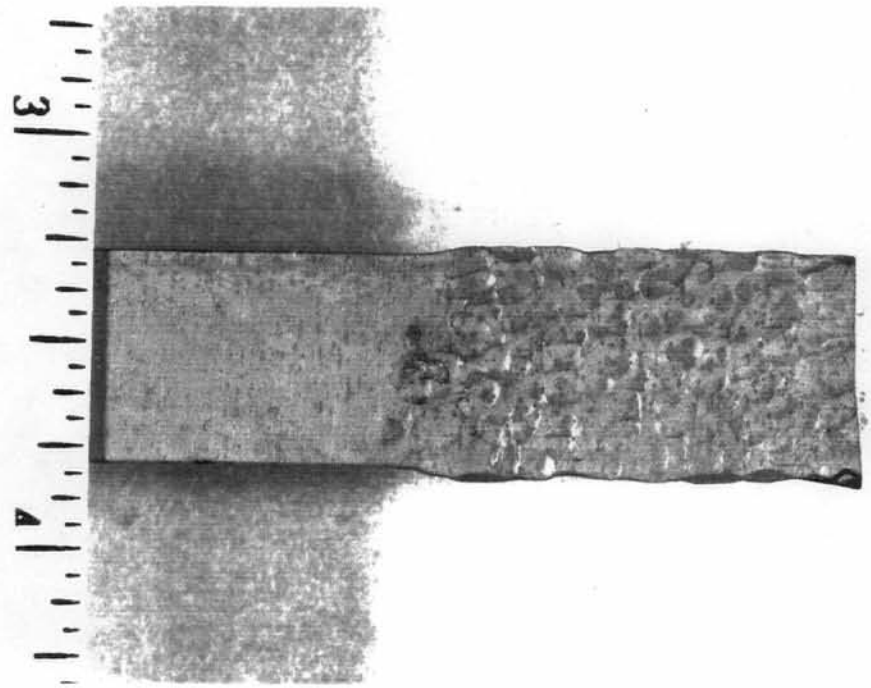

FIGURE 4.18

Photograph of As-Tested Severe Peened Sample, HT-1.

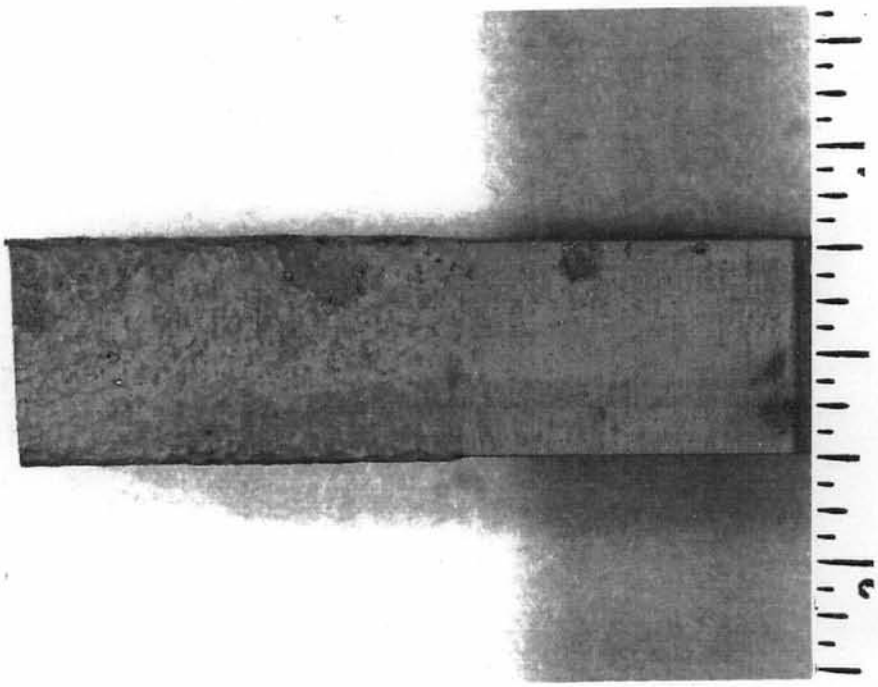

FIGURE 4.19

Photograph of As-Tested Mildly Peened Sample, HT-1.

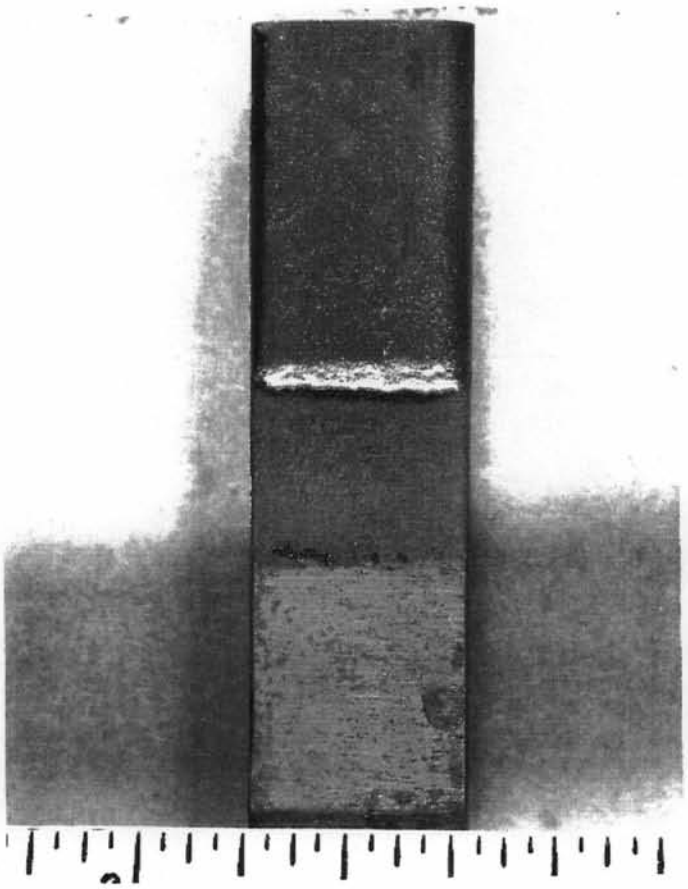

FIGURE 4.20

Photograph of As-Tested Coated Sample, HT-1.

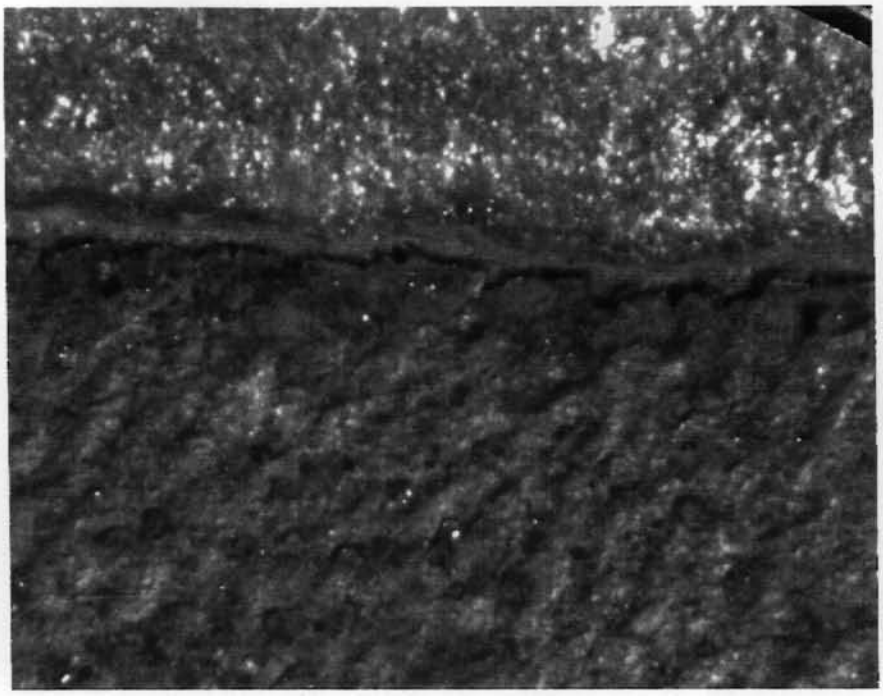

FIGURE 4.21

Coated Sample Coating/Base Metal Interface
Showing Accelerated Localized Corrosion, HT-1, 20X.

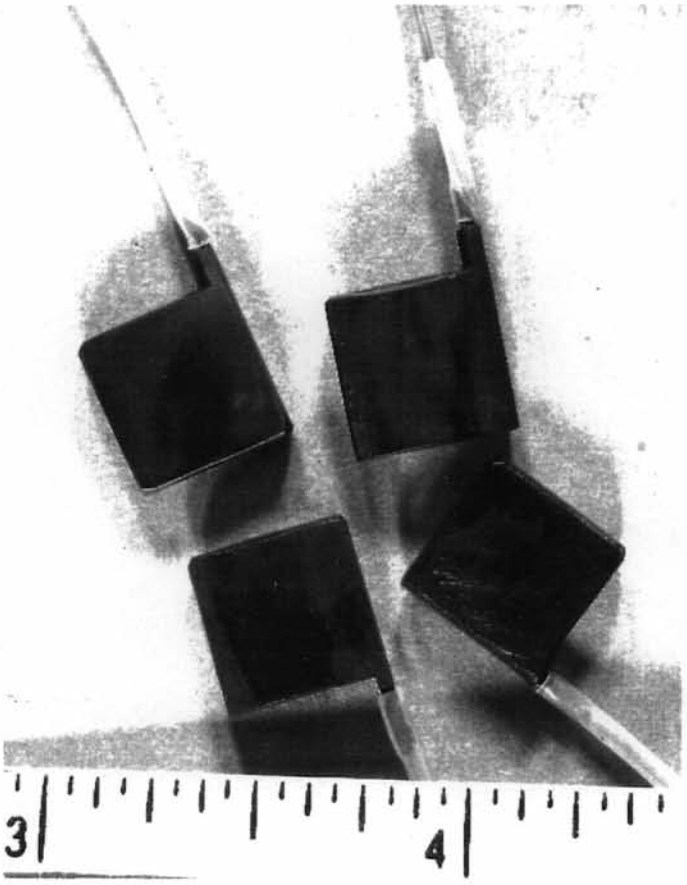

FIGURE 4.22

Photograph of As-Tested Samples for Test HT-3
Showing Dark Thin Oxide Film.

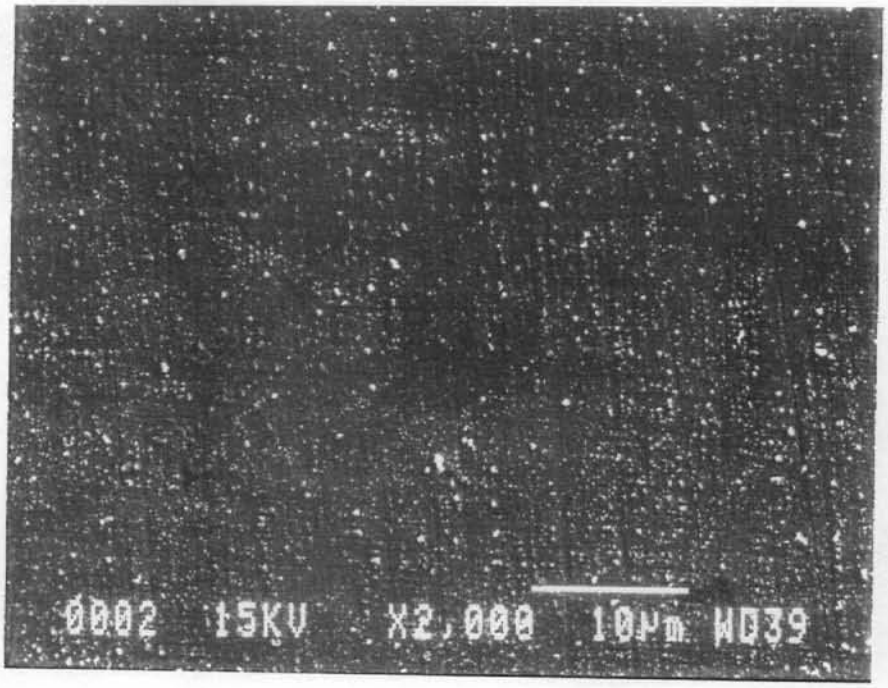

FIGURE 4.23

SEM Micrograph of HT-3 As-Tested Surface.

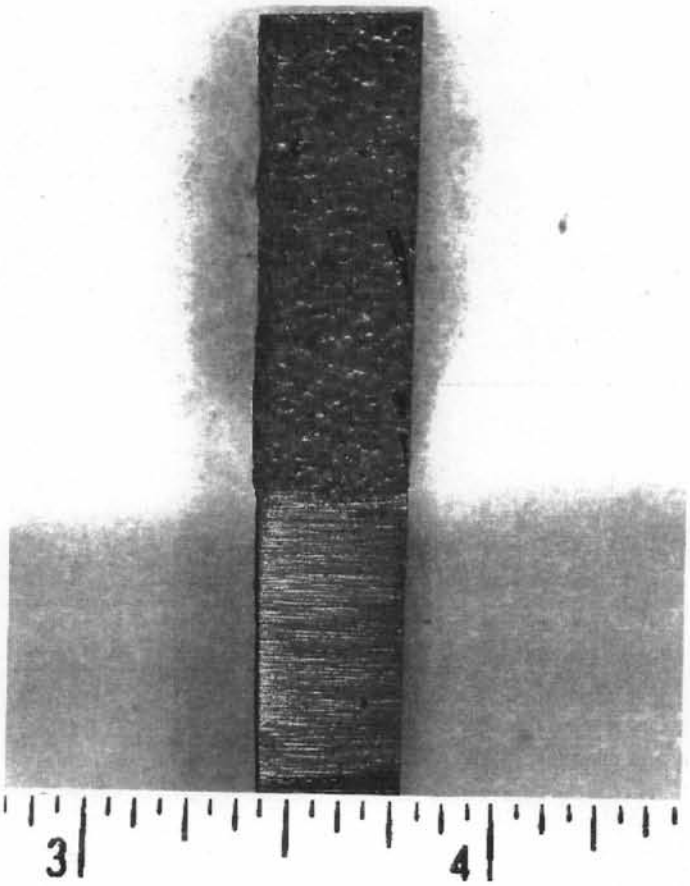

Figure 4.24

Photograph of Mildly Peened Sample, HT-3.
Note Lack of Visible Corrosion.

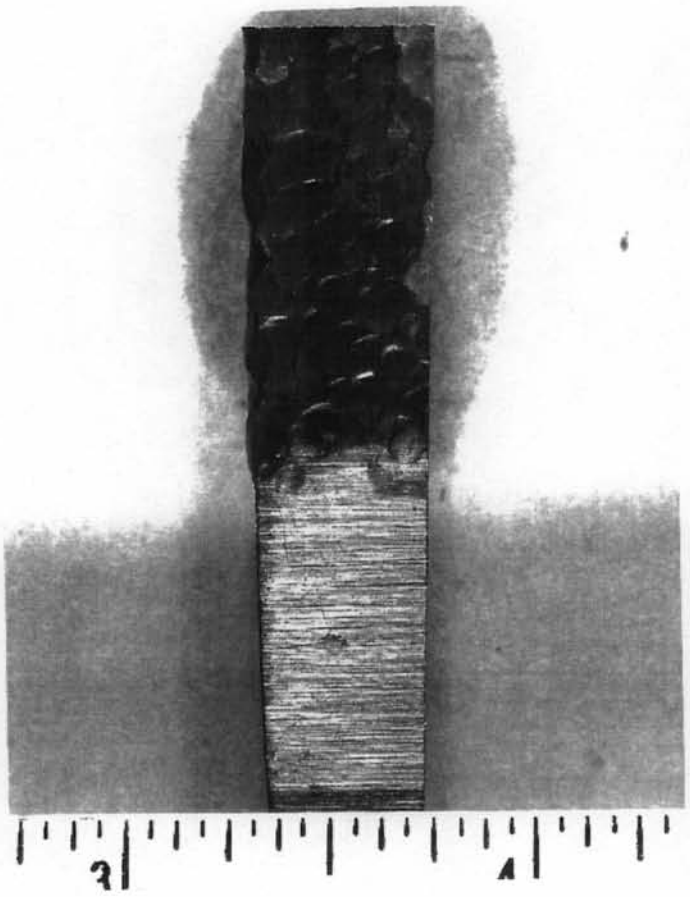

FIGURE 4.25

Photograph of Severe Peened Sample As-Tested, HT-3.

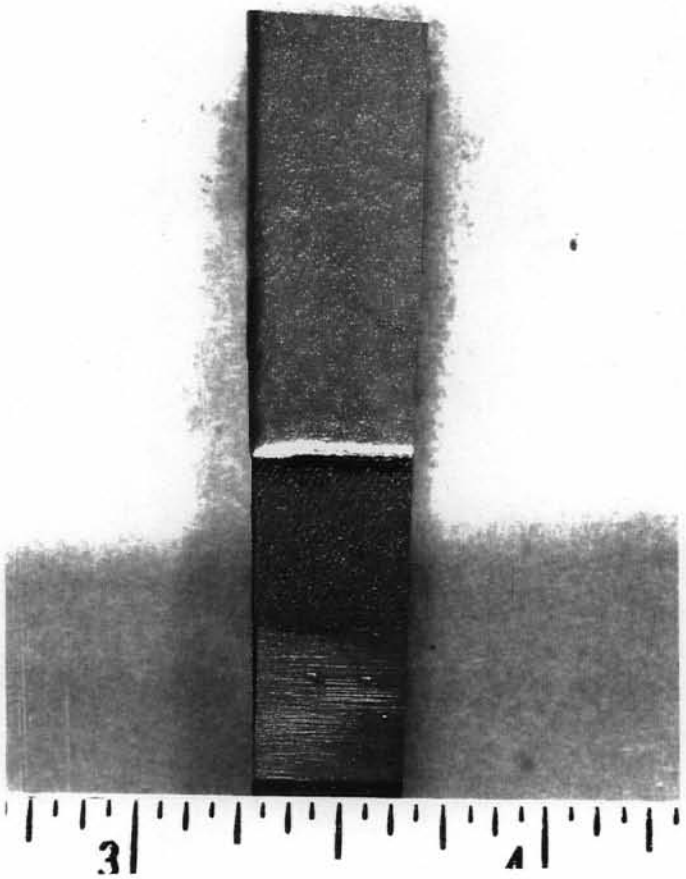

FIGURE 4.26

Photograph of Coated Sample As-Tested, HT-3.
Note Localized Corrosion at Coating/Base Metal Interface.

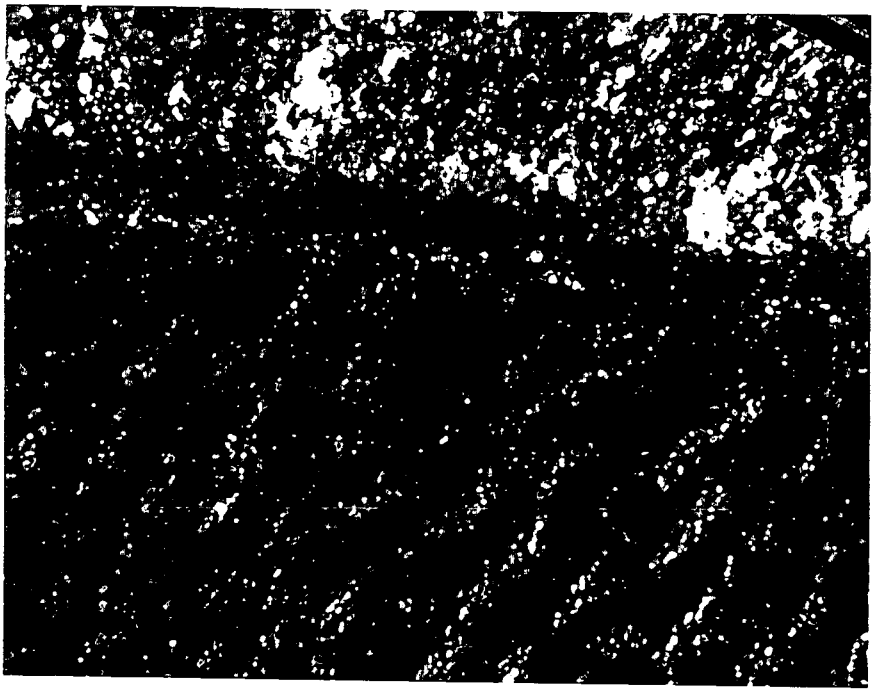

FIGURE 4.27

Coating/Base Metal
Interface of Sample Shown in Figure 4.26
Showing Localized Corrosion, 20X.

5.0 EVALUATION OF GIRTH WELD REGION

5.1 Thermal Monitoring Program

5.1.1 Description

A program was developed to monitor the temperatures of the Steam Generator in the area of the girth weld and the feedwater nozzle. Thermocouples were placed on the outside of steam generator 21 on the feedwater nozzle and the girth weld. The locations of the thermocouples are shown in Figure 5.1. The girth weld thermocouples, numbered 9 and 10, were of greatest interest with respect to the mechanism of cracking in the girth weld. Thermocouples 1 to 8 were located on the feedwater piping and nozzle and provided information on the temperatures in these two areas. The location of the thermocouples on the girth weld relative to the location of the feed nozzle and the feed ring is shown in Figure 5.2.

The thermocouples were monitored remotely utilizing a computer controlled data logging system. This system logged data when a significant change in the trending of the data occurred.

5.1.2 Temperature Results

The temperature data, acquired from June 23, 1990 until August 13, 1990 by the monitoring program, was reviewed to determine the most significant operating transients for the steam generator girth weld region during this period. The most significant transients occurred during the reactor startup on June 23, 1990 and during a unit shutdown initiated for a planned outage to repair a steam leak on July 27, 1990.

Temperature versus time plots were made of the girth weld thermocouple data for these two periods. Figure 5.3 shows the data from thermocouples 9 and 10 for the unit shutdown which was initiated at 22:33 on July, 27, 1990. The most rapid change in temperature occurred at approximately 02:00 and resulted in a ΔT of approximately 13°F with a period of approximately 30 minutes.

Figure 5.4 shows the data for these same thermocouples during the unit startup on June 23, 1990. In this event, the most rapid change in temperature occurred at approximately 02:00 and resulted in a ΔT of approximately 20°F with a period of approximately 20 minutes.

Of these two transients, the startup transient with the ΔT of 20°F with a cyclic period of approximately 20 minutes was the most severe. Finite element heat transfer analysis was performed to determine the inside wall surface temperature change that would result in the measured outside wall temperature. The ΔT of 20°F measured on the outside surface would result from an inside temperature ΔT of 30°F with the same period (20 minutes). This inside surface thermal transient was utilized to calculate thermal stresses.

5.2 Stress Analysis

A complete stress analysis of the girth weld region of the steam generators was performed to assist in understanding the effect of the stress distributions on the initiation and propagation of girth weld cracks.

5.2.1 Pressure Stress

A stress analysis was performed for an internal pressure in the steam generator of 660 psig. The analysis used the ANSYS computer code [4]. An axisymmetric model of a

portion of the steam generator extending from the upper cylinder to the lower cylinder was prepared. Figure 5.5 shows the extent of the overall model and Figure 5.6 shows the finite element mesh at the girth weld region. The model was prepared to assure full consideration of the interaction effect of the upper shell and the transition cone and to assure an accurate representation of through wall stresses.

The maximum values of the axial and hoop stress components occur at the center-line of the girth weld, at the geometrical discontinuity between the steam generator upper cylinder and transition cone shells. In addition, this discontinuity effect on the inside surface stress is further increased by the stress concentration resulting from the "knee" caused by the joint between the cylinder and the cone. There is an additional bending stress component due to the structural discontinuity which results from pressure on the ID surface.

Figure 5.7 shows the through-wall distribution of the axial stress and the hoop stress at the center of the girth weld. This shows that at the inside surface of the girth weld the axial stress is approximately 50% larger than the hoop stress. These analyses also indicate that at a depth of approximately 1 inch from the inside surface of the shell, the axial stress value is reduced to a level below the hoop stress value.

5.2.2 Thermal Stress

The temperature data acquired from the thermal monitoring program was analyzed to determine the resulting thermal stresses. As stated earlier, the most significant transient recorded at the outside surface of the girth weld was caused by an inside ΔT of 30°F with a cyclic period of approximately 20 minutes. A thermal stress

analysis was performed for the girth weld region of the steam generator using an inside surface temperature sine wave variation with an amplitude of 30°F and a period of 20 minutes. The analysis used the same 3-D model described in Section 6.2.1. The maximum axial stress on the inside surface occurs at the knee of the girth weld and has a value of 8.5 ksi.

This stress is small in comparison to stresses required to cause significant fatigue crack growth, and the number of cycles during this operating period was limited. The next largest thermal transient occurred during the unit shutdown. It was a single cycle of approximately 4.0 ksi.

The measurement of these temperature transients and the calculation of these stresses resulted in the conclusion that the mechanism of cracking was less likely to be controlled by a fatigue or corrosion fatigue mechanism, and was more likely by a stress corrosion mechanism.

5.3 Fracture Mechanics Analysis

5.3.1 Two-Dimensional Fracture Mechanics

The initiation and propagation of circumferential cracks at the inside surface of the girth weld is dictated by the axial component of stress at this location. The effect of the through-wall axial stress distribution on cracks of various sizes was investigated using classical solutions of two-dimensional (2-D) fracture mechanics.

Mode I stress intensity factors (K_I) were computed for semi-elliptical surface cracks in flat plates subjected to a combination of membrane and linear bending stress. The axial stress distribution used is for 660 psig pressure shown in Figure 5.7. Cracks of various depths

(a) and aspect ratios (a/2c) were evaluated. The stress intensity factor results are presented in Figure 5.8.

Figure 5.8 shows that the K_I values for small aspect ratio cracks continue to increase with increasing crack depth. The K_I values for larger aspect ratios of 0.4 and 0.5 reach a maximum value at a crack depth of approximately 1 inch, then tend to level off and to decrease for deeper cracks.

5.3.2 Three-Dimensional Fracture Mechanics

To develop a more accurate knowledge of the effects of the actual stress distribution and geometric configuration, and to determine the distribution of the stress intensity factor, K_I, around the crack front, a 3-D fracture mechanics analysis of the steam generator girth weld region was performed. The fracture mechanics capabilities of the ANSYS finite element code were used in the analysis. The loading considered was 660 psig internal pressure.

The procedure to obtain the desired K_I values consisted of three steps, each step using a sub-model of that used for the prior step. The initial model, referred to as the coarse model and shown in Figure 5.9, was made using 3-D solid elements (ANSYS element STIF45). It was comprised of a 45° arc of the steam generator circumference and a portion of both the upper cylinder and the transition cone. The right hand side of the model shown in Figure 5.9 was the location of the circumferential crack and was a symmetry plane, i.e., the circumferential crack is symmetric about this plane. Two nodes at the inside surface of this symmetry plane are unconnected so as to represent, in a coarse manner, the effect of the circumferential crack at this location. Pressure was applied to the inside surface, axial tensile

loads were applied to the upper edge of the upper cylinder, and the lower edge of the transition cone was restrained in the vertical direction. Symmetry boundary conditions were applied on the two shell thickness planes.

In order to refine the displacements in the region of the circumferential crack, a sub-model of the coarse model, referred to as the intermediate model and consisting of tetrahedrons (ANSYS element STIF92), was used. This model is shown in Figure 5.10. This model, shown in the deformed condition, has the semi-elliptical crack faces modeled using nodes that are unconnected in the axial direction. Nodal displacements from the coarse model were input on the boundaries of this intermediate model and a displacement solution obtained.

Finally, to compute the K_I values at the crack, the local region of the crack front was modeled as shown in Figure 5.11 using singular crack tip elements (ANSYS elements STIF95). Displacements from the intermediate model were input on the boundaries and the distribution of the stress intensity factors, K_I, along the crack front were computed on the basis of the crack face displacements.

The results for the crack sizes analyzed are shown in Figure 5.12. Eight models were run and the crack size (a) and the crack length (2c) are provided. The values of K_I are shown at various locations on the crack front. For example, the value of KI12 is the stress intensity value calculated on the ID surface of the shell.

The maximum stress intensity values all occurred at the maximum depth of the crack (KI20) at the plane of symmetry. These values are presented in Figure 5.13. Comparing the results of the 2-D analysis in Figure 5.8 with the 3-D analysis results in Figure 5.13, it is seen

that for the smaller aspect ratios and at approximately a 1 inch depth, the 3-D analysis gives values of K_I which are lower by approximately 30%. The 3-D analysis results are considered to be more accurate since the 2-D analysis utilizes several simplifying assumptions, e.g., the use of an infinite plate, neglecting the shell curvature and discontinuity geometry, and linearizing the stresses.

It is useful to utilize the results of the 3-D model to consider the effects of the stress intensity around the crack surface. Figure 5.14 shows ratio of the K_I at the crack tip to the K_I at the surface of the shell. These results illustrate that a crack with a small aspect ratio (shallow long crack) has a much higher crack tip K_I than crack edge K_I, indicating that the crack would have a tendency to grow deeper more quickly than longer. As the crack becomes more semi-circular (a/2c = 0.5), the ratio between the tip and the edge becomes equal to one, indicating that the crack will grow more uniformly and tend to remain semi-circular. In this stress field, free surface cracks tend to grow towards a semi-circular shape.

In order to assure an accurate prediction of the stress intensity and crack behavior, consideration of residual stresses is required.

5.3.3 The Effect of Residual Stress

The axial component of residual stress at the inside surface of the girth weld, caused by the welding process and partially relieved by post-weld heat treatment, will influence the initiation and propagation of circumferential cracks.

The girth weld between the steam generator upper cylinder and transition cone is the final closure weld of the

secondary shell. This weld was made in the field and was a double bevel, full penetration weld made using the manual arc welding technique. The post-weld heat treatment, while not optimum, was in full compliance with the ASME Boiler and Pressure Vessel Code, Section III, 1965 which was in effect at the time of the fabrication of the steam generator.

It is not feasible to ascertain the exact magnitude of the axial residual stresses at the inside surface of the girth weld. An estimate of the stress level may be obtained based on available data and industry experience. It is known that the as-welded residual stress distribution will be of the form shown in Figure 5.15, and that the maximum value of the stress will be approximately equal to the yield stress of the material. In addition, experience indicates that for the post-weld heat treatment applied in the field, the remaining stress should be approximately 20% of the initial value. Thus, the residual tensile stress after post-weld heat treatment should be approximately as indicated in Figure 5.16, with a maximum tensile value on the inside surface of approximately 10 ksi.

Combining the postulated residual stress with the pressure stress, the through-wall distribution of axial tensile stress at the girth weld will be as shown in Figure 5.17. This combined stress shows that when the effects of residual weld stress are combined with the axial pressure stress, the axial stress component (driving a circumferential crack) becomes compressive for cracks deeper than approximately 1 inch.

The through-wall stress distribution shown in Figure 5.17 was utilized to calculate stress intensity factors, K_I. Classical 2-D fracture mechanics solutions were utilized. These results are provided in Figure 5.18 and show that

for crack depths greater than approximately 0.7 inch, the stress intensity factors reduce in value. In addition, based on the data comparing 2-D and 3-D results, the maximum K_I value for the most severe cracks subjected to combined pressure and residual stress will be approximately 20 ksi$\sqrt{in.}$

5.4 Conclusions from the Stress Analysis and Fracture Mechanics

The stress analysis and fracture mechanics analysis explain the behavior of the cracking. The thermal stresses from plant operation are calculated to be low and below the level that would cause fatigue growth. The interaction of the pressure and the residual stresses cause a stress intensity factor which decreases at the depth that cracks are observed in the plant. The fracture mechanics results, when calculated with the consideration of residual stresses, corroborate the observation that cracks in the girth weld area grow to a maximum depth of approximately 1 inch and then level off or decelerate.

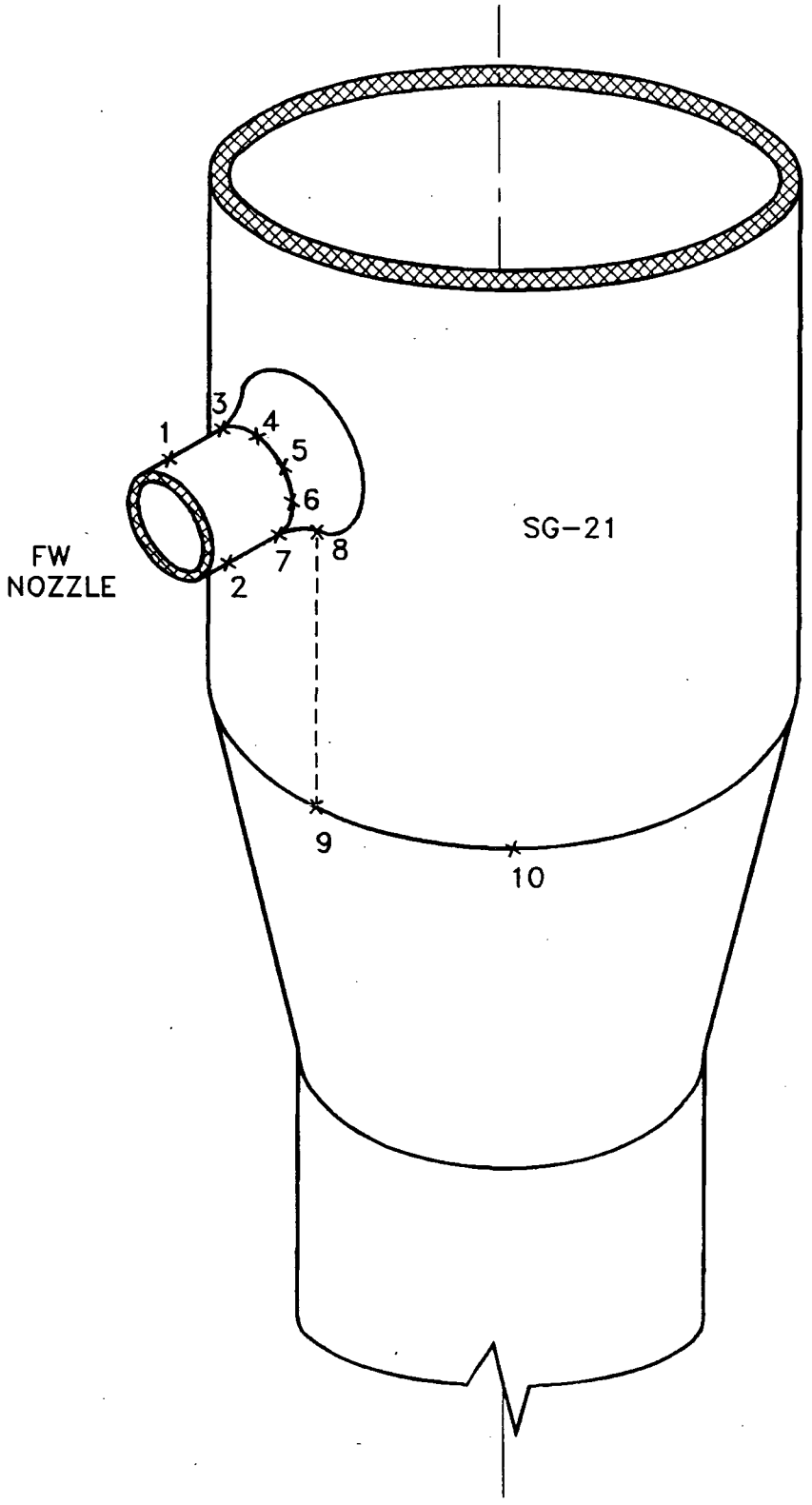

FIGURE 5.1

Location of the Thermocouples 1 to 10
Steam Generator 21

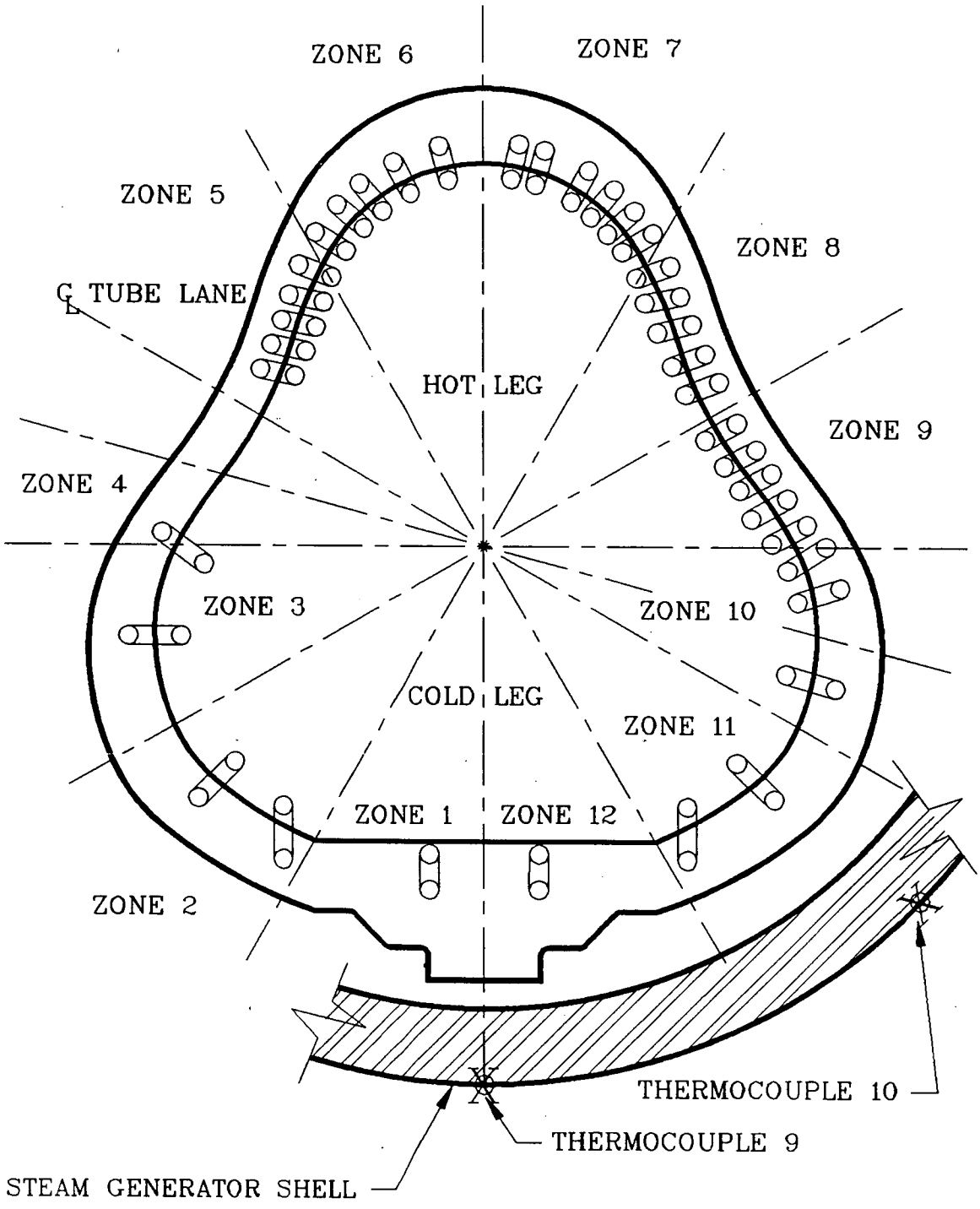

FIGURE 5.2

Location of the Thermocouples 9 and 10 on the Girth Weld Relative to the Location of the Feed Ring

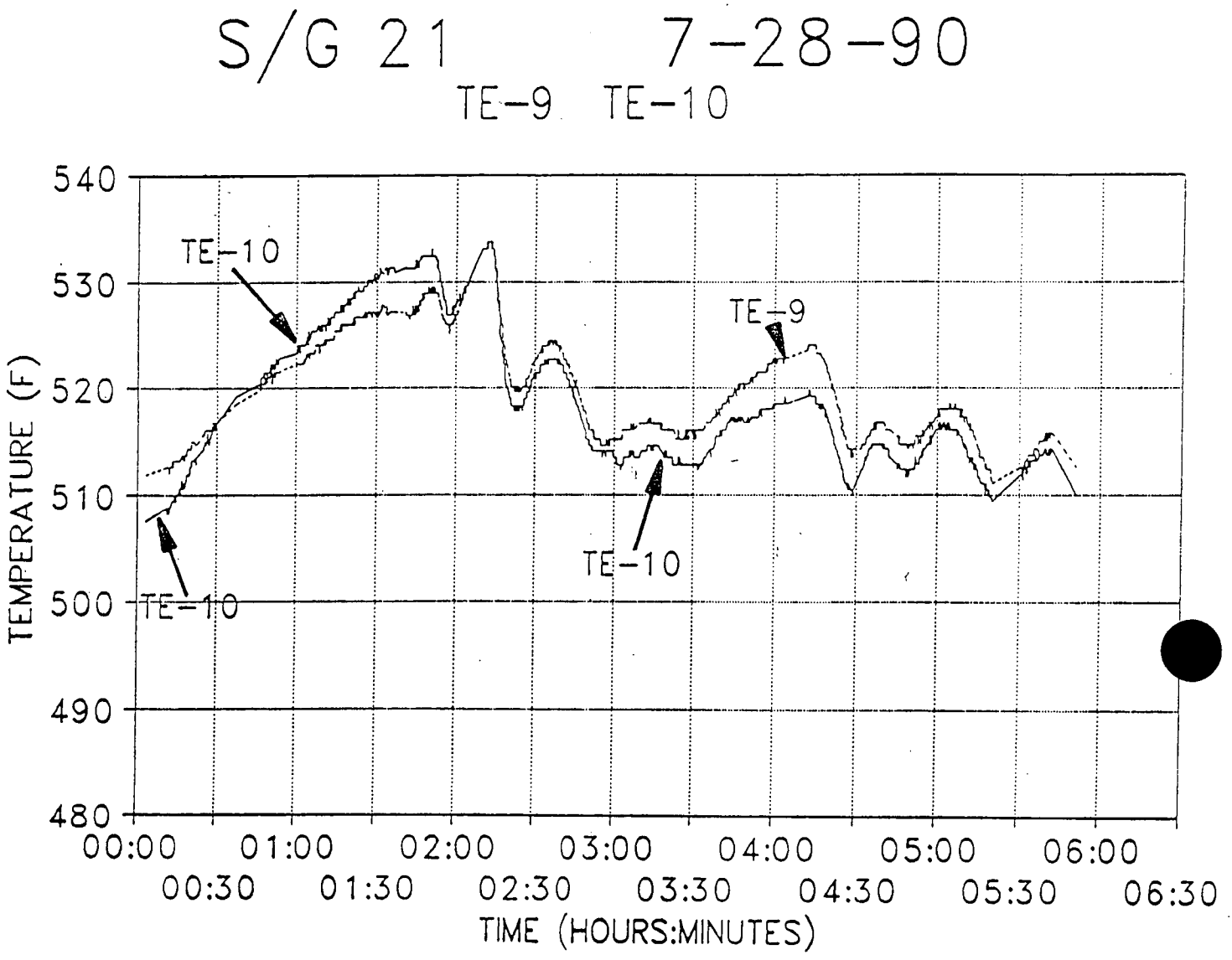

FIGURE 5.3

Data from Thermocouples 9 and 10 for the 7/27/90 Unit Shutdown

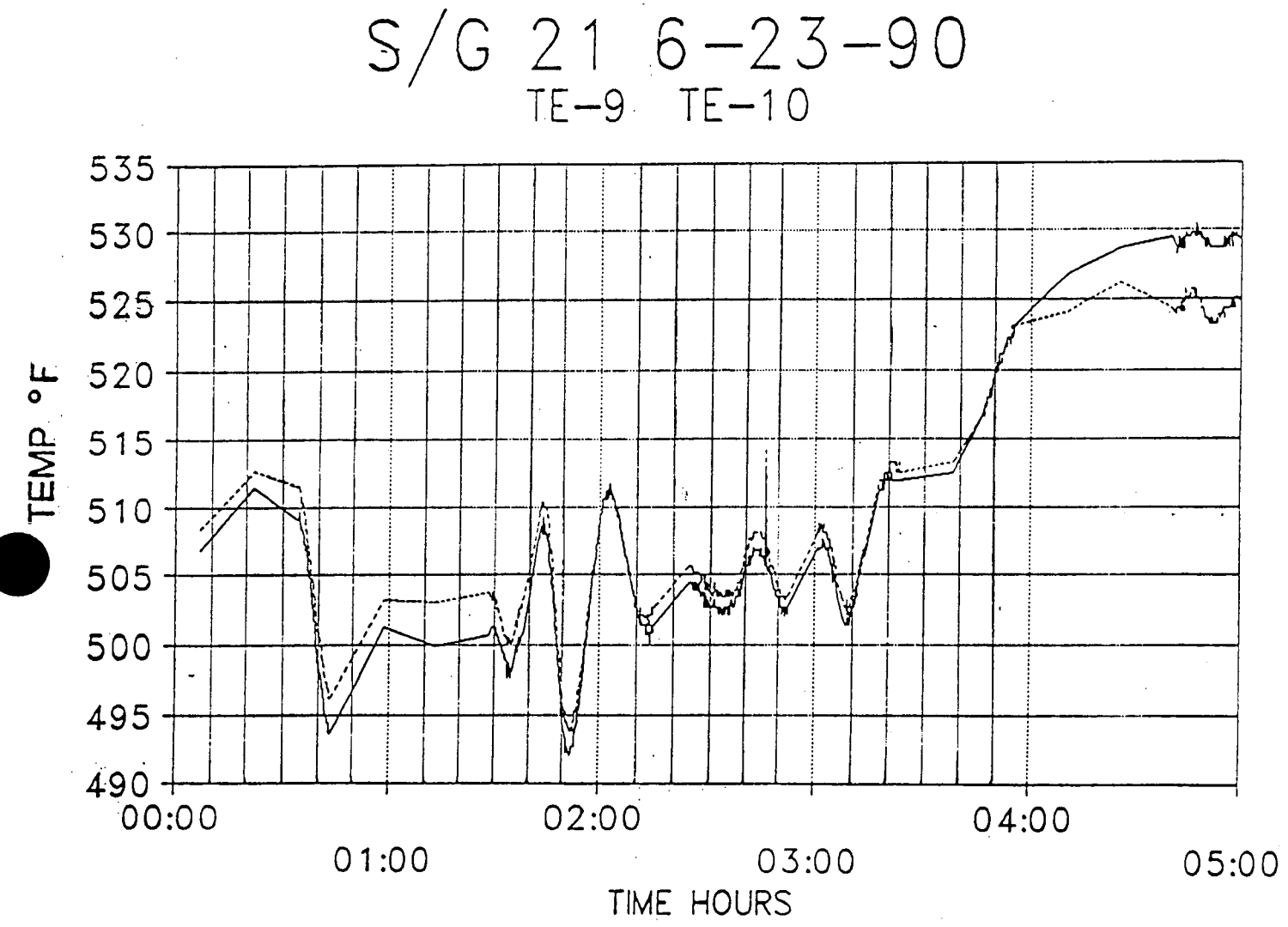

FIGURE 5.4

Data from Thermocouples 9 and 10 During Unit Startup on 6/23/90

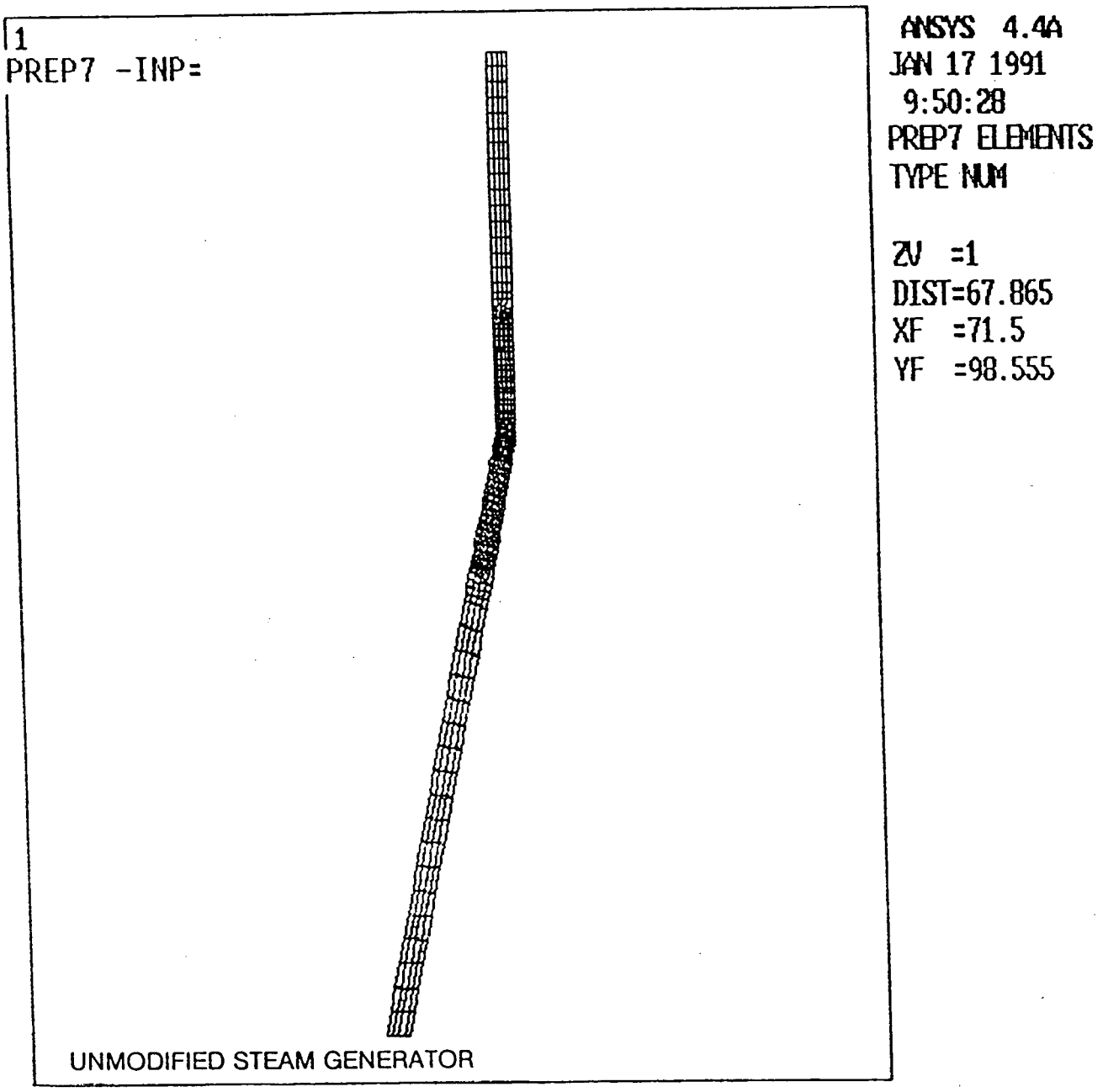

FIGURE 5.5

Full Finite Element Model of the Girth Weld Region

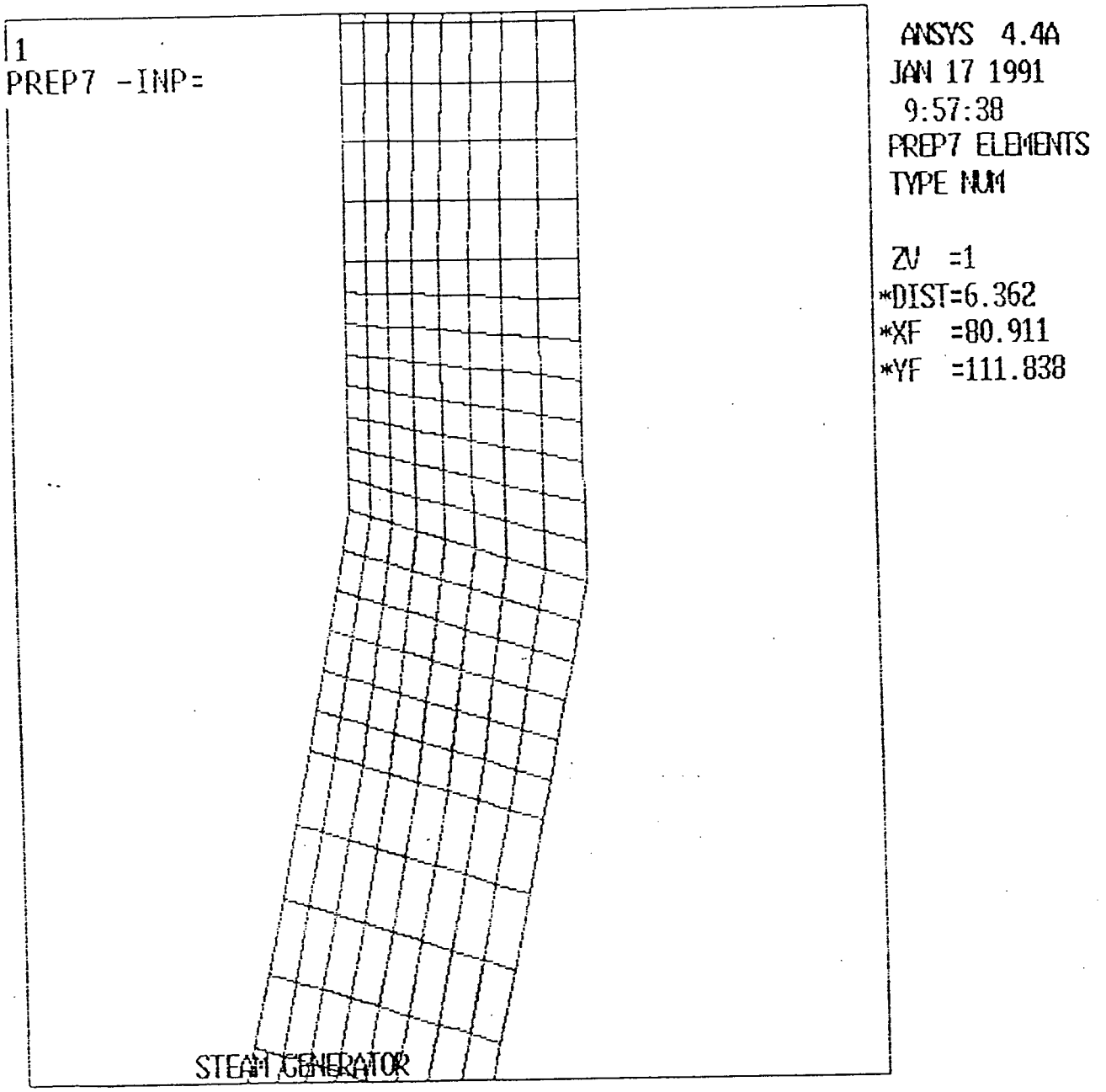

FIGURE 5.6

Local Finite Element Mesh at the Girth Weld Region

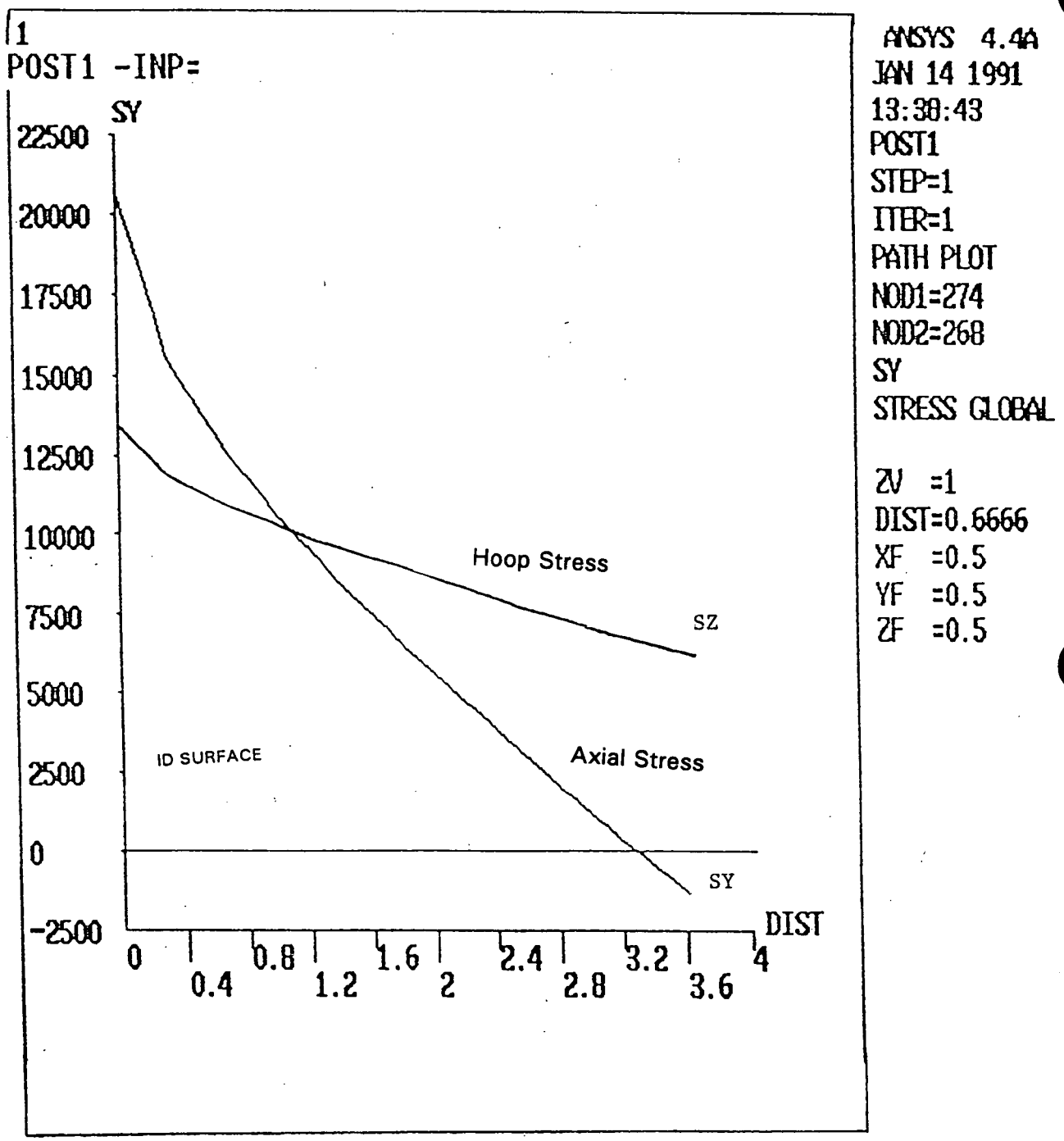

FIGURE 5.7

Through-Wall Distribution of the Axial Stress and the Hoop Stress at the Center of the Girth Weld

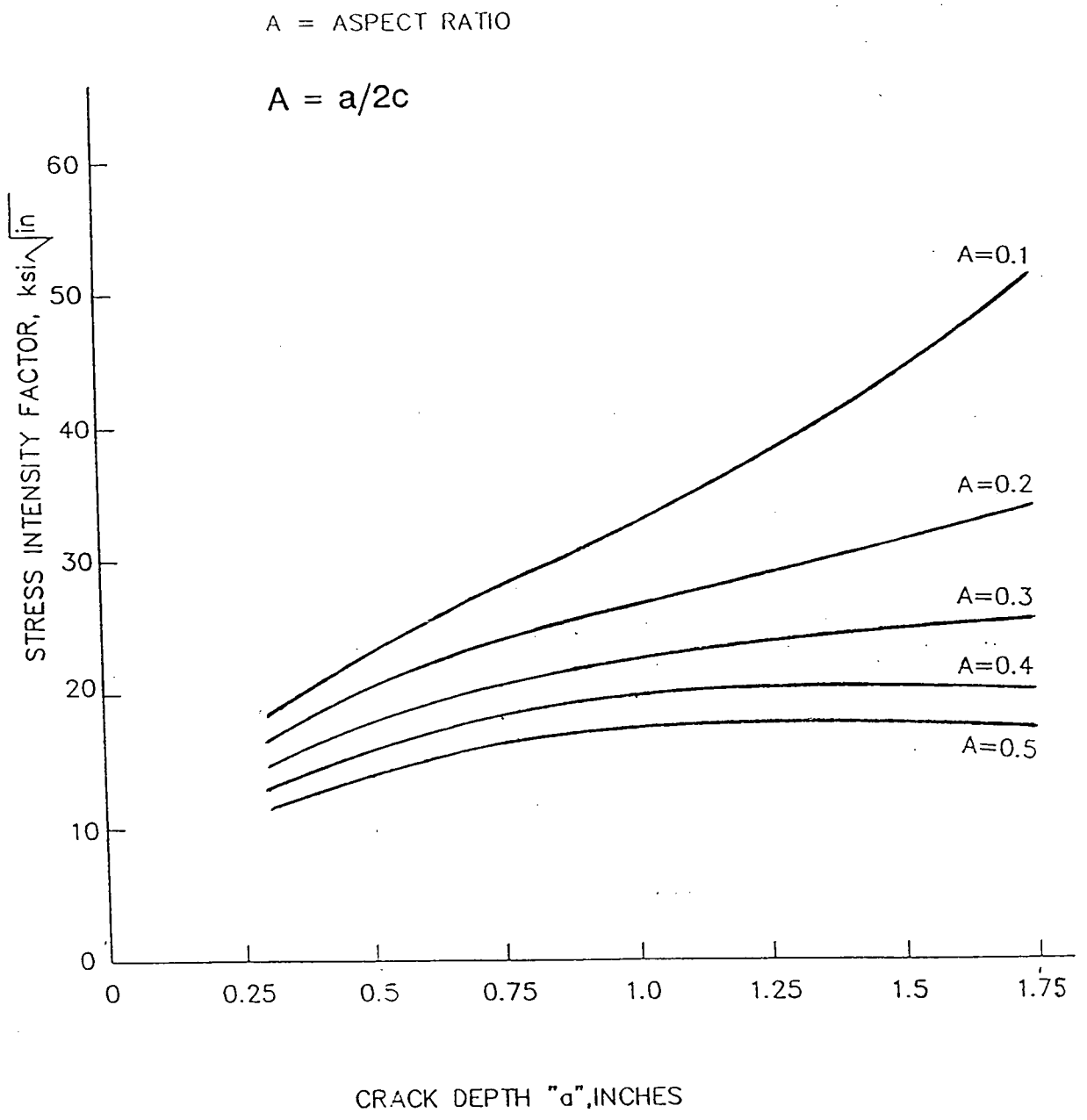

FIGURE 5.8

Stress Intensities for Cracks of Various Depths (a) and Aspect Ratios (a/2c) for the Pressure Axial Stress Distribution Shown in Figure 5.7

COARSE MODEL

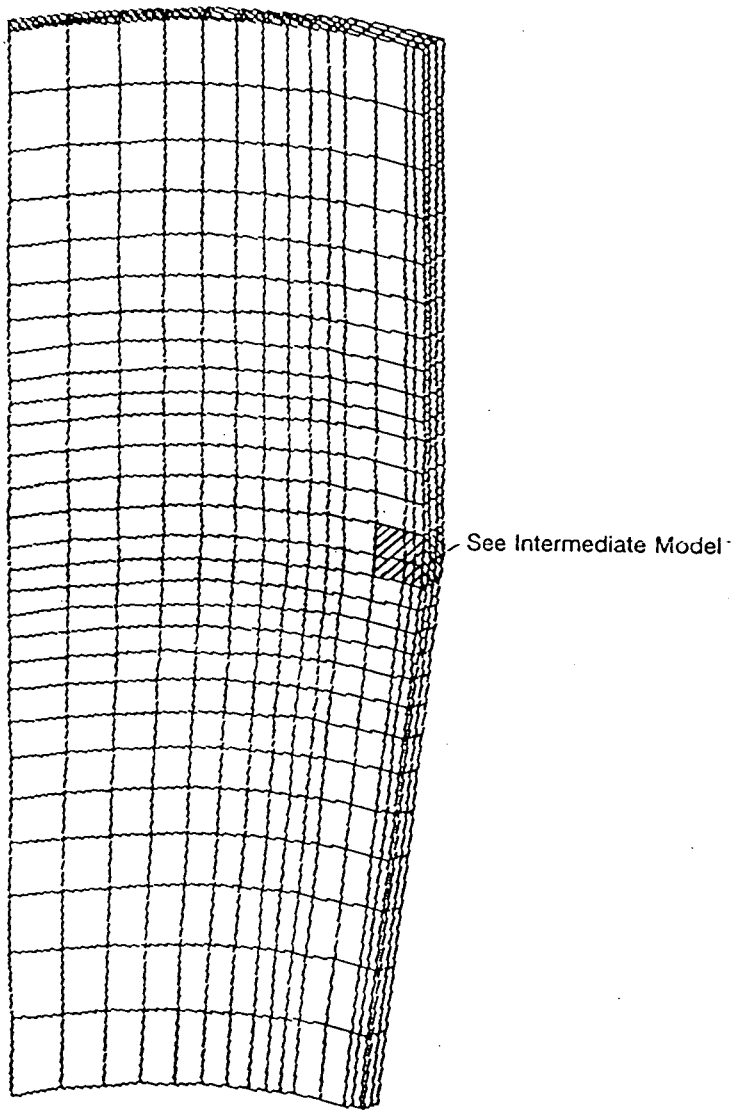

FIGURE 5.9

The Coarse Model for the 3-D Fracture Mechanics Analysis

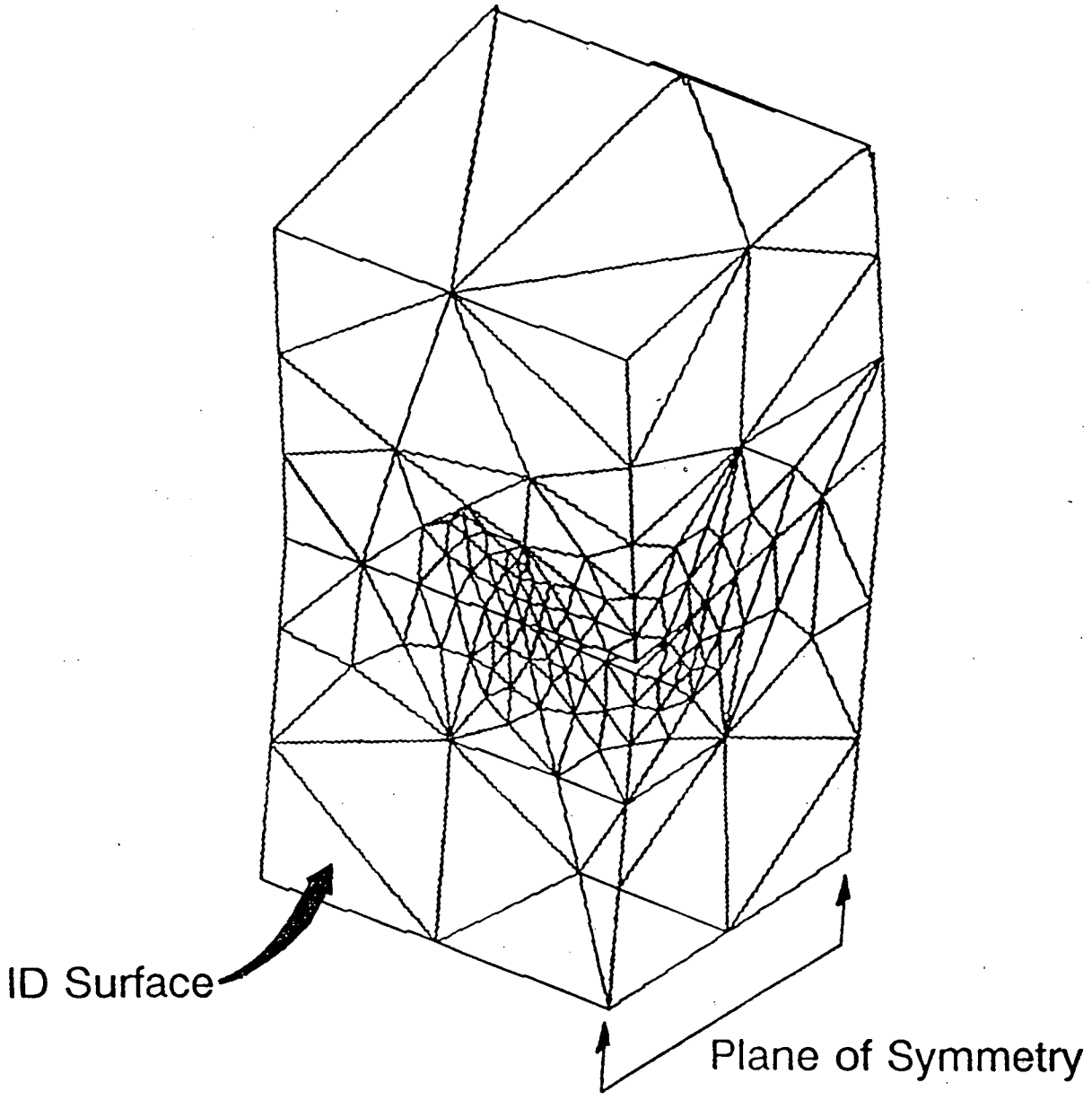

FIGURE 5.10

A Sub-Model of the Coarse Model, Referred to as the Intermediate Model

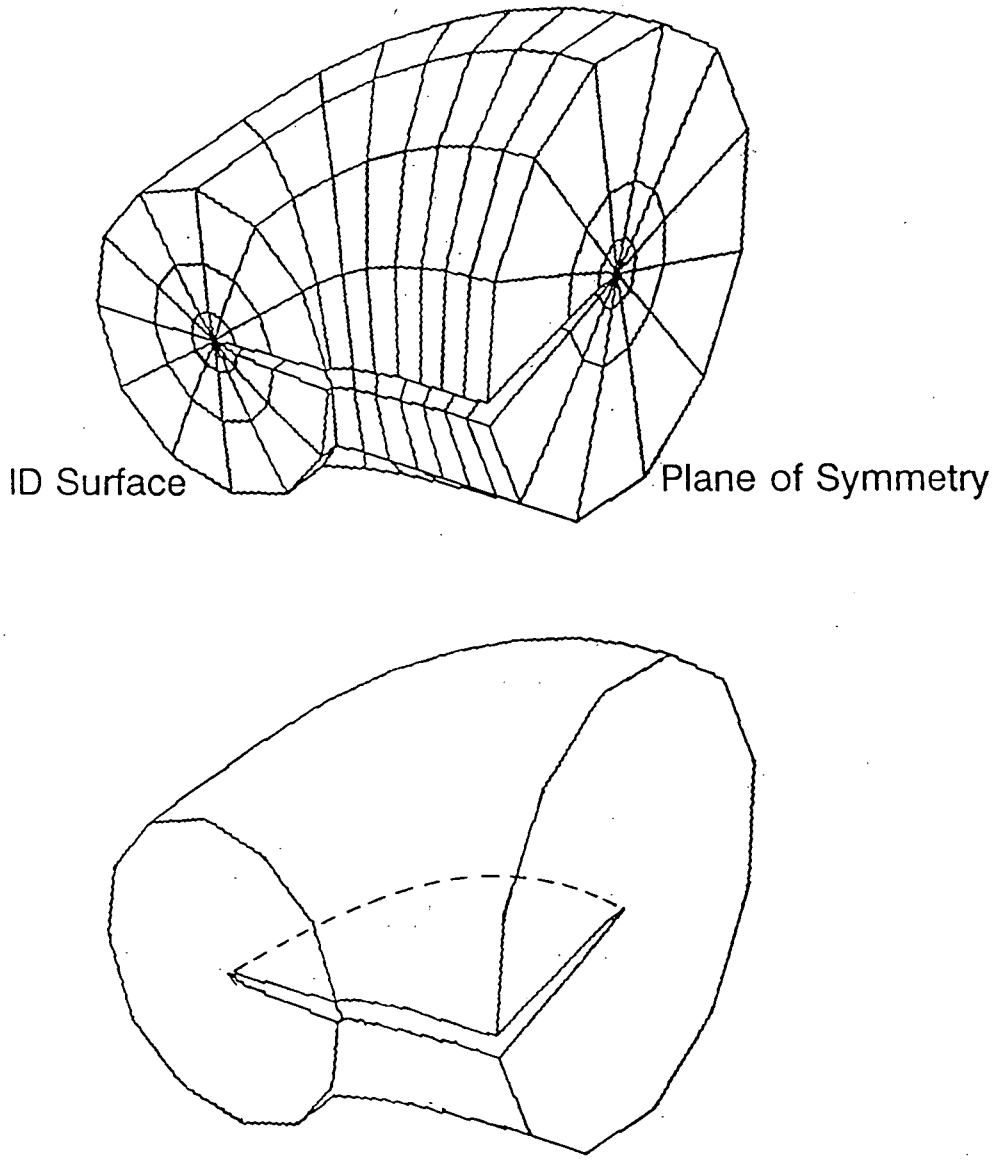

FIGURE 5.11

The Crack Front Model

STRESS INTENSITY FACTORS (KSI-IN$^{1/2}$)

MODEL	A	B	C	D	J	F	G	H
a	1.0	1.0	1.0	0.5	0.5	0.25	0.25	0.25
2c	3.0	5.0	7.0	1.5	2.0	0.50	0.75	1.25
Aspect Ratio (a/2c)	.33	.20	.14	.33	.25	.50	.33	.20
KI12	18.2	15.3	11.9	14.2	12.5	11.4	10.1	8.1
KI13	17.6	16.2	15.0	13.8	13.5	11.8	11.0	10.0
KI14	17.8	18.9	18.5	14.4	14.0	10.7	11.1	11.8
KI15	17.6	20.0	20.3	13.4	14.7	10.8	11.4	11.8
KI16	17.6	20.1	21.1	14.9	15.9	10.0	11.3	12.8
KI17	17.6	20.9	21.4	14.5	16.1	9.9	11.2	13.0
KI18	17.6	21.0	21.6	14.8	16.2	10.6	12.0	13.6
KI19	17.6	20.5	21.7	14.0	15.7	8.9	11.4	13.1
KI20	17.6	21.5	21.8	15.1	16.7	10.5	12.2	13.7

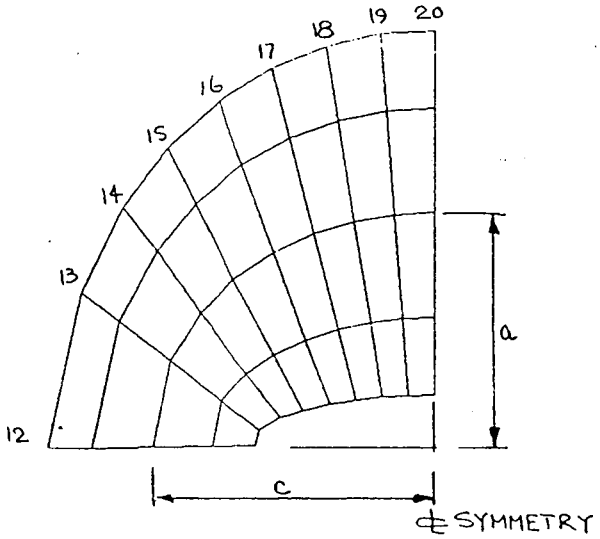

FIGURE 5.12

The Results for the Crack Sizes Analyzed in the 3-D Fracture Mechanics Model

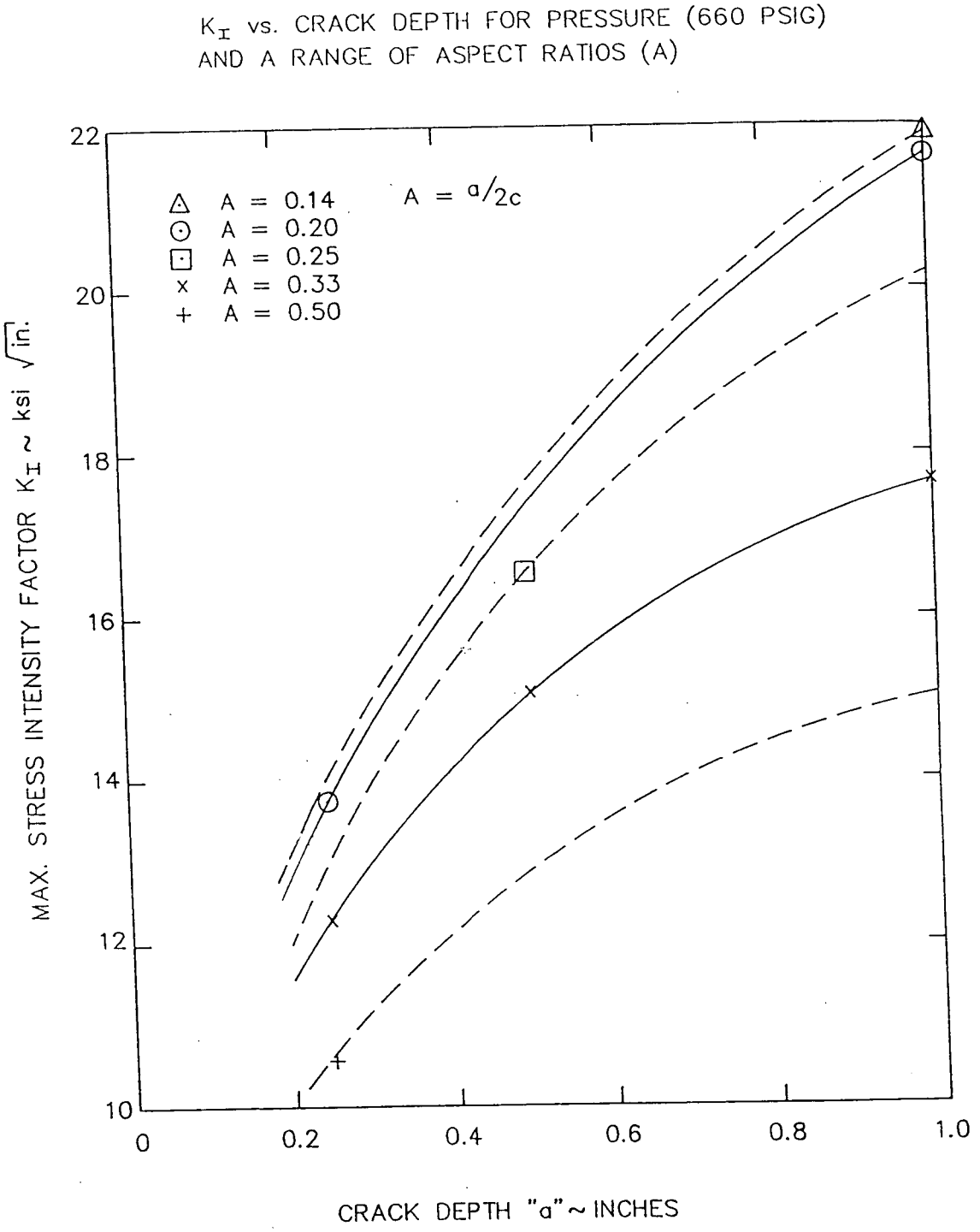

FIGURE 5.13

Maximum Stress Intensity Factor Values

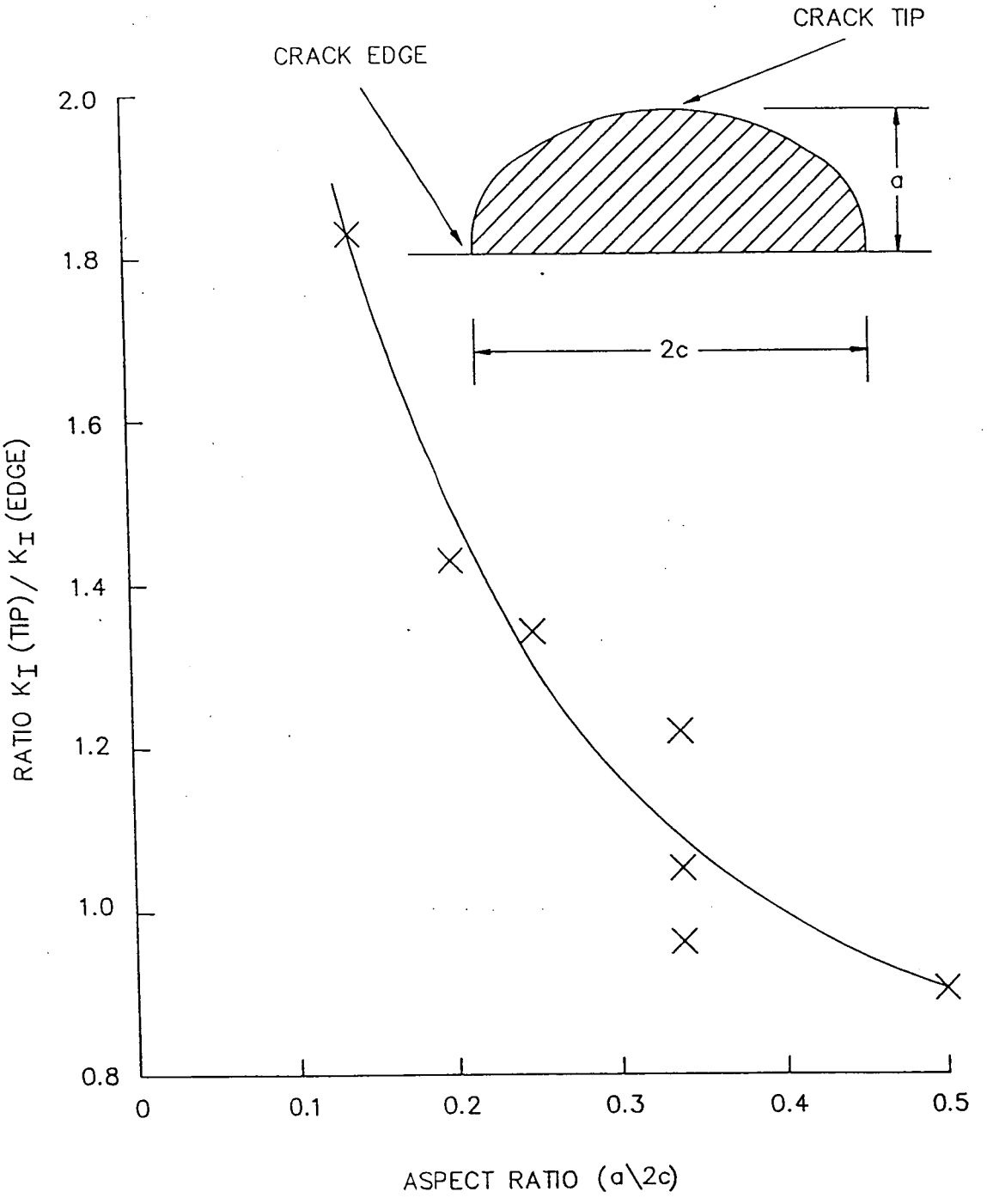

FIGURE 5.14

The Effect of Crack Aspect Ratio (a/2c) on the Distribution of the K_I Values Around the Crack Front

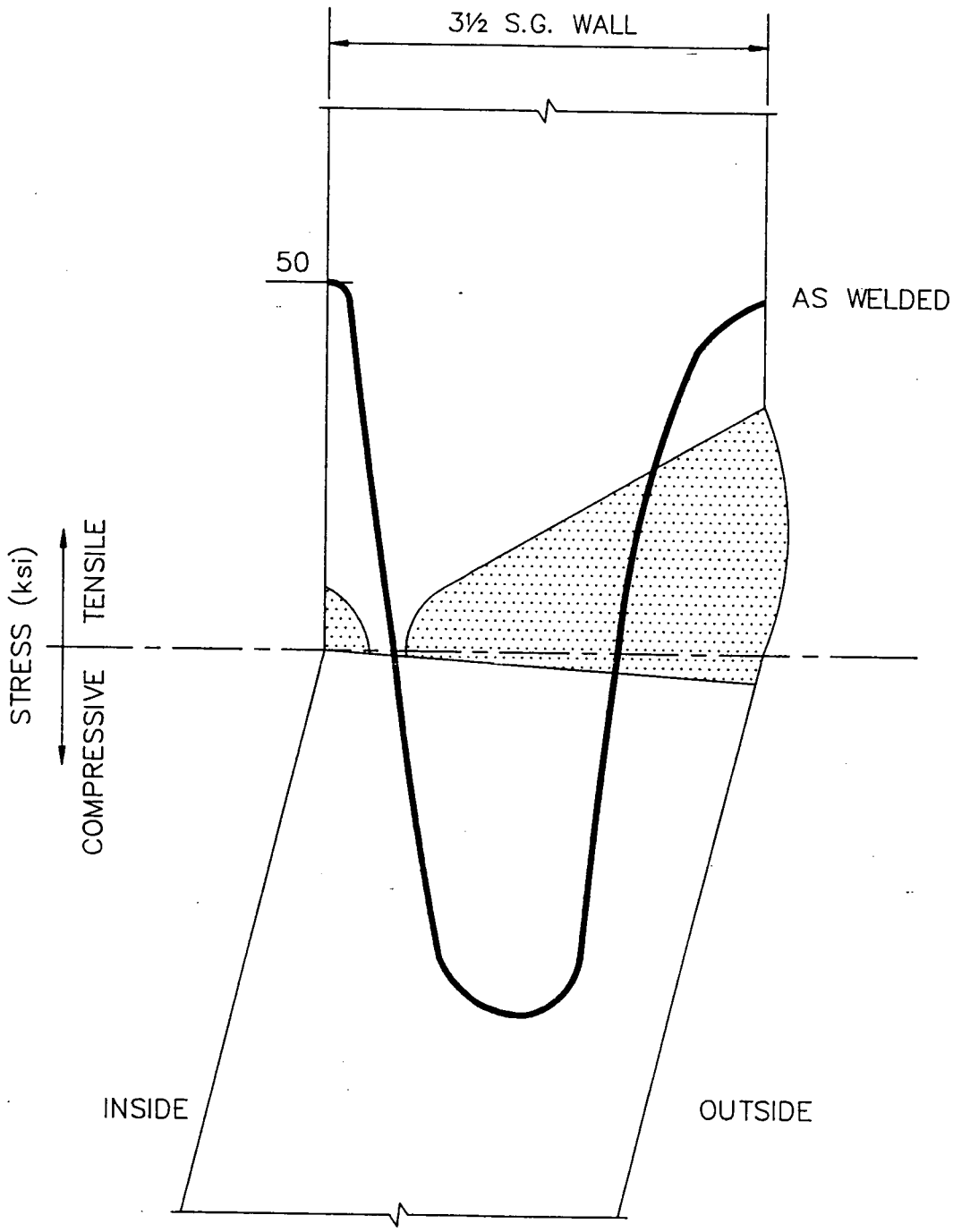

FIGURE 5.15

As-Welded Stress Distribution

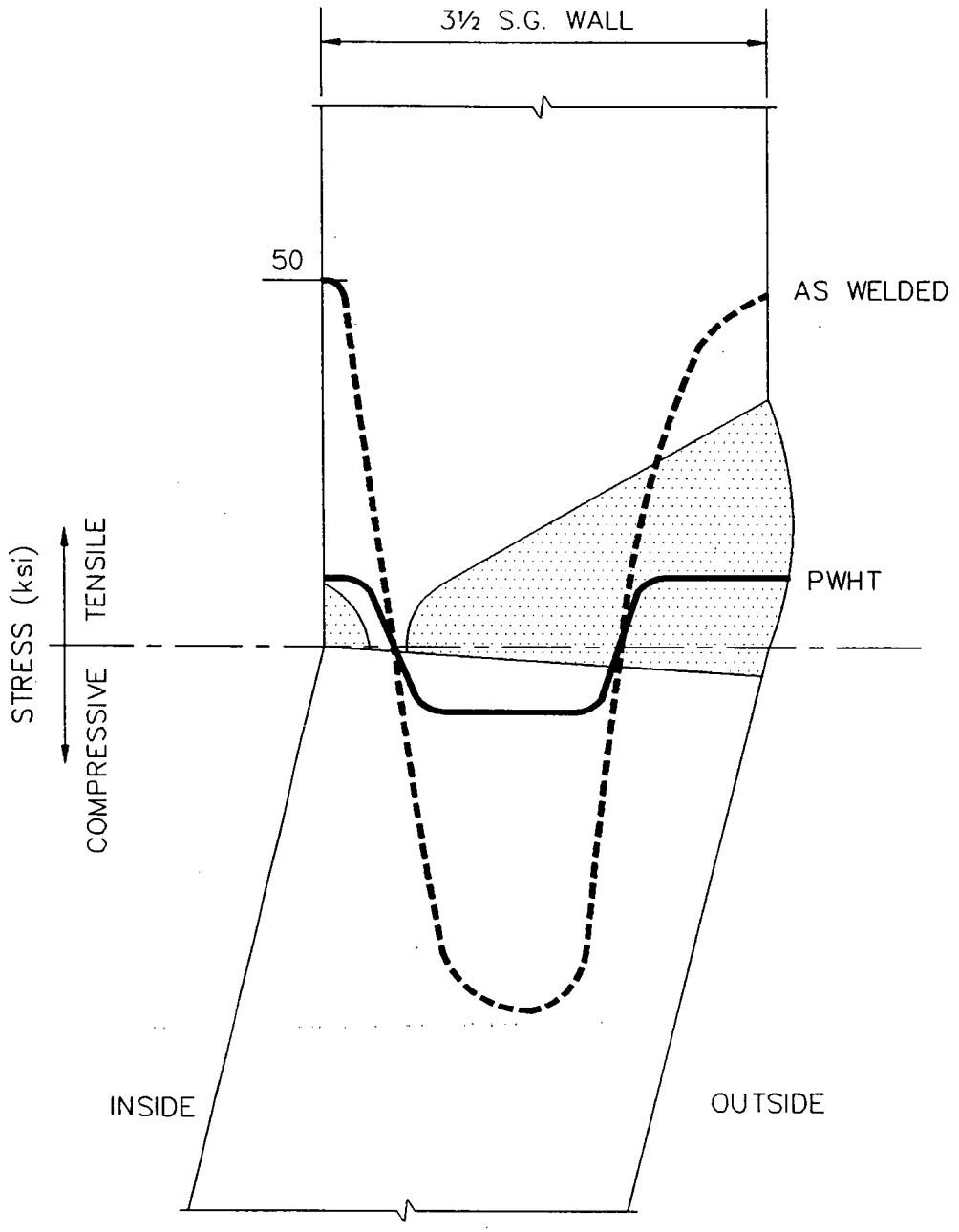

AXIAL RESIDUAL STRESS DISTRIBUTIONS THROUGH GIRTH WELD

FIGURE 5.16

The Residual Stress After Post-Weld Heat Treatment

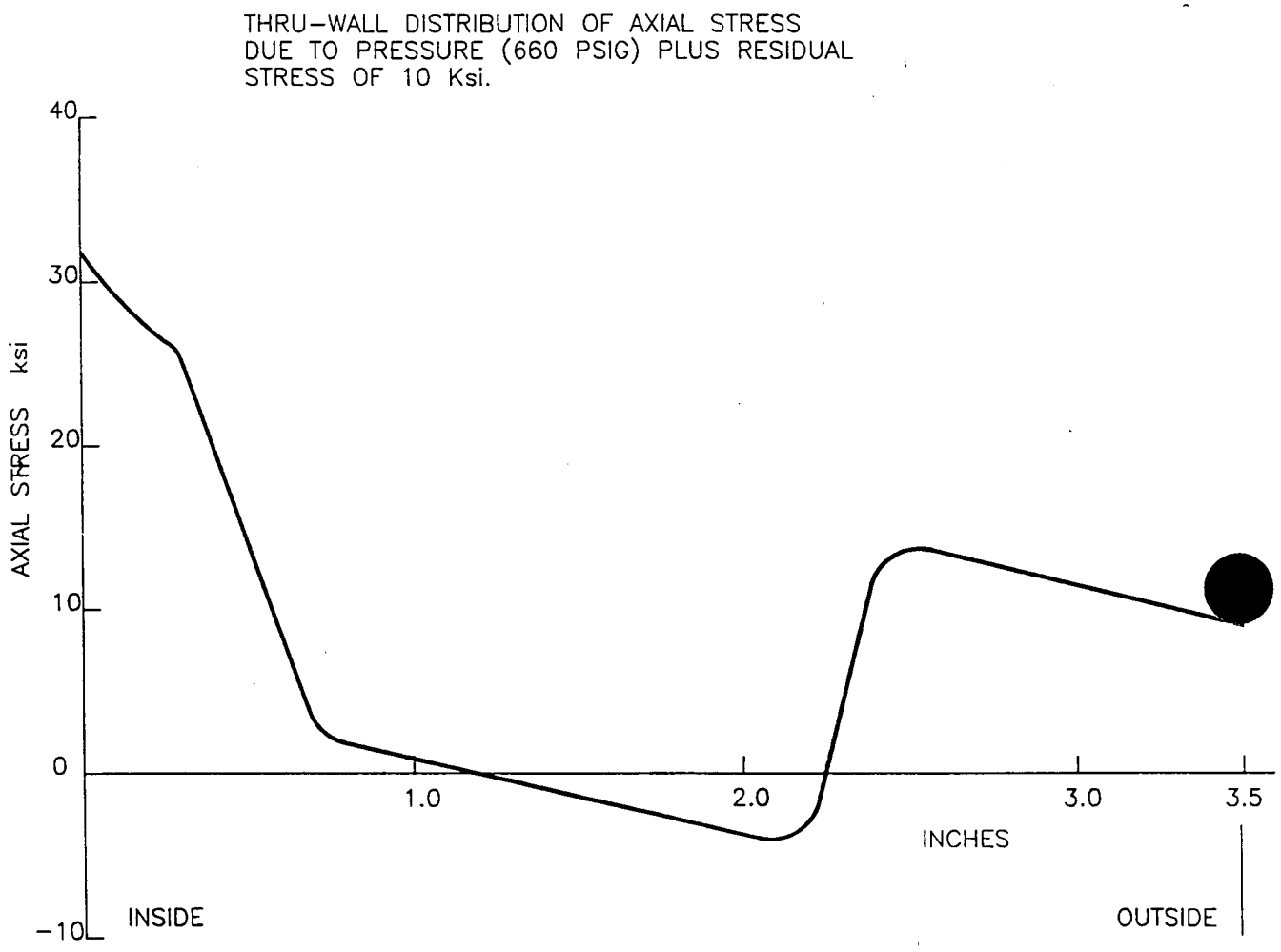

FIGURE 5.17

Combined Residual Stress and Pressure Stress
Through-Wall Axial Tensile Stress Distribution

K_I vs. CRACK DEPTH FOR PRESSURE (660 PSIG) PLUS RESIDUAL STRESS (10 Ksi) FOR A RANGE OF ASPECT RATIOS.

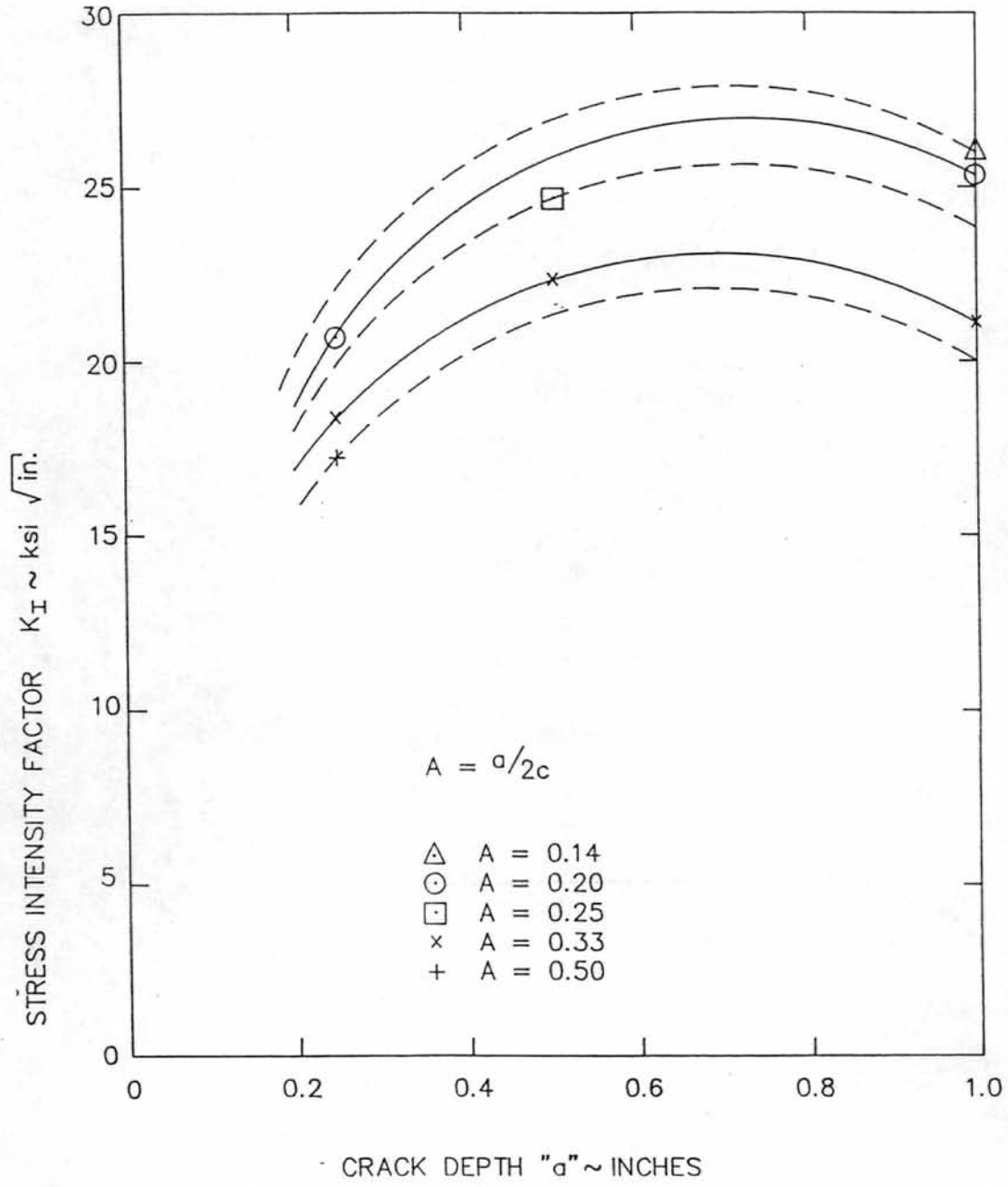

FIGURE 5.18

Stress Intensity Factors, K_I, for the Stress Distribution Shown in Figure 5.17

This page intentionally left blank.

6.0 REPAIR AND MITIGATING ACTIONS

6.1 Girth Weld

The original girth weld was removed by a robotic milling machine, producing a groove 6 inches wide and approximately 3/4 inch deep. Figure 6.1 shows the original weld, the machined groove, and the final welded contoured condition. The repair was performed remotely. Figures 6.2 through 6.4 show the operator's console for the girth weld repair robotics, the robotic milling machine and the milled welding groove, respectively. The weld metal used for the repairs was a Thyssen ER80S-G wire, specified to a sulfur content of less than 0.010%. The actual weld material sulfur content was verified to be below the specification. The chemical analysis of the filler metal is provided in Table 6.1. All of the filler metal used was manufactured from the same heat of material. The low sulfur filler metal reduces the quantity of sulfide inclusions that can be formed in the weldment. Laboratory tests have shown that sulfide inclusions in steel can develop into preferential pitting and corrosion sites. By reducing the available constituents for inclusion formation, the number of inclusions and hence, pit locations, are reduced.

The welding was performed by automatic Gas Tungsten Arc Welding, utilizing robotic welding machines. The completed welds were contoured and smoothed to provide a minimum 20 inch radius and an approximate 64 RMS finish. The radius provides a smoothly contoured transition between the upper barrel and the transition cone, thereby minimizing the geometry stress concentration effect. The radius is a significant improvement over the original condition in which the crown of the weld was readily apparent. Figures 6.5 through 6.8 show the robotic welding machine, the as-welded surfaces, and the contoured

girth weld surfaces, respectively. The smoothly contoured girth weld was examined by MT. Some MT indications were removed by light surface grinding and reinspected to verify their removal. Other areas were ground and were rewelded.

During MT examinations performed after the repair welding, MT "ghost" indications were found. These MT indications were different in nature in that they were "fuzzy" and not sharply defined as are most cracks. PT examination of some unground "fuzzy" indications did not reveal cracking. MT of the boat samples at the site failed to reproduce the "fuzzy" indications. Boat samples of these indications failed to show cracking by metallography in the Massachusetts Institute of Technology and Consolidated Edison metallurgy laboratories or by MT after removal from the steam generators. The "fuzzy" indications were due to localized magnetic permeability variations in the material as a result of the welding. All "fuzzy" MT indications were either ground out and rewelded or examined by PT to verify that cracking was not present.

Following the MT examinations, RT was performed prior to the post weld heat treatment, in accordance with the 1986 Edition of the ASME Boiler and Pressure Vessel Code Section III. UT was performed after the post weld heat treatment.

The post weld heat treatment was performed at 1125°F ± 25°F for 4 hours. The feedwater pipes and instrument lines were cut to permit steam generator thermal growth during the heat treatment. Following the post weld heat treatment, MT examinations were performed on the repair welds. UT was performed on the girth weld to complete the repairs. Additional UT examinations were conducted to provide a baseline for future girth weld inspections.

6.2 Inspection Ports

The crack in Inspection Port 2 of Steam Generator 24 was ground out and removal verified by PT. The repair of the grind out to the original diameter was accomplished by the half-bead welding technique using E8018-C3 filler metal. A steam cut on the gasket seating area was also repaired by the same technique. The repairs were examined by dry powder MT. The half-bead weld repairs are described in the ASME Boiler and Pressure Vessel Code, Section III, NB 4622.9.

6.3 Feedwater Nozzle Sealing Sleeve

A feedwater nozzle sealing sleeve assembly was installed to reduce the amount of feedwater which leaks past the existing thermal sleeve into the feedwater nozzle bore. Leakage of cold feedwater has resulted in thermal fatigue of the feedwater nozzle under the thermal sleeve during periods of cold feedwater or auxiliary feedwater injection.

The sealing sleeve, Figure 6.9, was installed in all four steam generator feedwater nozzles after the feedwater pipe at the feedwater nozzles were cut for the girth weld post weld heat treatment.

The sealing sleeve was installed as follows. Four stop blocks were welded onto the existing carbon steel thermal sleeve. A pad ring was then welded to the thermal sleeve. The pad ring provides the sealing surface for the sealing ring and was therefore machined to be concentric with the sealing sleeve. The sealing sleeve assembly, with a compressed spiral spring and sealing ring, was inserted into the thermal sleeve. The sealing ring was released to press against the pad ring. A water cooling coil device was then inserted into the thermal sleeve/sealing sleeve

to provide cooling to prevent relaxation of the spring during the post weld heat treatment of the sealing sleeve to the feedwater nozzle weld. The sealing sleeve was then welded to the feedwater nozzle. The feedwater nozzle was also welded to a short length of feedwater pipe. The purpose of the short feedwater pipe section was to permit post weld heat treatment of the two welds to the feedwater nozzle with the cooling device in place. Examinations of the welds at various stages of assembly was by MT.

6.4 Other Plant Actions

6.4.1 Oxygen Control of Auxiliary Feedwater

Oxygen control has been augmented. During normal plant operation, low levels of oxygen in steam generator feedwater is maintained by operation of the condenser as a deaerator. At full power, the dissolved oxygen in the feedwater averages approximately 2 ppb. By comparison, the industry guideline limit is 10 ppb. However, during hot standby, water is drawn from the Condensate Storage Tank (CST) which, in the past, has had a higher oxygen content. A modification has been completed which now "blankets" the water in the CST with nitrogen. The nitrogen is maintained at a slightly positive pressure during all plant conditions preventing the entry of air into the CST.

Hydrazine is also added to the CST. The hydrazine provides additional scavenging of any oxygen in the CST and also increases the pH during auxiliary feedwater injection.

6.4.2 Copper Removal Program

A copper removal program has been in progress for several years. The Moisture Separator Reheaters (MSR) and high pressure and intermediate pressure feedwater heaters have been retubed along with one third of the condenser. The remaining condensers and the low pressure heaters are scheduled for replacement in the 1993 and the 1995 outages. This will remove all copper bearing equipment from the feedwater system.

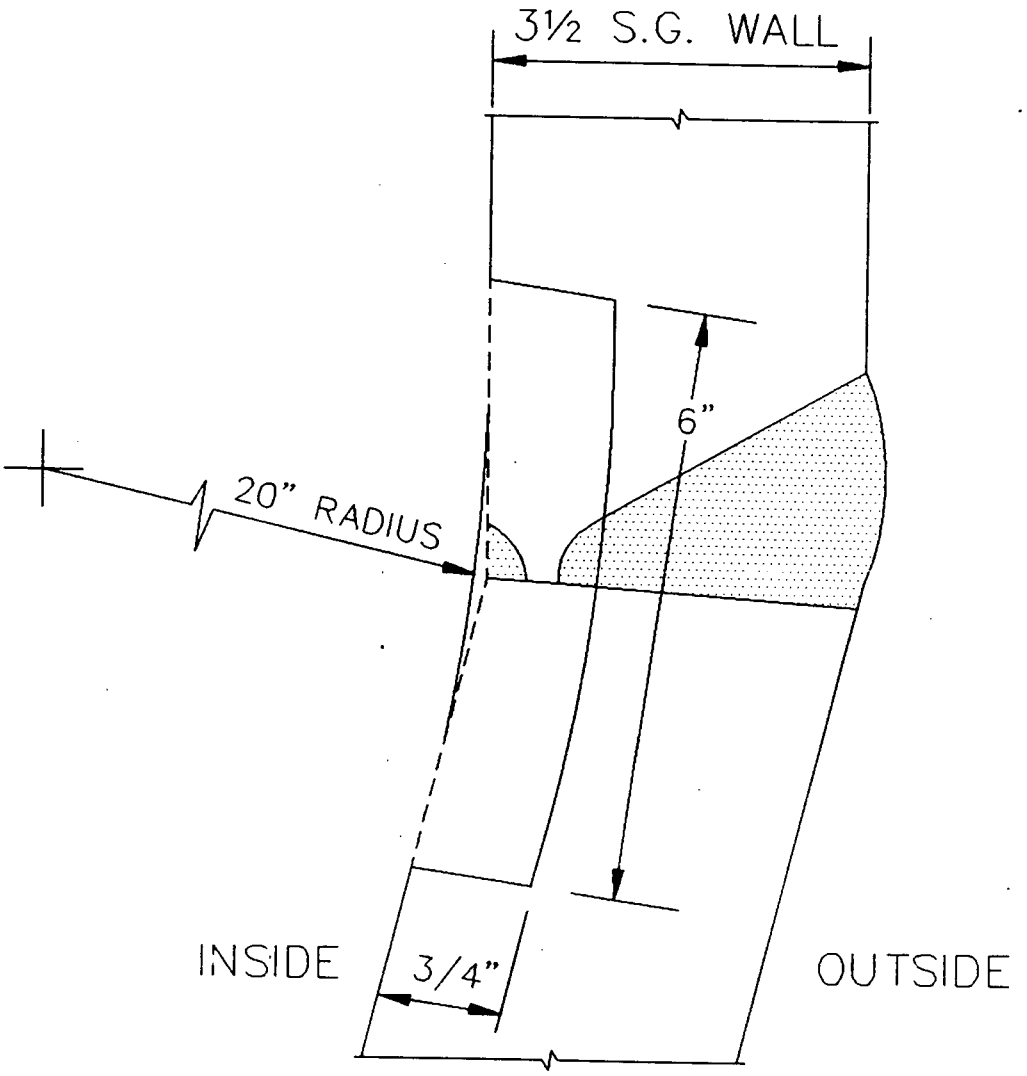

FIGURE 6.1

Girth Weld Showing 20 Inch
Contour Radius

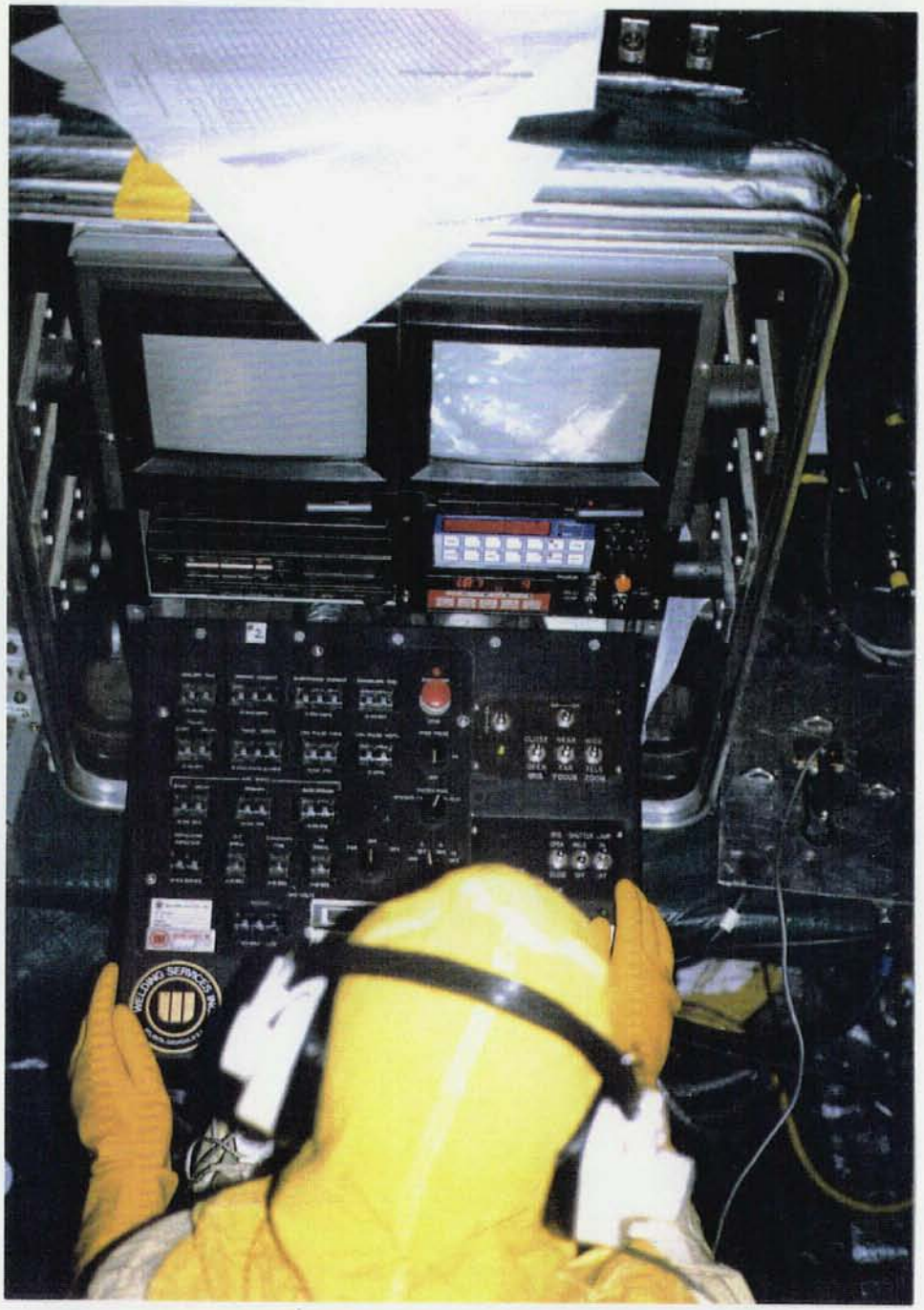

FIGURE 6.2

Operator's Control Console for Robotics

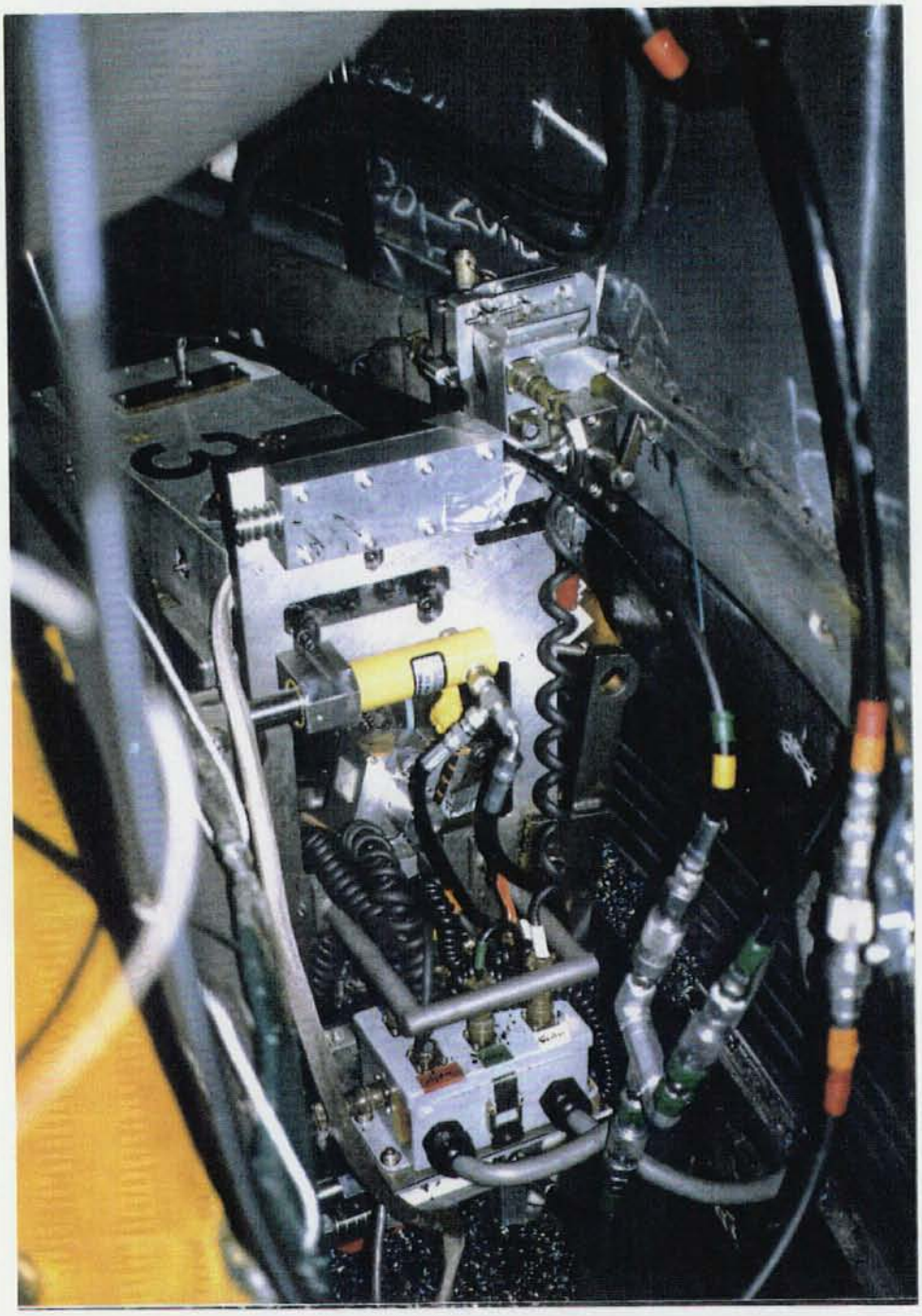

FIGURE 6.3

Robotic Milling Machine

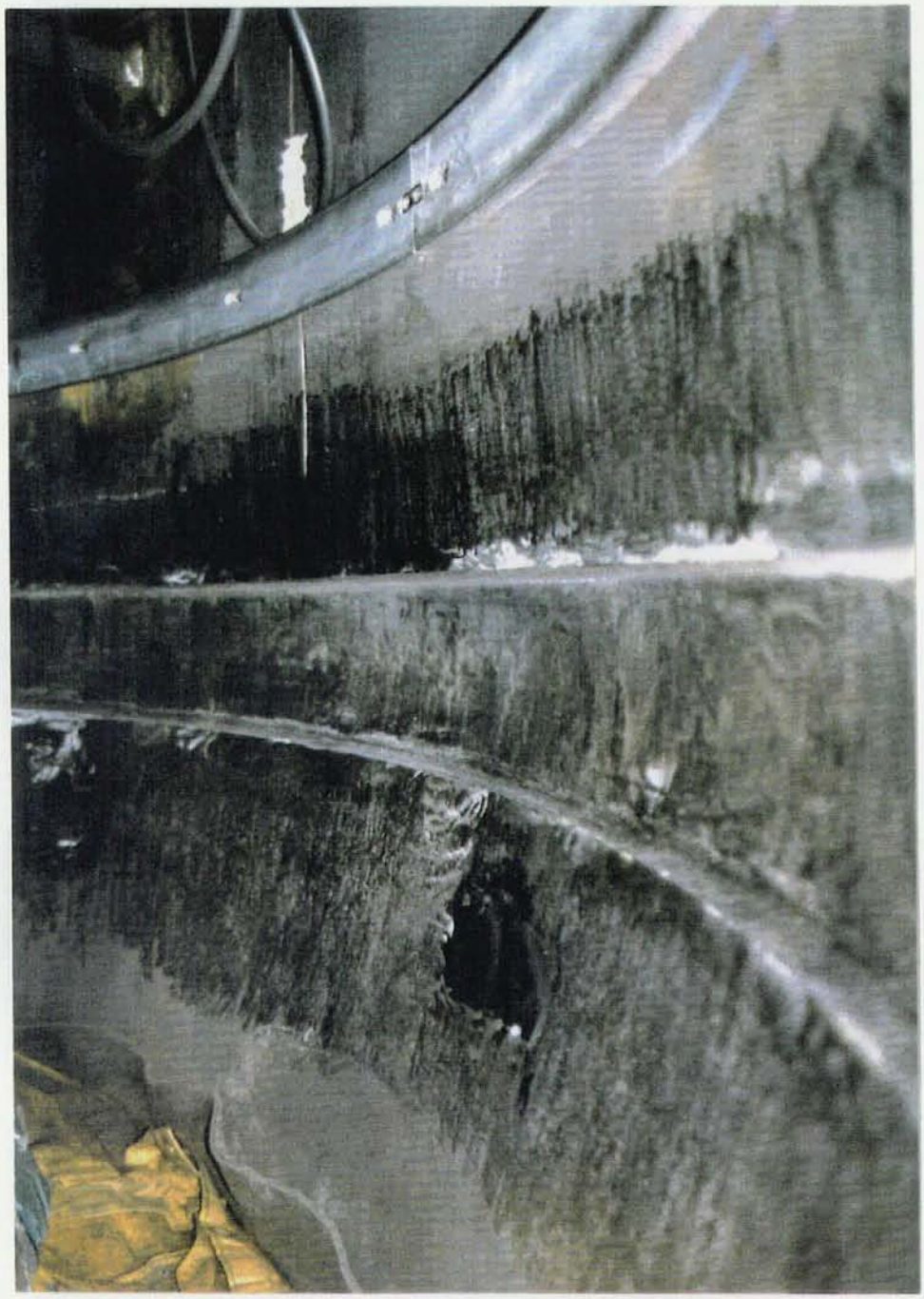

FIGURE 6.4

Milled Welding Groove

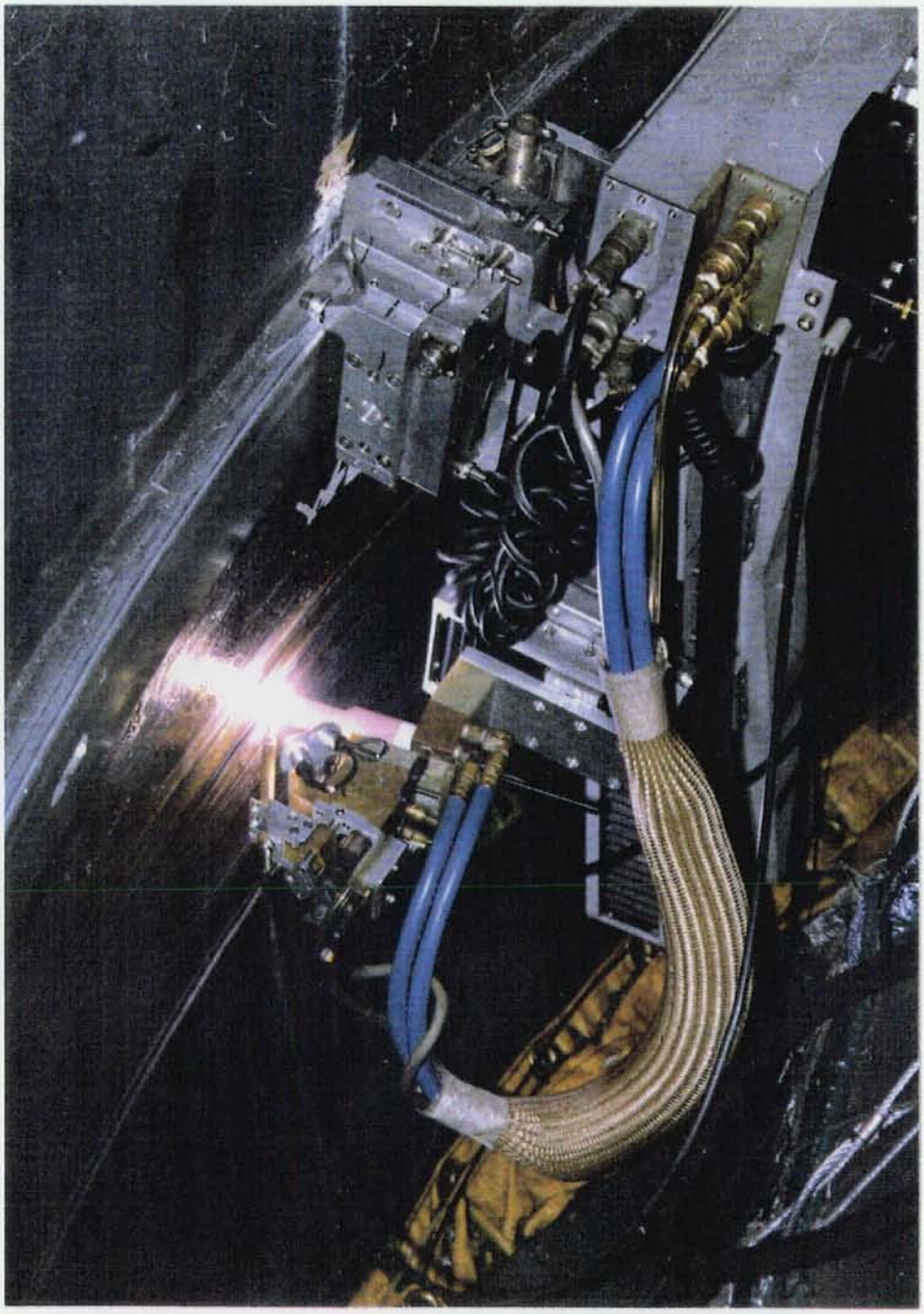

FIGURE 6.5

Robotic Welding Machine

FIGURE 6.6

Girth Weld As-Welded Surface

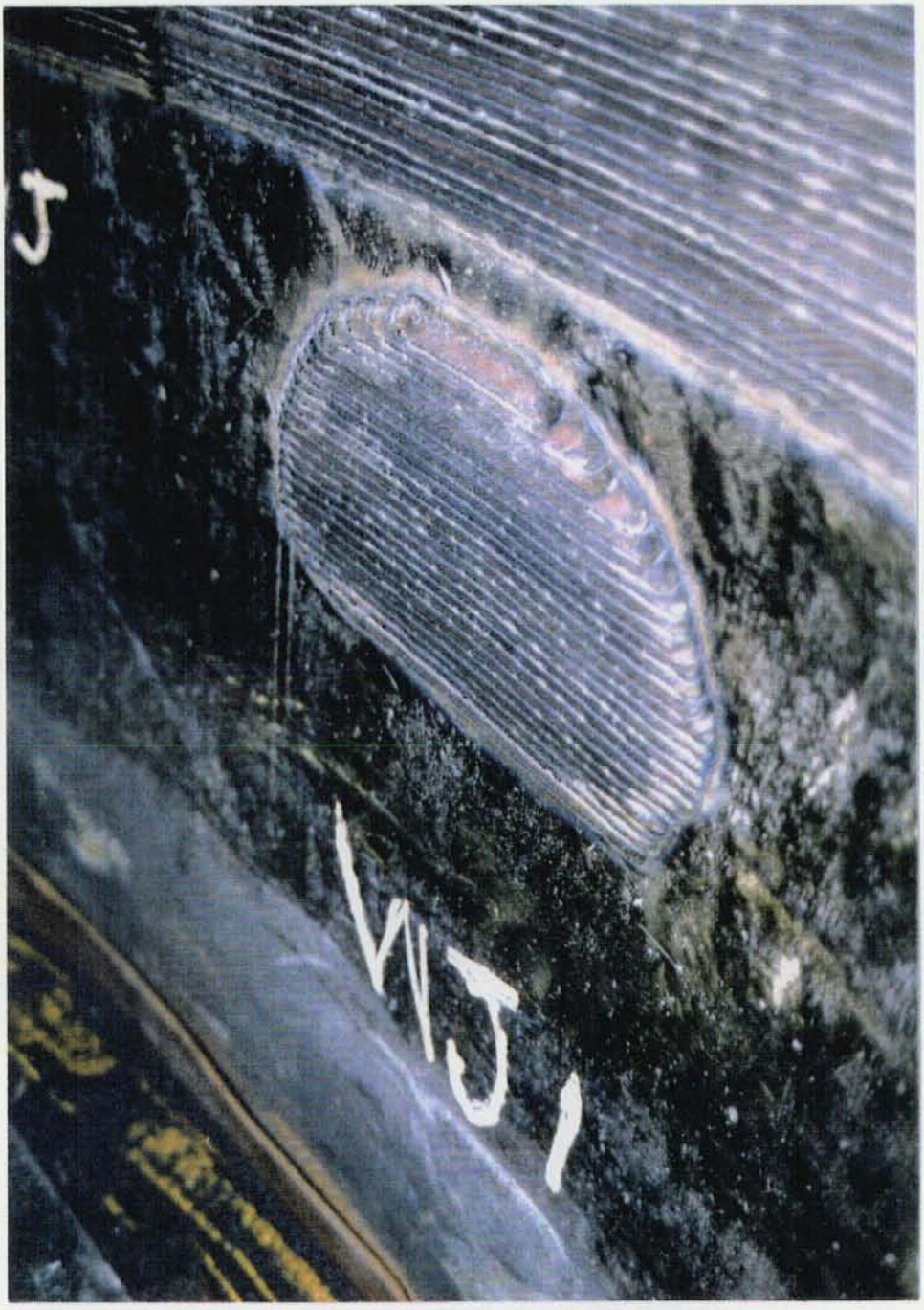

FIGURE 6.7

Below Girth Weld As-Welded Surface

FIGURE 6.8

Girth Weld Surface After Contouring

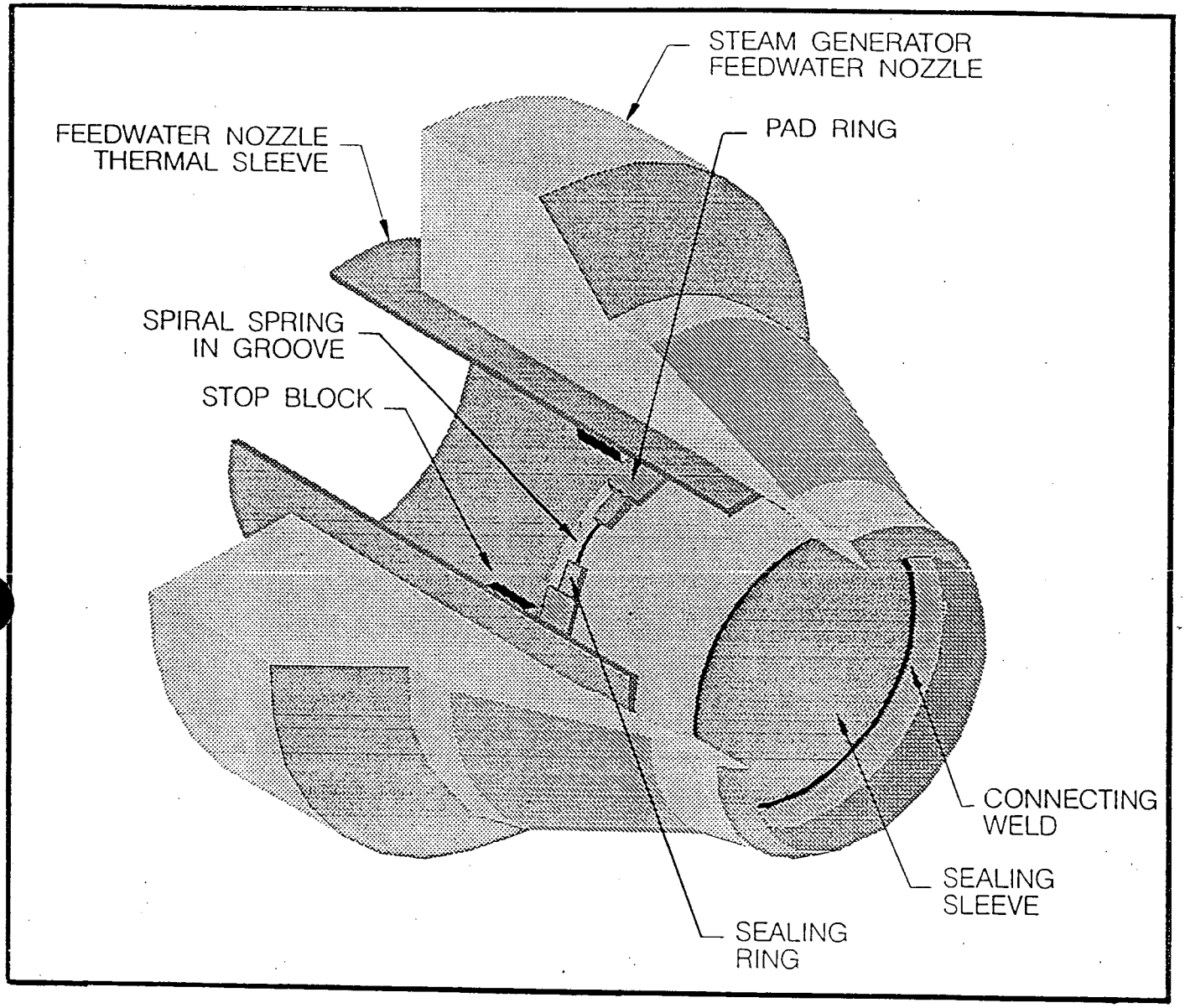

FIGURE 6.9

Feedwater Nozzle Sealing Sleeve

Filler Metal Mill Certification Chemical Analysis

ER80S-G

Thyssen Heat #485936

Element	Percent
Carbon	0.115
Silicon	0.58
Manganese	1.10
Chromium	0.04
Molybdenum	0.46
Phosphorus	0.14
Sulfur	0.005
Aluminum	0.014
Arsenic	0.004
Copper	0.06

TABLE 6.1

7.0 QUALIFICATION OF THE GIRTH WELD REPAIR

The region of the steam generator shell which includes the girth weld provides the pressure boundary for the secondary side of the steam generator. This region of the shell is subjected to normal operating loads including pressure, the secondary side fluid transients, and seismic loadings. The repaired weld must satisfy the requirements of the ASME Code including full consideration of fatigue loadings. This section documents the qualification of the steam generator shell in the region of the repaired girth weld to the requirements of the ASME Code.

7.1 Qualification Procedure and Loadings

The girth weld is a location of a structural discontinuity between the upper cylinder and the transition cone. The stresses at the girth weld are evaluated for compliance with the requirements of ASME Boiler and Pressure Vessel Code Section III. Shakedown to elastic behavior is checked by comparing the primary-plus-secondary stress range to the allowable value of $3S_m$. The fatigue usage factor, based on the alternating total stress, is compared to the allowable value of 1.0.

The pressure and thermal transients on the secondary side of the steam generator, and their associated number of cycles, are summarized in Table 7.1. The temperature changes and the rates of those changes were reviewed in detail and the severity of the transients evaluated. The most significant thermal stresses result from the Feedwater Cycling, the Reactor Trip, and the Loss of Power transients.

The secondary shell of the steam generator, including the region of the subject girth weld, is classified as an ASME Class A nuclear pressure vessel. The qualification is

performed in accordance with the requirements of the original code of records, the ASME Boiler and Pressure Vessel Code, Section III, 1965, titled "Nuclear Vessels". This edition of the Code included well developed fatigue requirements for evaluation of pressure boundaries which are very similar to the requirements in use today. The design pressure of the secondary side of the shell is 1,085 psig and the design temperature is 600°F.

7.2 Method of Analysis

A finite element model of the steam generator girth weld was prepared. The model represented the repaired condition including the 20 inch blend radius as shown in Figure 7.1. The ANSYS computer code was utilized. The model is an axisymmetric finite element model of the steam generator shell. The model extends in the axial direction 48 inches above the girth weld and 75 inches below the girth weld. The number of elements through the thickness is greater at the region of the girth weld where additional detail is required. Eight elements are provided through the thickness at the girth weld. Figure 7.2 shows the cross-section of the model with the repaired girth weld geometry, and Figure 7.3 shows the finite element mesh at the region close to the girth weld.

For the pressure case, a unit pressure load of 100 psi was applied to the inside surface of the shell and an equivalent axial pressure load boundary condition was applied to the top edge of the model. Displacement conditions at the upper and lower boundaries permitted the shell to move freely in the radial direction. The lower boundary was restrained in the direction of the Y-axis. Stresses at the specific pressures required for the evaluation were obtained by ratioing the stress values obtained for the 100 psi case.

For the thermal cases, the time varying fluid temperature was applied to the inside surface of the steam generator shell. Temperature solutions for the thermal transients were obtained over the time of the transient and time histories of the inside surface stress at the girth weld were prepared. To determine the maximum secondary stresses due to the thermal transients, the equivalent linear stress routine of ANSYS was used to plot the inside surface secondary stress versus time. The maximum secondary-plus-peak stress at the inside surface of the girth weld was obtained from plots of the ANSYS inside surface thermal stress results versus time.

7.3 Effects of the Weld Blend Radius

The effects of the repair weld contour radius was evaluated. Various weld radii were considered as shown in Figure 7.4. The use of the 20 inch radius increased the thickness of the shell by 0.15 inch. The pressure stress and the thermal stress for these different cases were evaluated. Figure 7.5 shows the comparison of the pressure stress for the original configuration and the 20 inch radius configuration. This is a plot of the axial surface stress variation in the axial direction with the centerline of the girth weld at the 3 inch location. Note that the maximum pressure stress, which occurs at the centerline of the girth weld, is 20,600 psi for the original configuration and 16,200 psi for the 20 inch radius repaired configuration. This reduction in the stress is largely due to the greater thickness and the reduced stress concentration.

The reactor trip transient was also analyzed to demonstrate that the increase in thickness does not significantly increase the thermal stresses. The maximum stress for the 20 inch radius case was 15% lower than for

the original configuration. This reduction is largely due to the reduction in the stress concentration.

Comparison of these analyses shows that the stresses due to pressure and thermal transients are lower for the repaired weld than for the original design.

7.4 Results

7.4.1 Pressure Load at 100 psi

The stress results from the unit pressure load case are summarized in Figures 7.6 through 7.9. Figures 7.6 and 7.7 show the variation in the axial direction of the axial and hoop stress components. The maximum value of these stresses occurs very close to the center of the original girth weld. Figures 7.8 and 7.9 show through-wall plots of the axial and hoop stress for the location at which the maximum stress value occurs.

7.4.2 Thermal Transients

Representative stress results from the thermal transient analysis are summarized in Figures 7.10 and 7.11. The reactor trip thermal transient stress results without internal pressure are shown. Plots are given for the time variation of the axial stress at the inside surface of the girth weld and from these distributions, the maximum stress and the time at which the maximum stress occurred was obtained. The through-wall axial distributions are provided at the time at which the maximum stress occurs. These results were used for the stress range in the fatigue evaluation.

7.4.3 Code Stress Evaluation

The ASME Code evaluation was performed and the results of the evaluation are summarized in Table 7.2. As shown in this summary, the repaired girth weld meets all applicable stress and fatigue requirements of the ASME Code.

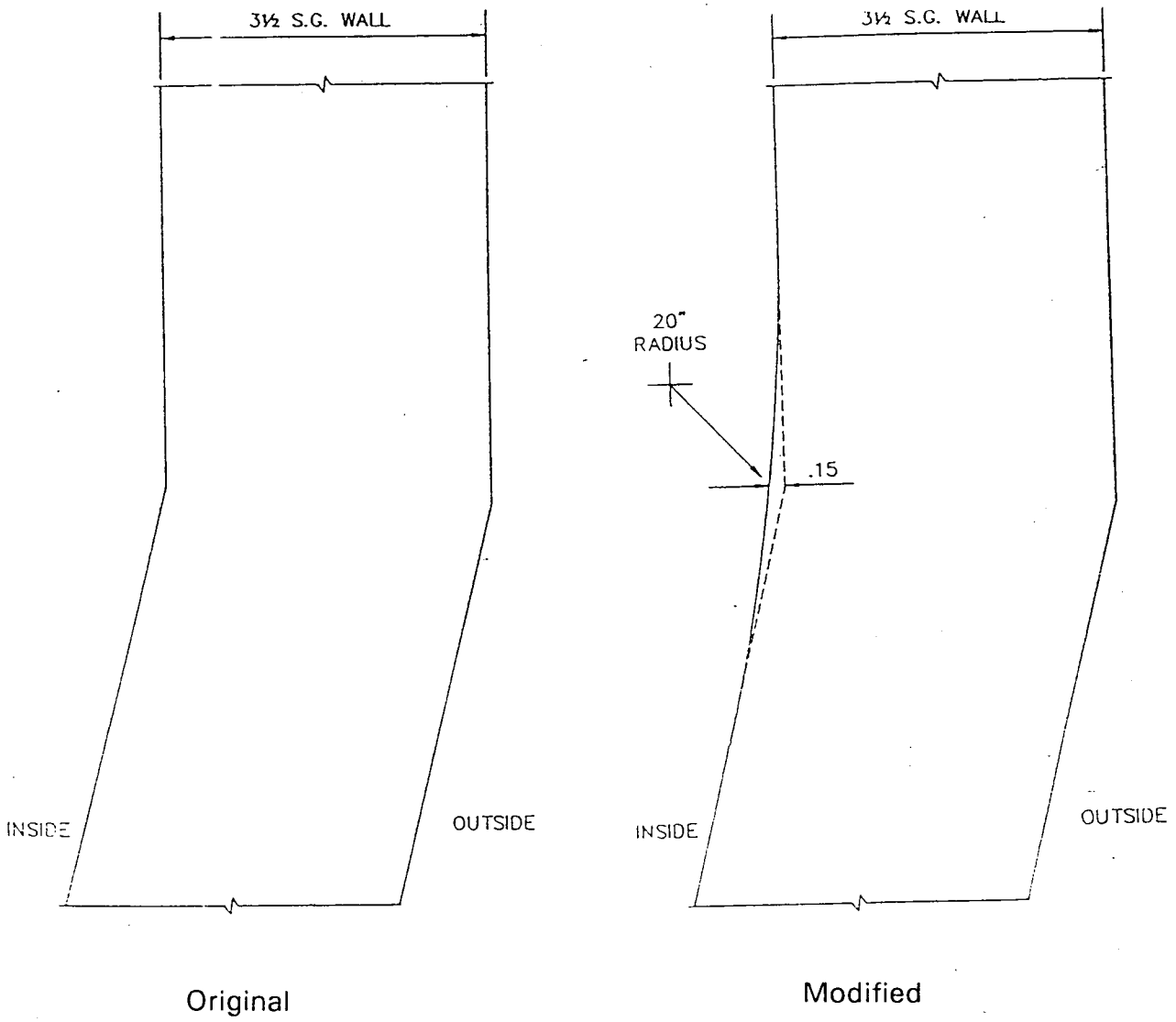

FIGURE 7.1

Cross-Section of Original Girth Weld and Modified Girth Weld

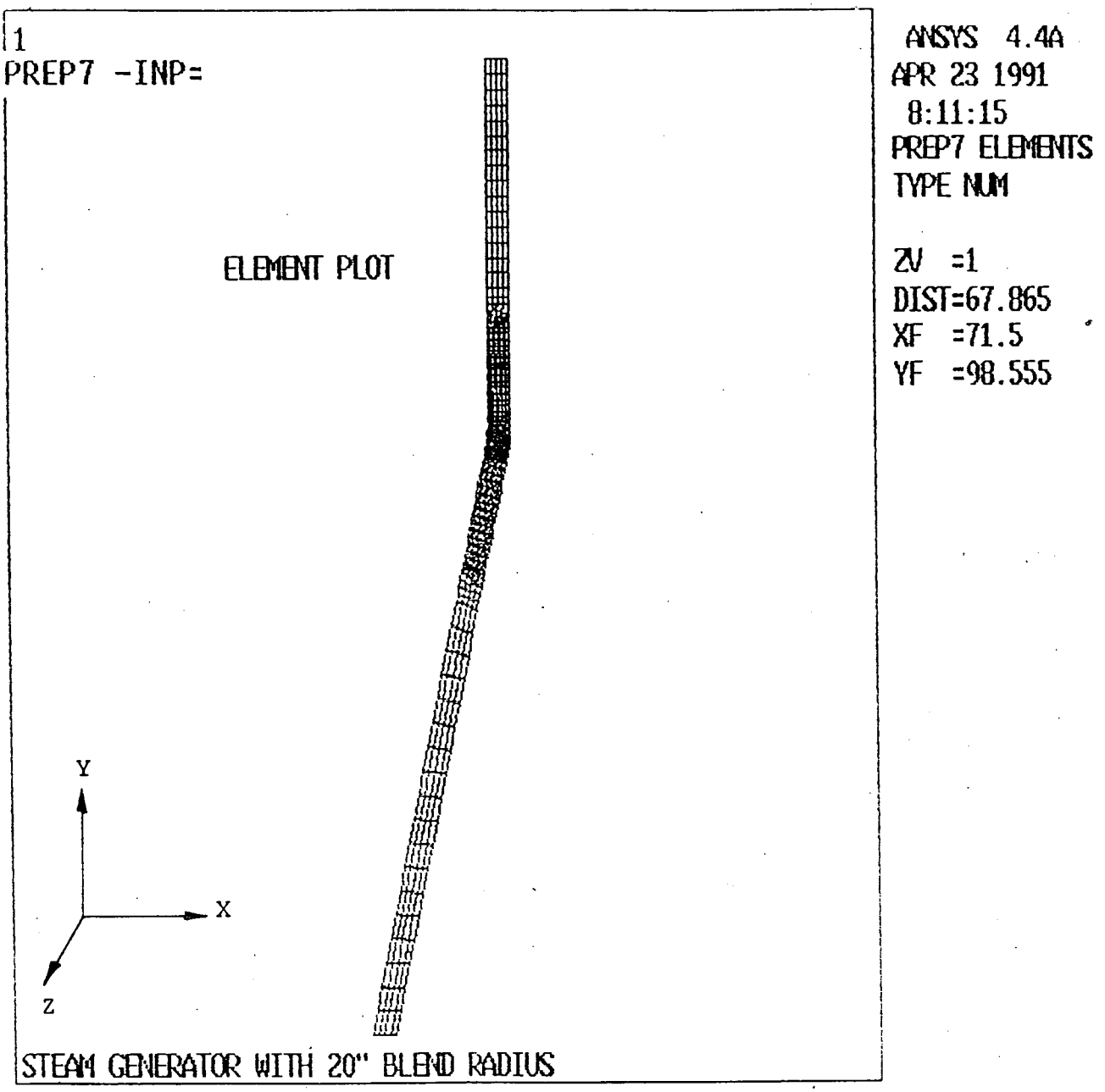

FIGURE 7.2

Axisymmetric Finite Element Model

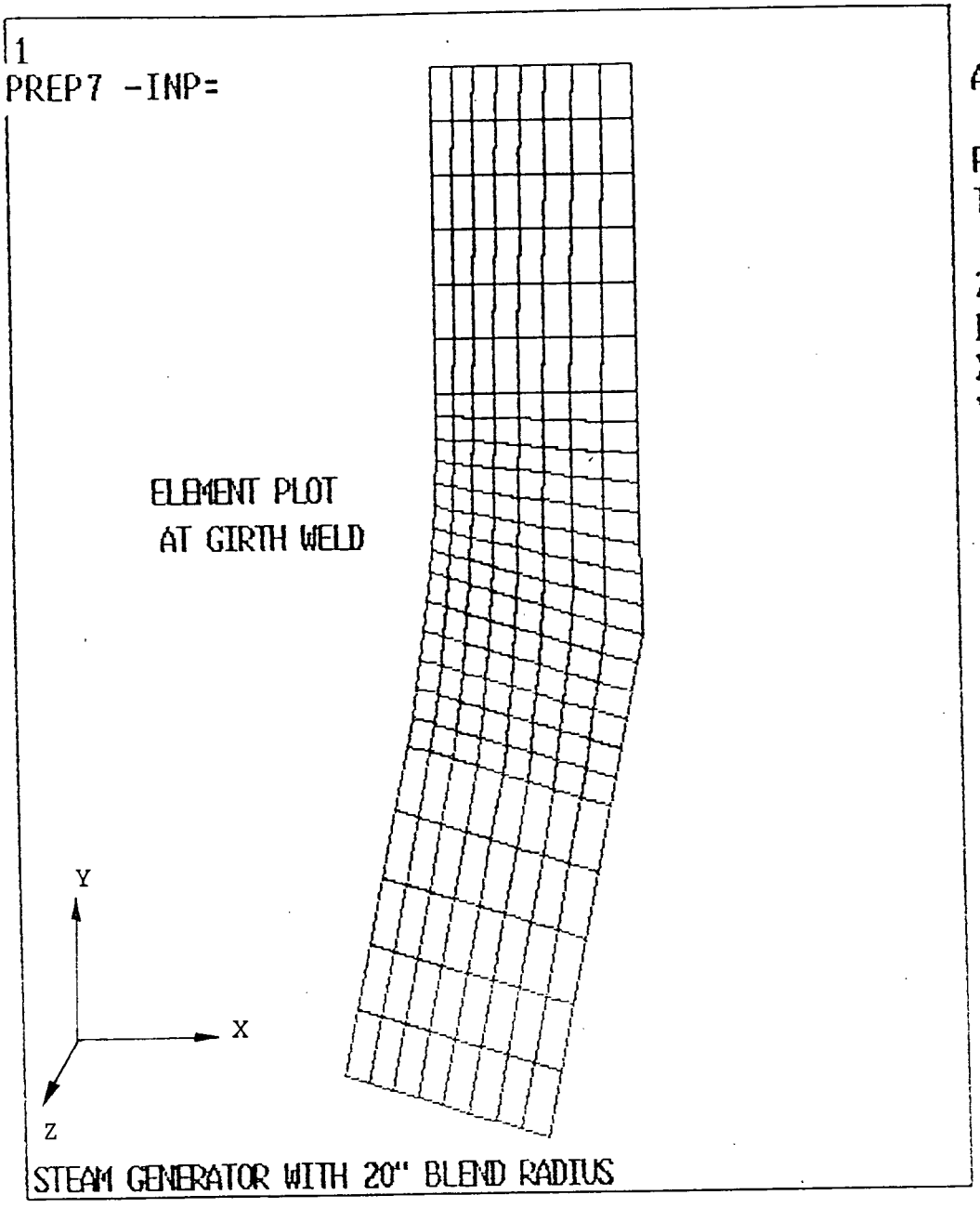

FIGURE 7.3

Finite Element Model Mesh at Girth Weld

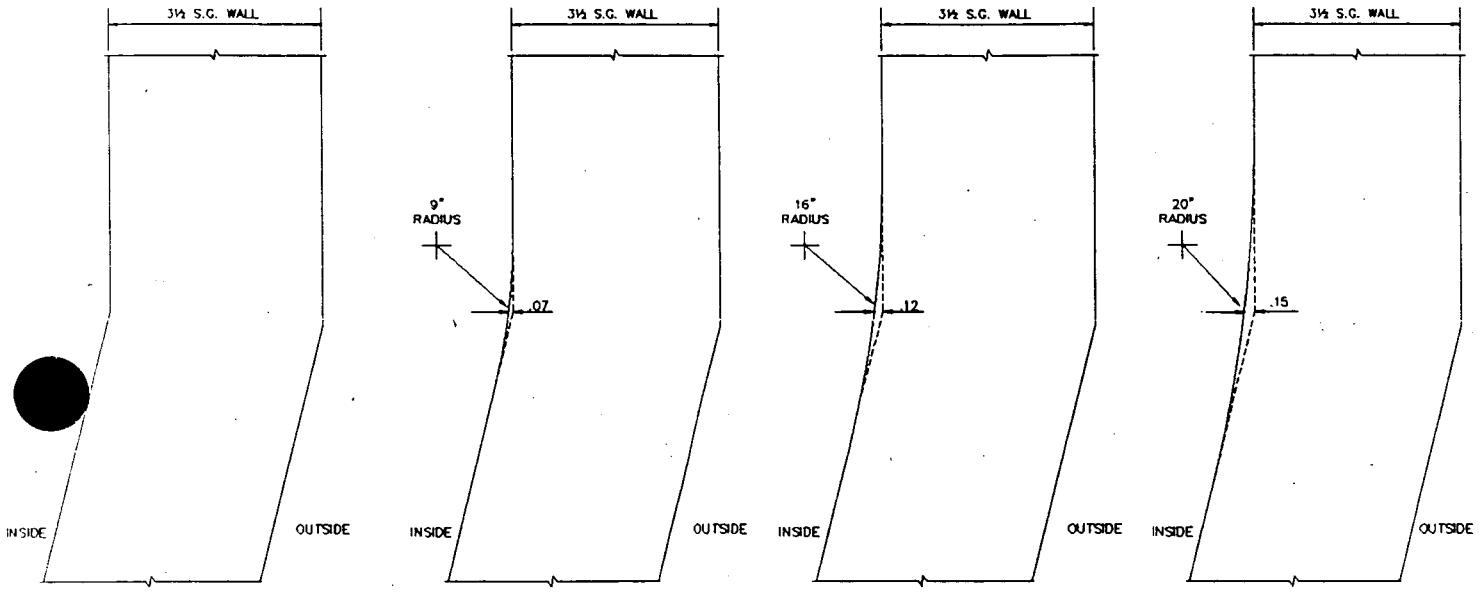

FIGURE 7.4

Variation in Girth Weld Contour Radius

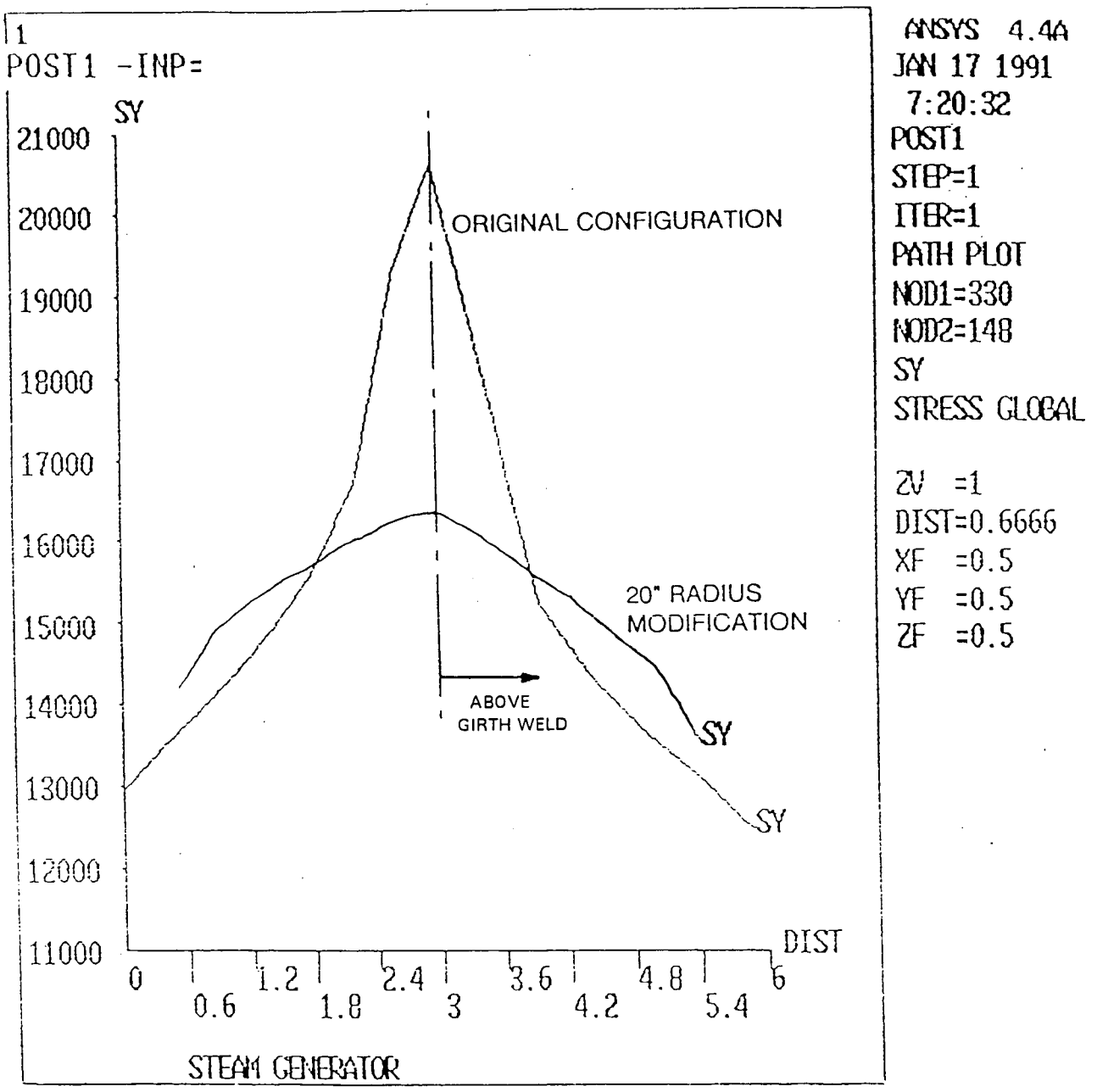

FIGURE 7.5

Effect of Girth Weld Contour Radius on
Pressure Stresses

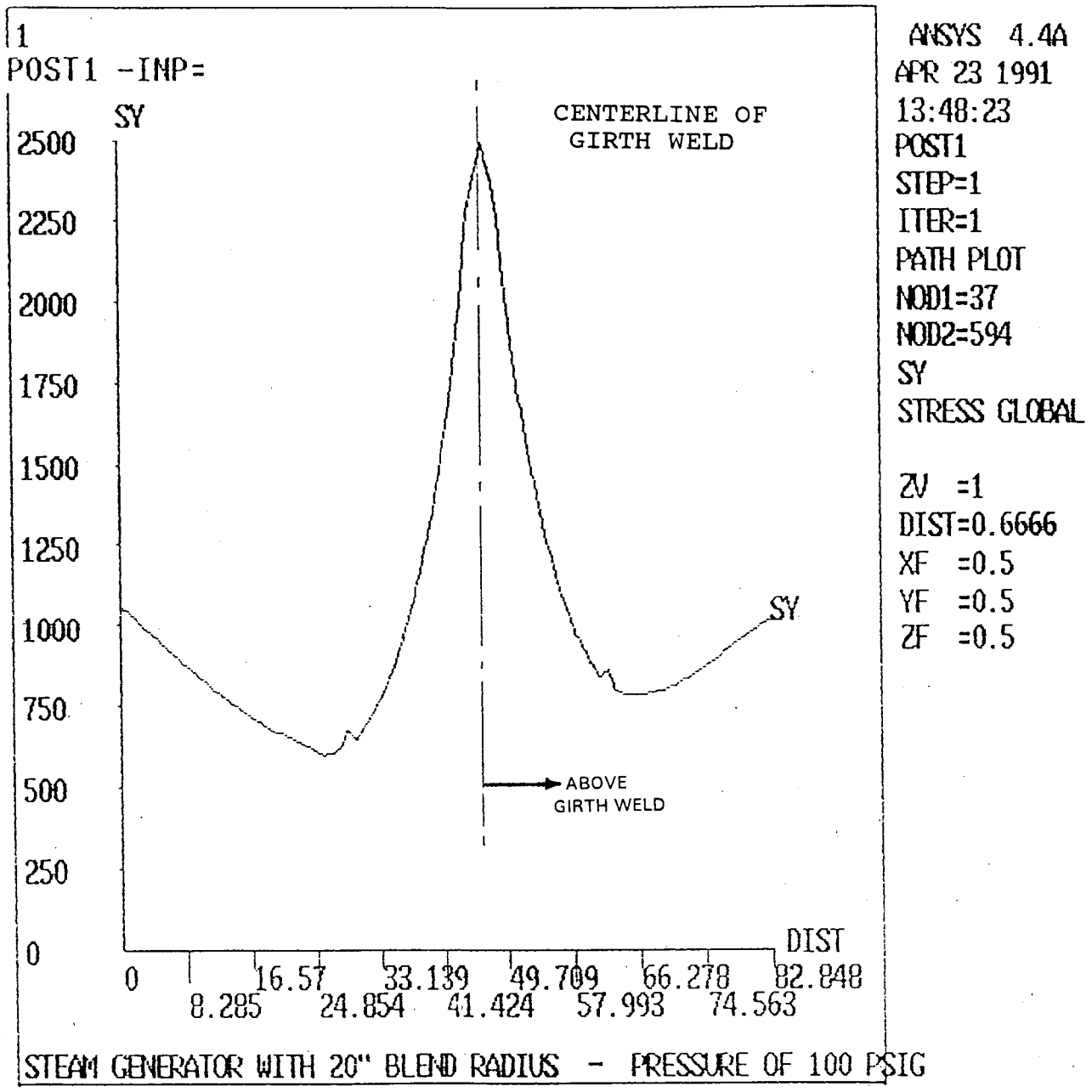

FIGURE 7.6

Axial Variation (inches) of Axial Stress (SY) for Unit Pressure Load (100 psi). Stress for Other Pressures Obtained by Ratioing

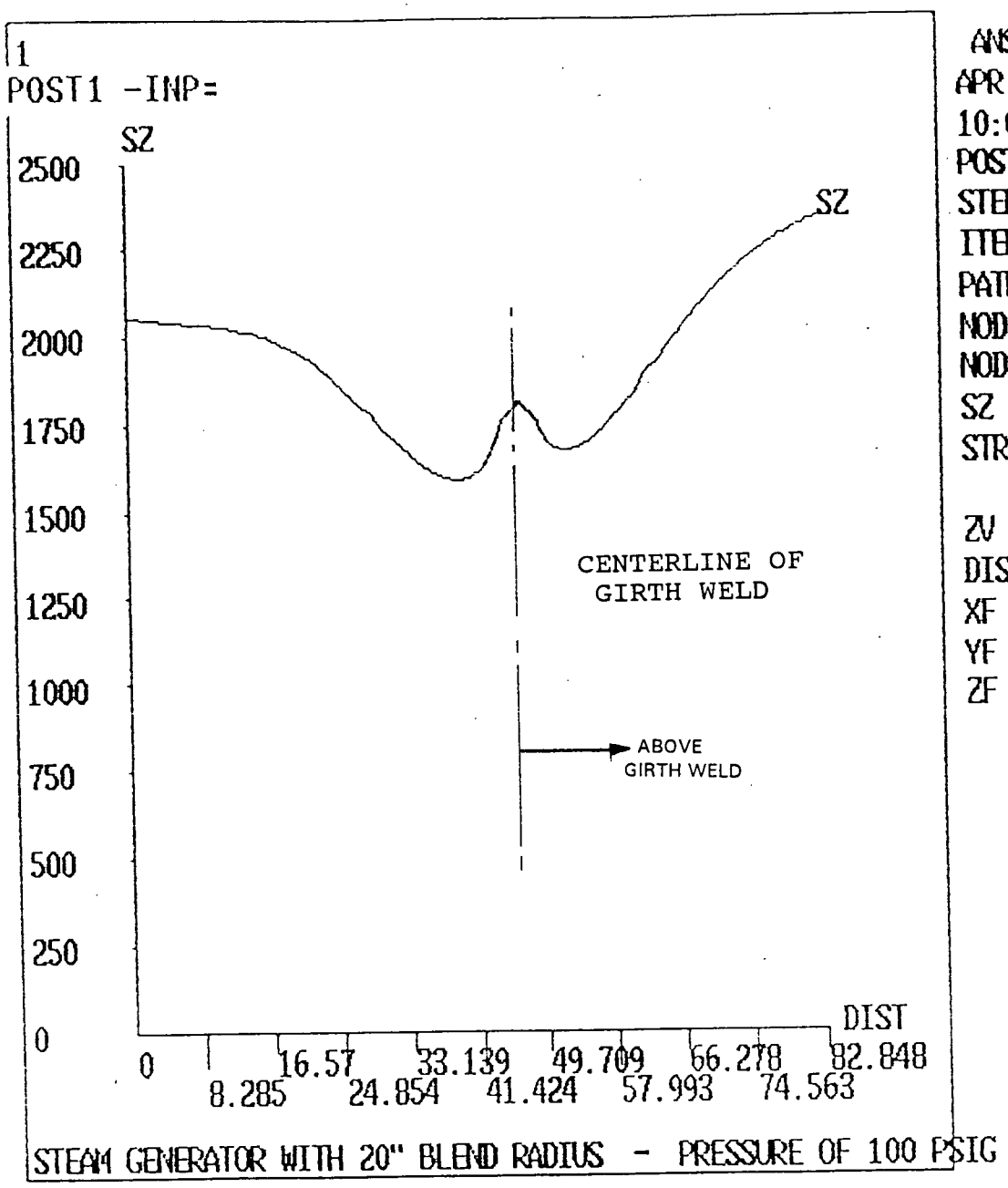

FIGURE 7.7

Axial Variation (inches) of Hoop Stress (SZ) for Unit Pressure Load (100 psi). Stress for Other Pressures Obtained by Ratioing

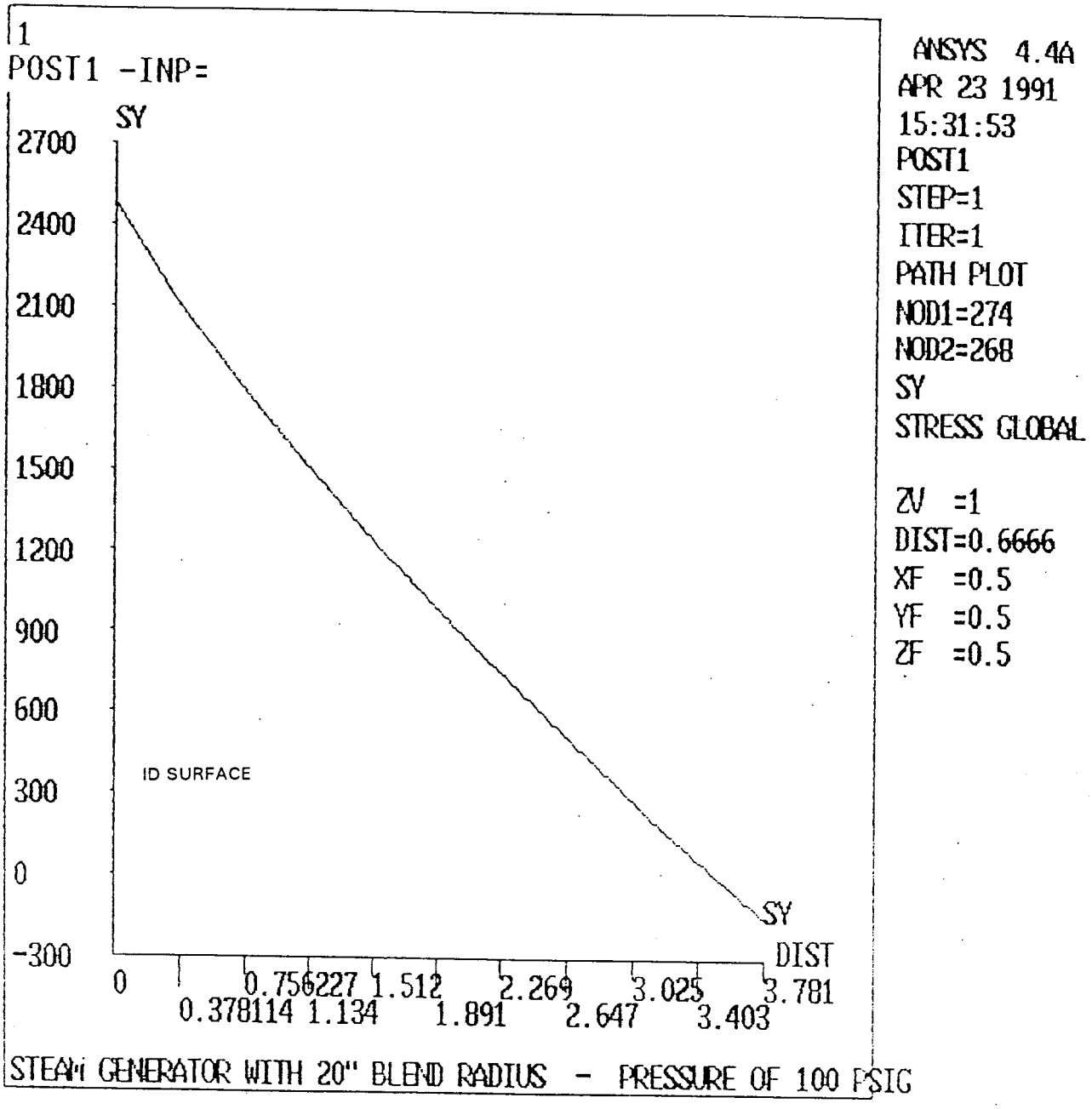

FIGURE 7.8

Through-Wall Distribution at Axial Location of Maximum Axial Stress (SY) for Unit Pressure Load (100 psi)

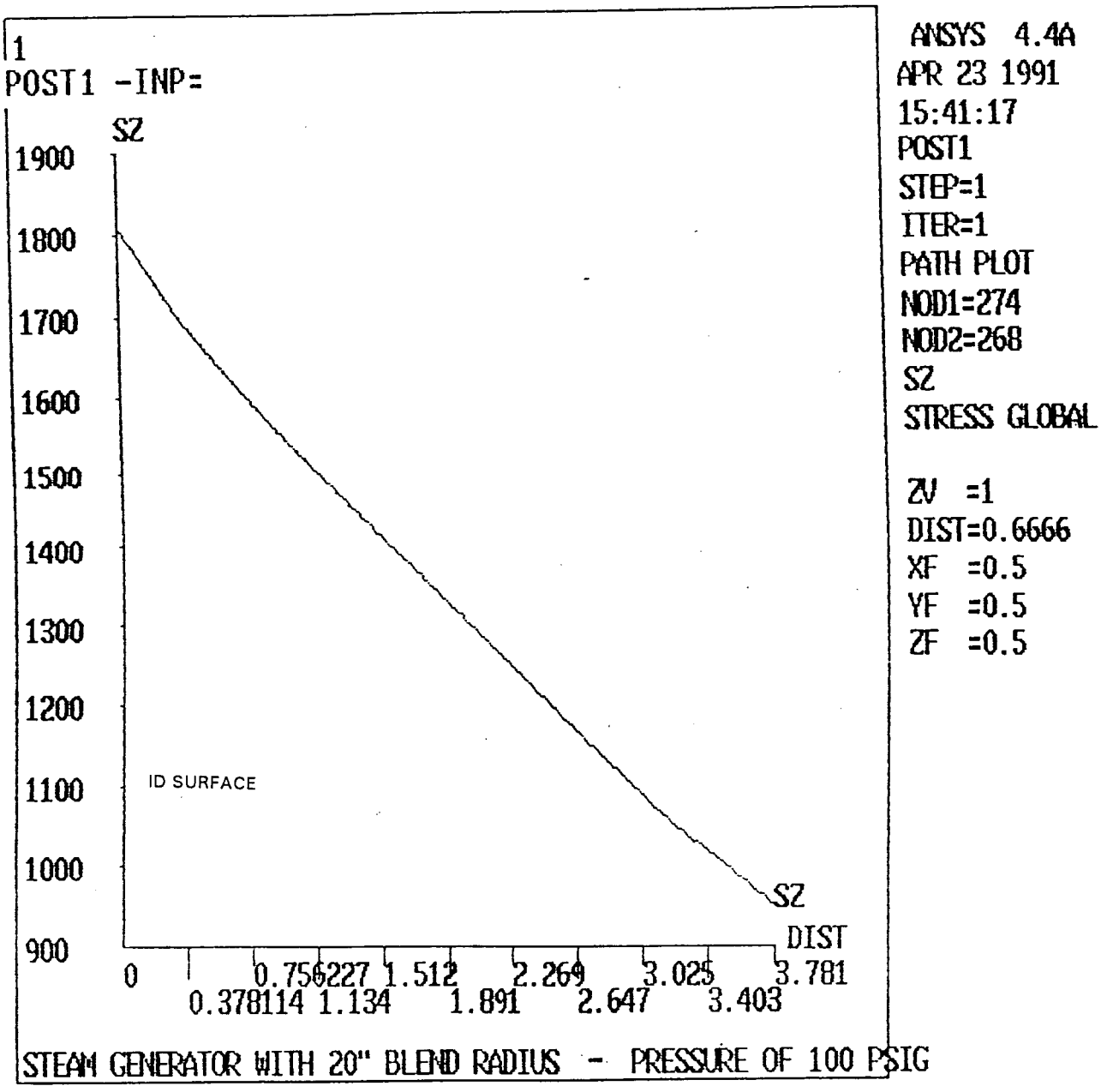

FIGURE 7.9

Through-Wall Distribution at Axial Location of
Maximum Hoop Stress (SZ) for Unit Pressure Load (100 psi)

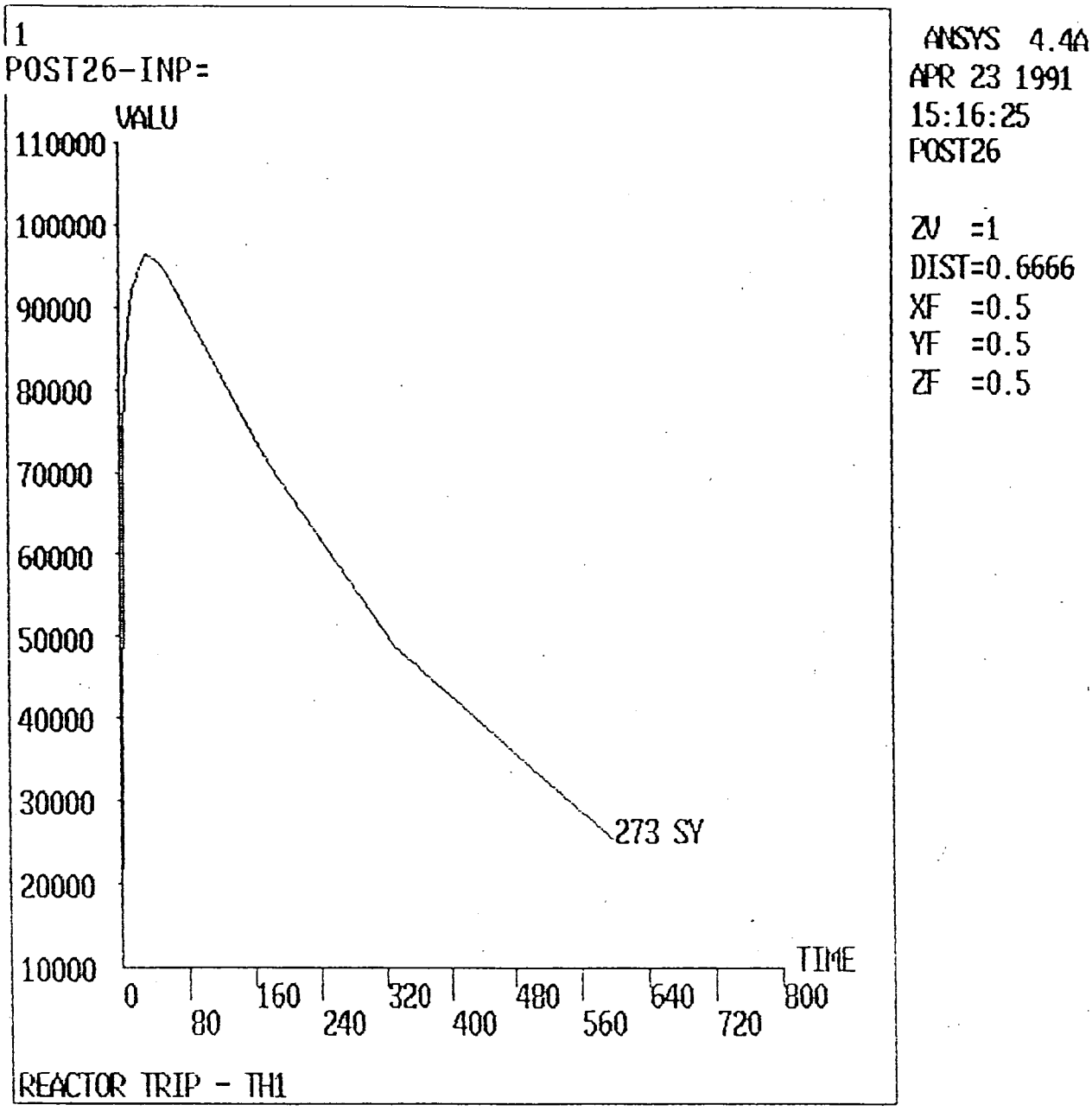

FIGURE 7.10

Reactor Trip - Time Variation of Surface Axial Stress (SY)
(Thermal Transient without Pressure)

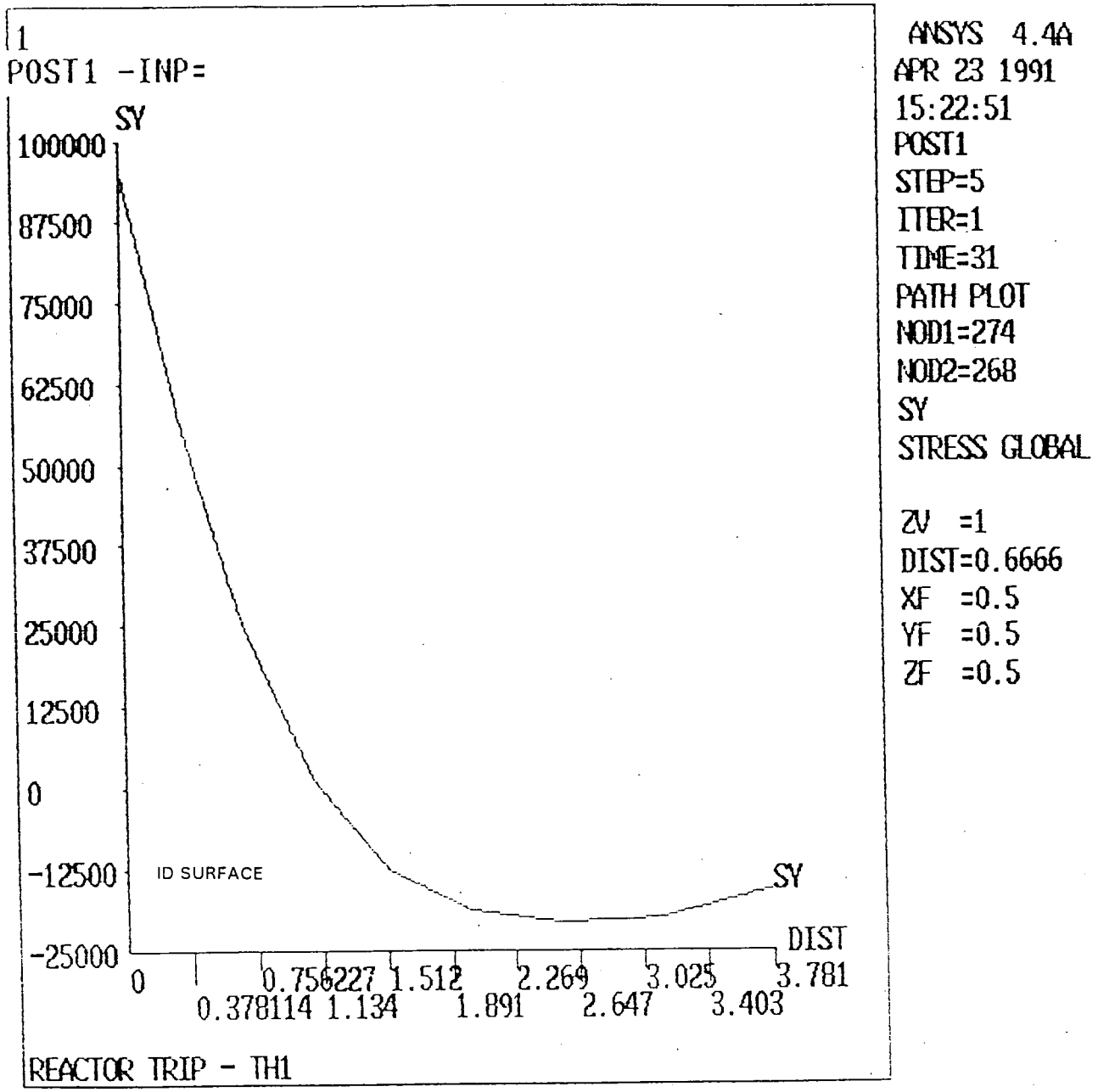

FIGURE 7.11

Reactor Trip - Through-Wall Axial Stress (SY) at the Time of Maximum ID Surface Axial Stress (SY) (Thermal Transient Without Pressure)

	Transient	Occurrences
1	Heat Up	200
2	Cool Down	200
3	Plant Loading	14,500
4	Plant Unloading	14,500
5	Small Step Increase	2,000
6	Small Step Decrease (50%)	2,000
7	Large Step Decrease	200
8	Feedwater Cycling Hot Standby	25,000
9	Steady State Fluctuation (+)	1,000,000
10	Steady State Fluctuation (-)	1,000,000
11	Reactor Trip	400
12	Partial Loss of Flow	80
13	Loss of Load	80
14	Loss of Power	40
15	Hydrotest	10
16	Pressure Leak	120

TABLE 7.1

Pressure and Thermal Transients for Secondary Side of Steam Generator

Load Condition	Stress Category	Upper Cylinder Stress	Upper Cylinder Allow.	Upper Cylinder Ratio	Girth Weld Stress	Girth Weld Allow.	Girth Weld Ratio	Transition Cone Stress	Transition Cone Allow.	Transition Cone Ratio
Design[1]	P_m or P_L	25.7	26.7	0.96	16.1	40.0	0.40	<25.7	26.7	<0.96
	$P_L + P_b$	25.7	40.1	0.64	16.1	40.0	0.40	<25.7	40.1	<0.64
Normal & Upset	$(P_L + P_b + Q)_{range}$	[2]			78.3	80.1	0.98	[2]		
Faulted[3][4]	P_m or P_L	25.7	56.0	0.46	16.1	84.0	0.19	<25.7	56.0	<0.46
	$P_L + P_b$	25.7	84.0	0.31	16.1	84.0	0.19	<25.7	84.0	<0.31
Test	P_m	[5]			[5]			[5]		
	$P_L + P_b$									
Fatigue Usage	-	[2]			0.13	1.0	0.13	[2]		

NOTES:
(1) Includes seismic OBE loads
(2) Enveloped by girth weld stresses
(3) Includes seismic DBE loads
(4) Faulted Conditions use Design Pressure and DBE; since DBE gives only axial stress, the Design Condition and Faulted condition stress intensity values are the same
(5) This condition is enveloped by the Design Condition

TABLE 7.2

Code Evaluation Summary for the Girth Weld Region

8.0 FEEDWATER NOZZLE SEALING SLEEVE QUALIFICATION

Following an inspection of the feedwater nozzle surfaces with the thermal sleeve removed, indication of nozzle cracking had been observed beneath the thermal sleeve in the 1990 outage. The location and schematic of the present feedwater nozzle arrangement is as shown in Figure 8.1. The cause of the nozzle cracking has been attributed to cold feedwater leaking past the existing thermal sleeve. This leakage flow path is schematically shown in Figure 8.2.

8.1 Sealing Sleeve Design

A feedwater nozzle sealing sleeve has been designed and installed to provide a barrier to prevent cold feedwater from entering the region of the steam generator feedwater nozzle beneath the existing thermal sleeve.

Feedwater flow enters the steam generator feedwater nozzle, flows into the thermal sleeve, through the feedwater ring and enters the upper steam generator chamber via J tubes. The existing thermal sleeve is a push fit into the feedwater nozzle. The sealing sleeve provides a protective barrier to leakage flow. A schematic of the sealing sleeve is presented in Figure 8.3.

The main components of the sealing sleeve, with reference to Figure 8.3 are as follows:

The sealing sleeve, Part #1, is welded directly to the steam generator feedwater nozzle at the outboard (feedwater pipe) end. This ensures a sealed leakage flow path to the incoming feedwater. At the inboard (steam generator) end, a groove is cut into the sleeve. The groove contains a spring (Part #2) loaded sealing ring (Part #3). The sealing ring

compresses against a pad ring (Part #5), but is free to slide on the pad ring to accommodate differential thermal movements of the steam generator, nozzle, and feedwater ring configuration. The pad ring is welded directly to the existing feedwater thermal sleeve (Part #6). For leakage flow to occur, flow has to take a convoluted path via the sealing ring. Blocks (Part #4) are provided to prevent the sealing sleeve from entering the feed ring in the event that the weld should fail.

This section of this report provides the basis for the design and acceptability of the sealing sleeve under all loading conditions.

8.2 Sealing Sleeve Qualification

The analysis performed on the sealing sleeve focused on qualifying the design for the following anticipated loading conditions:

- Fluid Flow Conditions
- Thermal and Pressure Transients
- Thermal Stratification
- Normal Load Qualification

The fluid flow evaluation considered both the added resistance of the sealing sleeve and potential flow induced vibration. All potential mechanisms of flow induced vibration were considered and evaluated. The design of the sealing sleeve was specifically made to limit "incoming" flow resistance and to minimize the potential for vortex formation at the end of the sleeve.

All feed system thermal and pressure transients were evaluated in a fatigue analysis. The most severe thermal transient considered was the reactor trip, where auxiliary feed is injected into the steam generator. Thermal stratification in the feedwater nozzle occurs when cold feedwater is slowly injected into a hot steam generator. Different levels of stratified flow were assumed and analyzed. The results of both the thermal and pressure transient analysis and the stratification analysis were utilized in an evaluation of the fatigue life of the sleeve.

Normal loads, including deadweight, seismic and normal thermal were also analyzed.

Flow Induced Vibration

A flow induced vibration analysis was performed to ensure the installation of the sleeve does not induce any significant vibration problems. The potential mechanisms of excitation considered were fluid instability, vortex shedding, and turbulence. The results of the calculations demonstrated that the critical velocities of fluid instability lay far beyond the range of the operating conditions. The frequency of the hydraulic force associated with vortex shedding was calculated and was found to be considerably less than the calculated natural frequency of the sleeve. Thus, resonance and the potential vortex shedding vibration is not feasible. Additionally, since the trailing edges of the sleeve are rounded, no noticeable hydraulic forces will result.

With respect to turbulence being a source of vibration, the diameter of the sleeve is larger than the characteristic length at which vibration would occur due

to flow turbulence. Turbulence, therefore, is a highly unlikely source of excitation.

Fluid Flow

The changes in feedwater flow rates and the potential for erosion/corrosion were also investigated.

The additional hydraulic resistance from the sealing sleeve was evaluated. This included one contraction and one expansion as the flow enters the sleeve and as the flow exits the sleeve. Since the installation of the sleeve will not change the pump discharge pressure or the steam generator operating pressure, it is calculated that there is less than 0.02% decrease in the flow. This flow change is negligible. The capacity of the feed system is sufficient to maintain the desired flow.

The installation of the sealing sleeve was also reviewed for potential susceptibility to erosion/corrosion induced wall degradation. The installation of the sleeve results in an insignificant increase in flow velocity. The nozzle configuration is such that its relative erosion rate is lower than other feedwater system components. The normal operating temperature of this system is also beyond the temperature regions of highest erosion/corrosion susceptibility. Erosion/Corrosion is not anticipated at the sleeve location.

In summary, the sealing sleeve will not significantly increase the flow rate through the nozzle nor the rate of erosion for pressure boundary components within and adjacent to the nozzle.

Thermal Transient Analysis

A thermal transient analysis using the ANSYS finite element model shown in Figure 8.4 was performed for the most severe transients. This 2-D axisymmetric model incorporated ANSYS STIF42, 2-Dimensional isoparametric solid and STIF55, 2-Dimensional isoparametric thermal solid elements. STIF55 is used as an axisymmetric ring element with 2-Dimensional thermal conductivity capability. The calculated stress results were then utilized to determine stress ranges for the defined design transients.

A stress concentration factor (SCF) was applied to the applicable component of stress to account for the stress riser at the toe of the weld connection of the sealing sleeve to the existing feedwater nozzle. These thermal transient stress results were combined with the results of the thermal stratification analysis to perform a fatigue analysis.

Thermal Stratification Evaluation

A thermal stratification evaluation was performed for three levels of an evaluated transient of stratified fluid flow as depicted in Figure 8.5. To accurately predict weld stresses during thermal stratification, an ANSYS 3-Dimensional finite element model was utilized as shown in Figure 8.6. The model is constructed utilizing ANSYS STIF45, 3-D isoparametric solid elements. The element is defined by eight nodal points having three degrees of freedom at each node. The results of this stratification analysis were then used to predict stresses for each of the design transients which will induce stratified flow. Based on the calculated stresses, the thermal fatigue life was calculated for the critical weld region of the sealing sleeve.

The maximum evaluated weld stresses occurred at the root of the fillet weld to the feedwater nozzles, along the hot water boundary nodes. These stresses were utilized in the fatigue analysis of the sealing sleeve.

Normal Load Qualification

Analyses were performed for the normal loads including sleeve deadweight, internal pressure, pressure differential across the sleeve, and seismic induced stresses. All the calculated stresses were acceptable.

Fatigue Evaluation

A fatigue evaluation was performed to the requirements of ASME Section III. The events previously described were considered in the calculation of usage factor. The fatigue usage factor was calculated to be less than 1.0 for the number of cycles postulated for a 20 year period, the approximate remaining life of the plant, and for the transients selected to be the most severe.

8.3 Summary

The results of the evaluation performed on the sealing sleeve for each of the anticipated loading conditions are acceptable.

The fluid flow evaluation considered both the added resistance of the sealing sleeve and potential flow induced vibration. The added resistance of the sealing sleeve is very low and will result in a negligible reduction in feed flow. All potential mechanisms of flow induced vibration were considered and are acceptable.

The results of thermal and pressure transient analysis and the thermal stratification analysis were utilized in an evaluation of the fatigue life of the sleeve. The stress analyses utilized conservative assumptions and indicated that the sealing sleeve is acceptable for 20 years of operation.

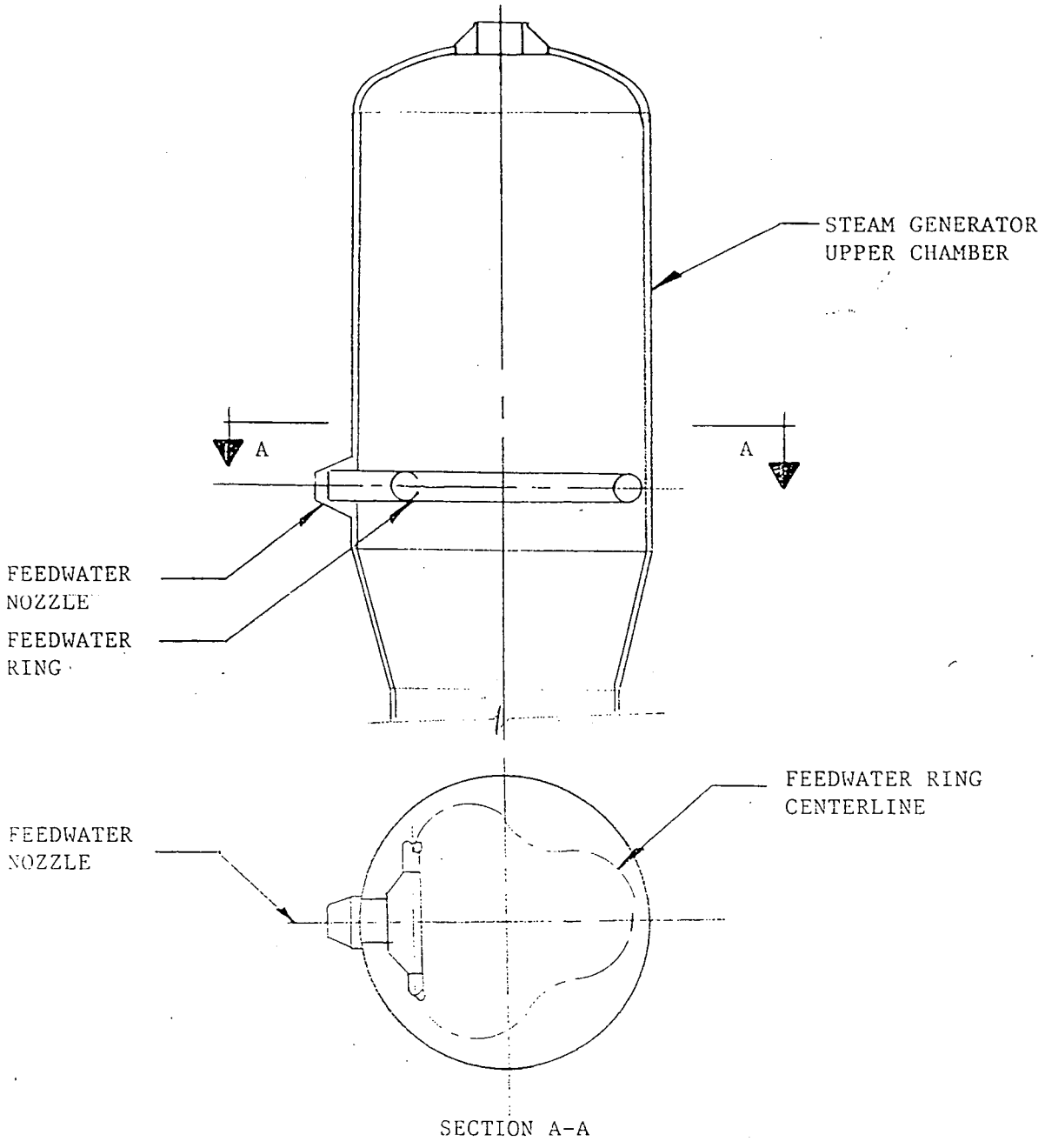

FIGURE 8.1

Series 44 Steam Generator &
Feedwater Nozzle Arrangement

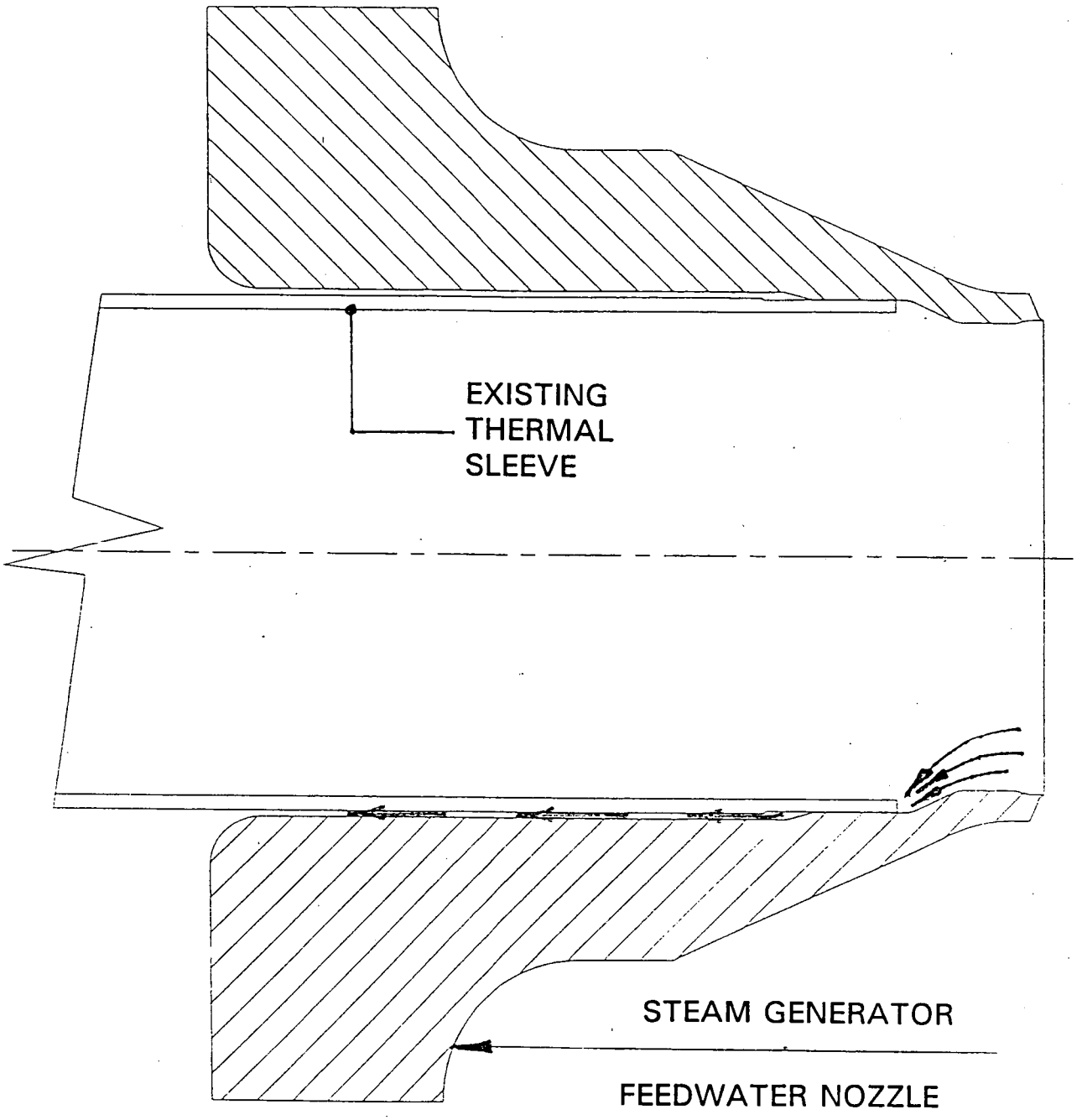

FIGURE 8.2

Existing Feedwater Nozzle and Sleeve
Leakage Flow Path Shown

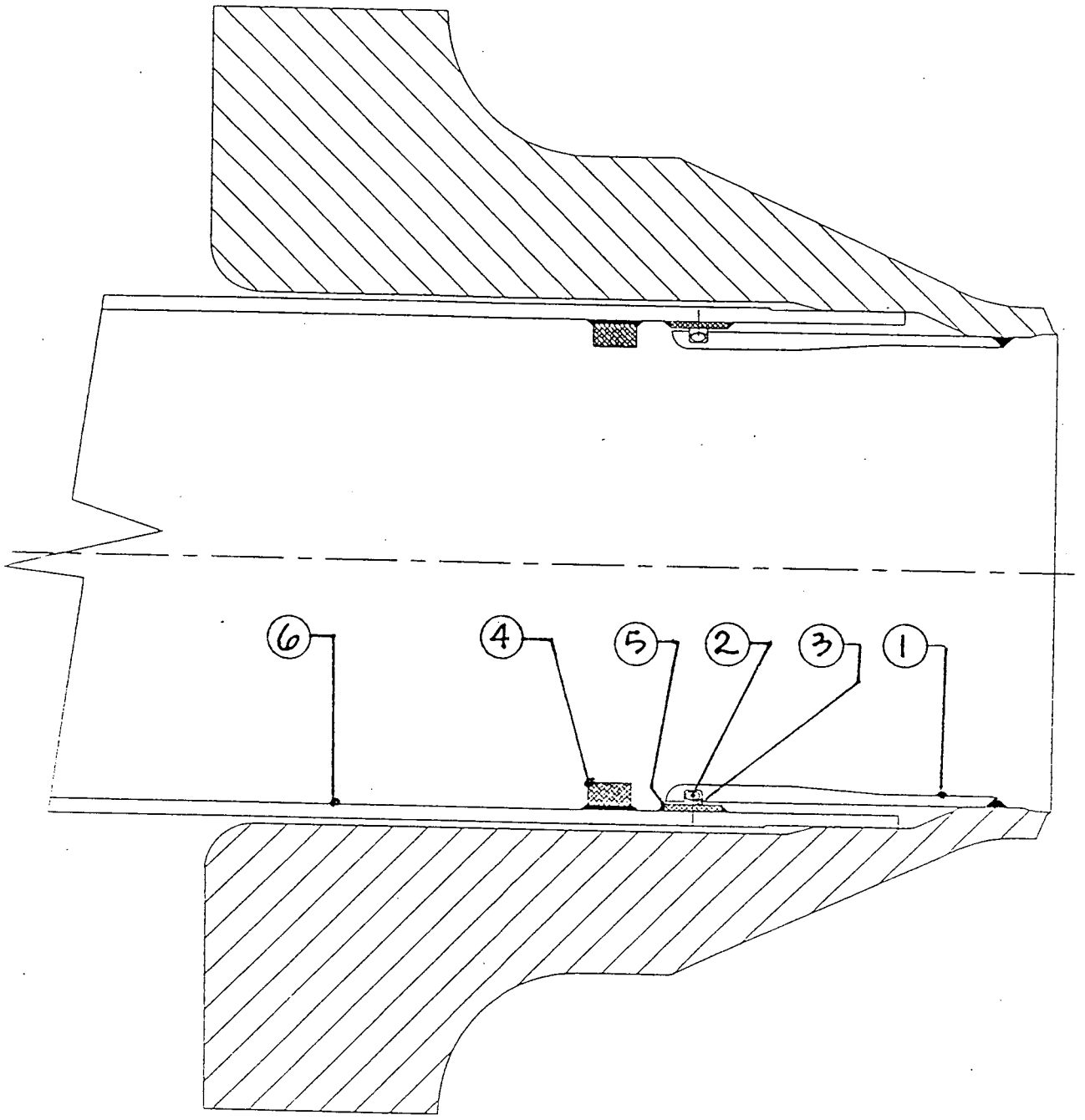

FIGURE 8.3

Feedwater Nozzle Sealing Sleeve

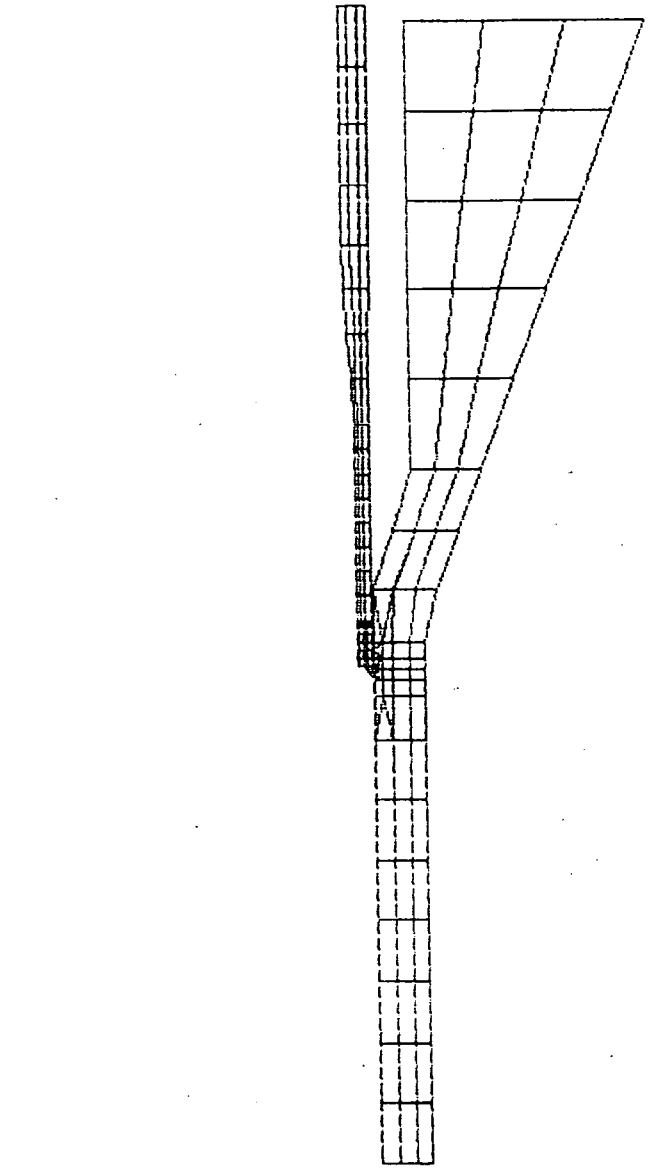

FIGURE 8.4

2-Dimensional ANSYS Finite Element Model

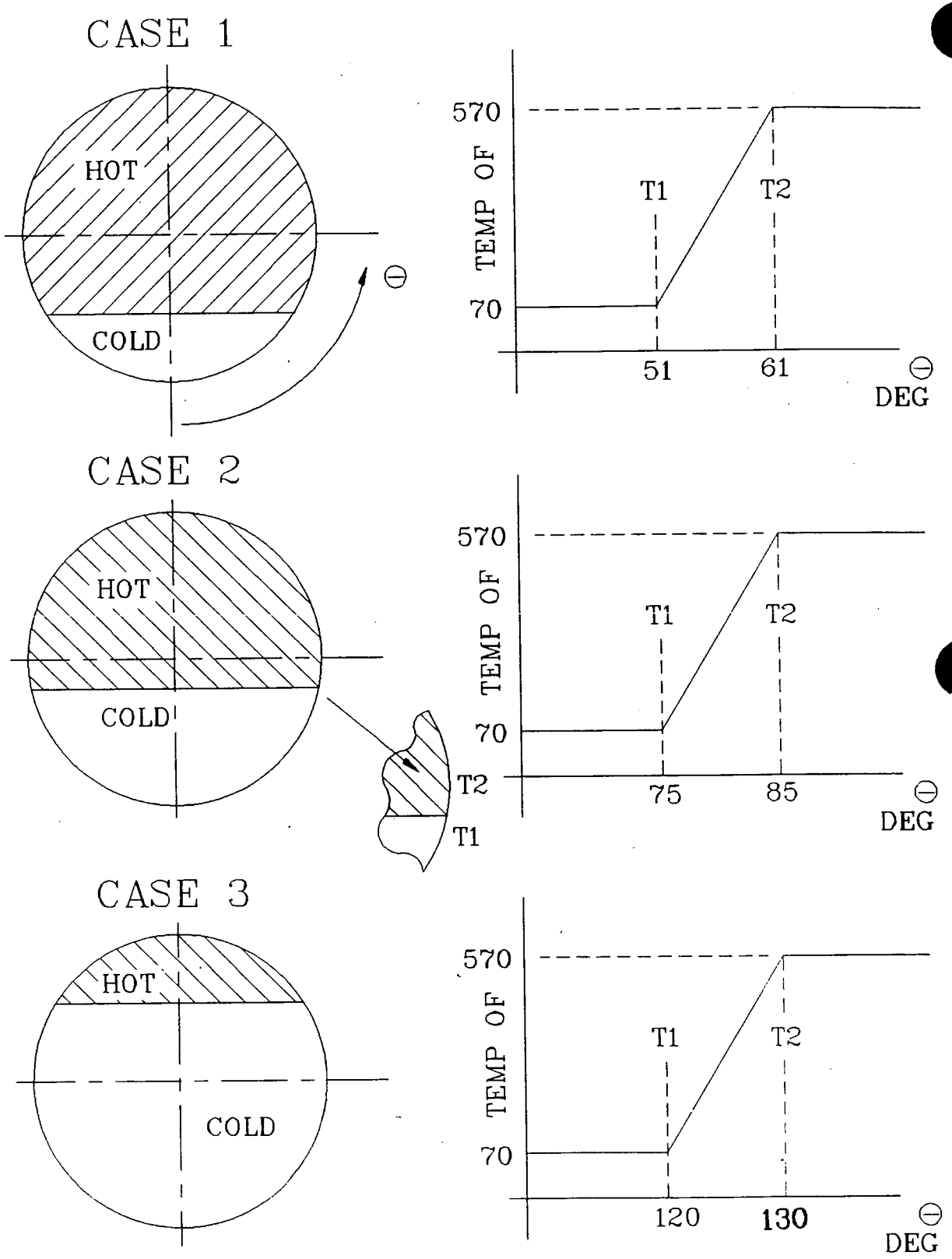

FIGURE 8.5

Thermal Stratification Temperature Profile

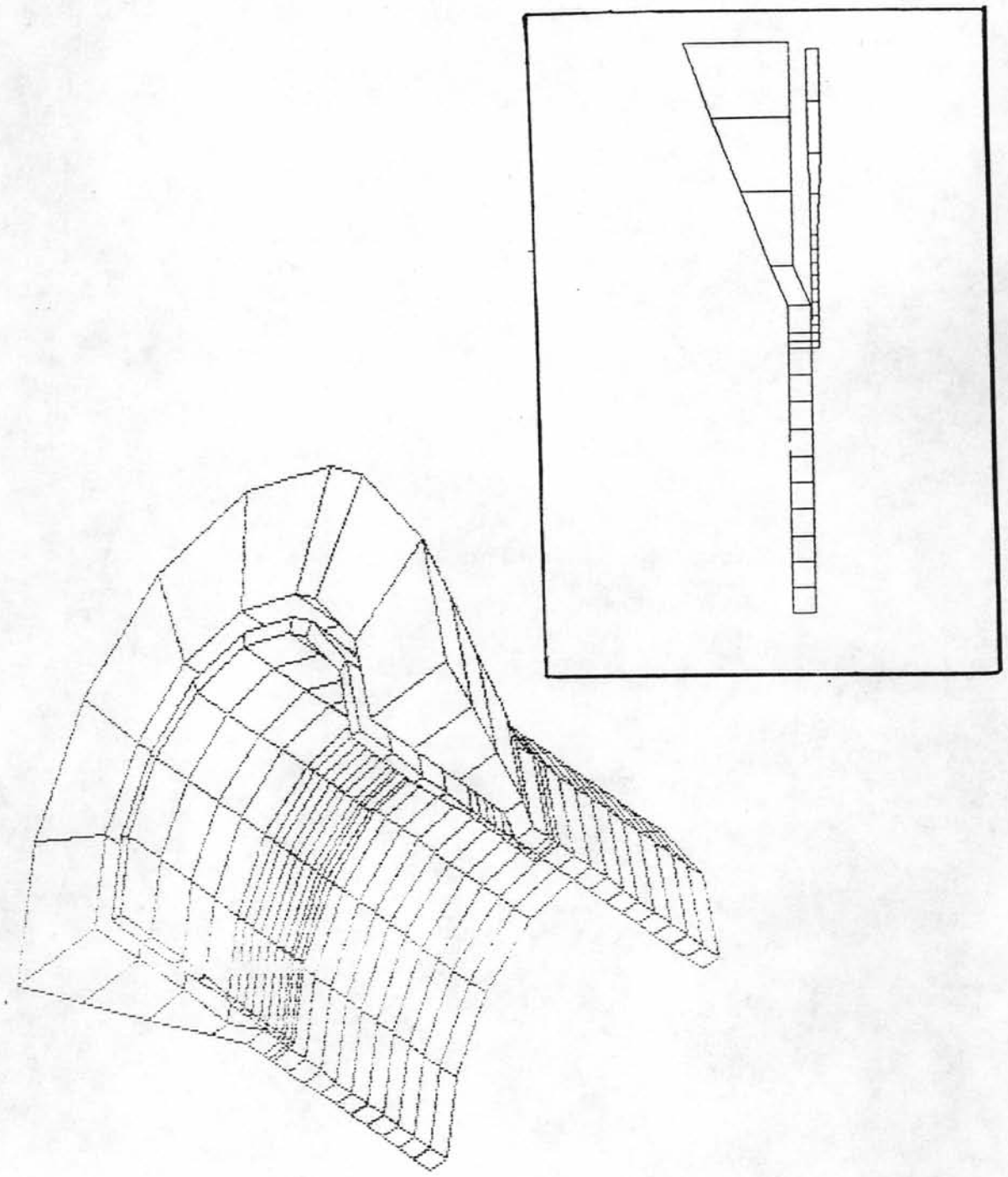

FIGURE 8.6

3-Dimensional ANSYS Finite Element Model

This page intentionally left blank.

9.0 **1993 INSPECTION PLANS**

The extensive repairs made during the 1991 refueling outage have restored the integrity of the steam generator shell to an "as-new" condition. The operating conditions are being maintained well within the specifications and industry guidelines. It is believed that further cracking of the steam generator shell will not occur. Nevertheless, Consolidated Edison will perform the following additional examinations during the 1993 refueling outage and will take appropriate measures based on the examination results:

1. GIRTH WELDS: UT examine a 20 inch band from the lower narrow range level tap downward in one steam generator. If cracks are found, similarly examine remaining steam generators.

2. PENETRATIONS: PT examine one 2 inch inspection port.

This page intentionally left blank.

10.0 REFERENCES

1. Indian Point Unit 2, Steam Generator Girth Weld Repair Report, Fall 1987 Outage, WCAP-11730, Westinghouse Electric Corporation, January, 1989. (WCAP-11731 Non Proprietary).

2. Indian Point Unit 2, Steam Generator Girth Weld/Feedwater Nozzles Report, Spring, 1989 Outage, WCAP-12293, Westinghouse Electric Corporation, October, 1989. (WCAP-12294 - Non Proprietary).

3. Indian Point Unit 2, Final Report of the Steam Generator Inspection, Repair, and Restoration Efforts During the 1990 Mid-Cycle Inspection, WCAP-12670, Westinghouse Electric Corporation, July, 1990 (WCAP-12671 Non Proprietary).

4. ANSYS Finite Element Analysis Software Systems, Houston, PA, Version 4.4A.

This page intentionally left blank.